Author's response

Referee comments and submitted author's responses are listed in black. Corresponding manuscript updates are marked in red.

-- Abstract, Introduction and Discussion*:* The conclusion that the oceanic storage of DIC and the drawdown of atmospheric CO2 in response to nutrient depletion all depend on the ocean circulation patterns (including the overturning strengths of NADW and AABW, and the volume fraction of the ocean last ventilated from the North Atlantic vs. Southern Ocean) is not new. The circulation effects on the ocean carbon pumps have been extensively studied using models and theoretical frameworks: the solubility pump (e.g., DeVries and Primeau, Atmospheric pCO2 sensitivity to the solubility pump: Role of the low-latitude ocean, GBC 2009), the biological pump (references already cited in the manuscript) and the disequilibrium pump (e.g. Ito and Follows, Air-sea disequilibrium of carbon dioxide enhances the biological carbon sequestration in the Southern Ocean, GBC 2013). One of the new points in this study is that the authors discussed the relative role of the three pumps in the net change of the simulated carbon cycle. But, because the forcing used to generate the different circulation patterns is arbitrary, their discussion of the relative roles does not seem very interesting. Overall, I feel that the authors need to highlight what new findings or insights this study can provide.

Response: In the study by Ito and Follows (GBC, 2013), mentioned by the referee, it was pointed out that more studies like these, where we analyse model output 'in terms of different carbon pump components' and their behaviour could aid in understanding the behaviour of climate models and carbon cycle models. The reviewer is correct that the circulation effect on the ocean carbon pump has been extensively investigated. There are two main advances here that are of importance to the community, and we will place greater emphasis on these in the revised manuscript:

1) The initial state, not only in terms of ocean circulation, but in terms of ocean carbon inventory and the origin of the already stored carbon (e.g. biological or solubility pump), is crucial for the outcome of a study investigating increased efficiency of the biological pump, and the effect of the initial state is quantifiable;

2) the relative contributions by Csat, Csoft, Ccarb, and Cdis to the ocean carbon inventory in the initial state depends on the model tuning strategy, yet these combine in a manner to give a response in total carbon that is more straightforwardly related to the circulation than any of the four components (Figs. 3-4).

Regarding 1) We show that differences in the initial states can explain discrepancies in e.g. a CO2 drawdown scenario where the efficiency of the biological pump increases. As the referee points out, this will help to explain why previous model intercomparison studies have seen a large spread in response among models to the same perturbation. Therefore, it can also be important for future model intercomparison studies, in explanations of results, but also in planning for common tuning strategies and experimental design. This will be important in model studies of both glacial and modern climate scenarios. Here, the findings in described in 2) make it easier to understand the outcome of the drawdown experiment and therefore provide a useful basis for explaining the role of the initial state. The findings presented in e.g. Fig. 6 are new, and have not been covered by the studies mentioned by the referee. Of most value here is that we show that it is possible to quantify, from theory, the effect of any bias in the model's initial state on its sensitivity to changes in the biological pump. We have chosen a variety of changes to the forcing in order to demonstrate that the result is robust. This result should be of value in understanding the biases individual models, in inter-comparison studies, and potentially for choosing tuning criteria.

Regarding 2) Firstly, the changes to the forcing that we make are certainly idealised, but they are not arbitrary. We are changing common circulation parameters, mainly within the limits of common tuning ranges, to produce circulation states that are relevant in the context of the amplitude of (palaeo-)climate change (see response to Referee #1, point 3). (The change used to produce a 100%-efficient biological pump is, of course, an intentional exception.) As we explore both an increase and a decrease of the same parameter, the equilibrium states resulting from the increase and decrease, together with the control equilibrium state, provide a range of states that can be expected from tuning of this parameter. By testing several parameters in the same manner, we show that different tuning strategies are expected to affect different reservoirs of the initial state carbon inventory. This leads us to the important conclusion that, depending on the strategy used in model tuning, the relative sizes of the reservoirs of DIC species will differ between models. As the referee points out, this has not been done in previous studies. As a consequence, such differences have not been taken into account in e.g. model intercomparison studies. We hope that our study can bring some attention to this problem.
Secondly, when comparing the different changes in forcing, our main intent is for the reader to compare the relative sizes of change of the different pumps when one parameter is changed (e.g. when the wind stress is changed, the most important contribution to the change in carbon inventory comes from the soft tissue pump, whereas if horizontal (isopycnal) diffusivity is changed, the contribution from the solubility pump and disequilibrium carbon dominate). Hence, the magnitude is not what is most important, but rather which carbon pump(s) is(are) affected by which tuning strategy. By doing this, we emphasize that the tuning strategy is important for determining which processes contribute to a model's ocean carbon inventory, and therefore its behaviour. Even if this conclusion is not entirely new, all the previous studies focus on one or two processes at a time. We therefore believe that the structured approach of the ensemble study, and the fact that all DIC species are investigated in the same manuscript, can provide a comparability that can be useful for the community.

→ We do, however, acknowledge the reviewer's point that these insights need to be better highlighted, and will make appropriate changes to the Abstract, Introduction and Discussion sections.
→ For the corresponding changes in the manuscript, see List of relevant changes and marked up manuscript comparison

-- Methods and Results: *General comment 1)* I assume that you don't have preformed nutrients (O2, PO4, DIC) written out in the model output? If you do, this eliminates the problem with O2dis, as you can calculate O2sat and then calculate the remineralised O2 and hence Csoft explicitly. Additionally, preformed O2 and PO4 would be much more useful in the parameterisation for ALKpre.
Response: We did not have preformed tracers in the output used for the first version of the manuscript. However, for the new version we have re-run the simulations to get the output for pre-formed tracers Cpre, O2pre, PO4pre and ALKpre. This eliminates the problems mentioned by the referee. It also eliminates the need for the regression model for ALKpre.
→ For the corresponding changes in the manuscript, see List of relevant changes and marked up manuscript comparison

-- All sections: *General comment 3)* If it's not too cumbersome, perhaps consider using descriptive abbreviations for the different SEs.
Response: We will include such abbreviations in the updated manuscript.
→ For the corresponding changes in the manuscript, see List of relevant changes and marked up manuscript comparison

-- p. 3, lines 4-5: Could you specify the order of magnitude of the change in CO2?
Response: The order of magnitude of the CO2 rise in deglacials, as observed in ice cores (e.g. Petit et al., 1999), is ~100 ppm. It is likely that circulation differences as large as in PMIP

LGM states (see e.g. Otto-Bliesner et al., 2007) could cause differences in deglacial CO2 on the order of tens of ppm, if such experiments were run with equally different circulation states in cGENIE. However, the order of magnitude of the potential discrepancies is not explicitly mentioned by Zhang et al. in the cited paper, and we would not want to speculate about the response of the models they are evaluating in their study.
→ no change has been made to the manuscript

-- p. 3, line 35: It's also important to note that these studies don't even have Cres due to infinitely fast gas exchange.
Response: Marinov et al. (2008a,b) do not have Cdis in their main ensemble of simulations, because of the fast gas exchange in these simulations. They do, however, study the disequilibrium component separately for a subset of 3 simulations, where they state that they apply 'regular' gas exchange. In this study, we cover a wider range of simulations that include Cdis. In Kwon et al. (2011), they assume the change in Cdis to be negligible in the theoretical derivation and therefore run most of the simulations with very fast gas exchange. They do, however, also analyse some simulations with a 'normal' gas exchange coefficient, in order to validate the theoretical model for atmospheric pCO2, but they do not explicitly study the disequilibrium response. The component of Cres that consists of calculation errors should be present in all of these studies, regardless of whether they have artificially fast or normal gas exchange. E.g. in Kwon et al., the calculation errors from the theoretical calculations of the changes in Csoft and Ccarb will be grouped together with Csat, which is not calculated.
→ For the corresponding changes in the manuscript, see marked up manuscript comparison

-- p. 4, lines 3-5: I don't find this paragraph necessary.
Response: The paragraph will be removed in the updated manuscript.
→ removed

* as much as possible of Section 2, Section 3.1.1 and Sections 3.2-3.4 will be put into an appendix. After re-running the model with pre-formed tracers (see Author's Response to Referees #2 and #3), the parts of the text that describe back-calculations to pre-formed nutrient from apparent oxygen utilization (see e.g. section 3.2, p. 10) and the regression model for preformed alkalinity (see section 3.3) can be removed entirely. This will be replaced by a short subsection (3.1.3), which describes the use of pre-formed tracers in the model.
→ See Appendices A and B

-- p. 4, lines 28-29: I don't believe that this is correct, as the pumps can have opposing effects. It should be specified that the net effect of all of the pumps must be to redistribute carbon from the surface to the deep ocean.
Response: We will rephrase the sentence as follows: 'If the net capacity of the carbon pumps to redistribute carbon from the surface to the deep ocean increased, this would act to decrease pCO2atm.
→ changed

-- p. 5, line 17: I think what you mean is that alkalinity is not set (or affected) by gas exchange, but referring to an "expected" value of Cpre is a little misleading.
Response: Since the regression model for ALKpre is no longer used, the two sentences at the end of this paragraph (starting with 'Unlike CO2…') will be removed.
→ removed

-- p. 5, lines 31-32: Please include Martin (1990), Paleoceanography, as this is one of the central references for increased soft tissue pump efficiency during glacials.

Response: We will add Martin (1990) in the updated manuscript.
→ added

*** Methods: The way the biological pump is simulated in the model is unclear. The authors included the carbonate pump in their models and analyses (expressed as Ccarb), but there is no description on how the carbonate pump is represented in the model. For example, are the sedimentation processes included in the model? How are the production and dissolution of calcifying organisms represented in the model? How is the strength/efficiency of the carbonate pump affected by the drawdown experiment? In the drawdown experiment (specified in lines #31-33 of page #9), the remineralization length scale of sinking organic particles is made very deep (10,000m), so that "any carbon that is taken up in organic material to be highly efficiently trapped in the deep ocean and not undergo any significant remineralization". Does it mean that most of inorganic nutrient is converted to organic form and stored in the abyss without being remineralized back to inorganic form? If this is the case, then the amount of organic matter would increase substantially in the drawdown experiment, and the carbon fixed in organic material should be an important component in the mass balance equations and can't be ignored in the theoretical derivations presented in the manuscript. Likewise, the equation "Ppre=P-Preg" would be incorrect. This needs to be clarified.

Response: The way the biological pump is simulated in the model is thoroughly described by Ridgwell et al. (2007). Since the description is lengthy and the paper is already long, we decided not to include the full description in the manuscript, but instead describe the most relevant part describing remineralisation (section 3.1.2) and reference the paper for the in-depth model description. We agree with the referee that it should be clarified that the explicit information on the biogeochemical cycling can be found in this paper (see manuscript changes below).
We also agree that we need to make some clarifications regarding the drawdown experiment. The referee asks 'Does it mean that most of inorganic nutrient is converted to organic form and stored in the abyss without being remineralized back to inorganic form?' Yes, that is exactly the case, and the referee correctly states that this means the amount of organic matter in the deep ocean significantly increases. The referee is also correct in saying that the theoretical derivation that neglects the organic matter no longer holds. Therefore, we do not use this derivation for the drawdown experiment (we only use it in the first step, where we compare the initial equilibrium states). For the drawdown experiment, we do not explicitly calculate the change in strength of the soft tissue pump, the carbonate pump, or the changes in disequilibrium. The theoretical derivation could be made valid for this case by assuming that 106 times the amount of particulate P in the deep ocean should be added to Csoft. However, we have chosen not to explore the changes in strength of the different pumps in the drawdown experiment, since it is a highly hypothetical case. We are mainly interested in the differences in CO2 drawdown between different ensemble members in the limit of a highly efficient biological pump. That the biological pump is made highly efficient is clear from the two orders of magnitude decrease in dissolved P in the ocean, which will also be clarified in the manuscript.
→ We will add a clarification in section 3.1, at the end of the second paragraph. This clarification reads "The model description of export flux of organic matter is based on available surface nutrients (see Ridgwell et al., 2007, Eq. 1-4), and instead of having a "standing plankton biomass" in the model, the export of particulate organic matter is derived directly from uptake of P. The carbonate precipitation rate is thermodynamically-based and relates export flux of CaCO3 to the flux of POC (see Ridgwell et al., 2007, Eq. 8). As investigation of carbonate system feedbacks are not the purpose of this study, interactive sediments are not used, and in terms of carbon cycling, the atmosphere-ocean is studied as a closed system."
→ We will also add to section 3.1.2, before the final sentence of the second paragraph, the sentence 'The remineralisation of CaCO3 in the water column is treated in a similar manner to particulate organic carbon."

→ Note that in the updated manuscript, these updates are all in Section 3.1, since Section 3.1.2 has been removed and incorporated into 3.1 (see List of relevant changes)

-- p. 7, lines 5-6: "and has a level of detail for the carbon system that made it particularly suitable for this study." This is very general; please specify why it is appropriate for this study (and/or why less complex models are not).
Response: The referee asks particularly about less complex models. A very simple ocean carbon system model such as miniBLING (Galbraith et al., 2015), which only has P, DIC and O2, would not be suitable for this study, because we are using ALK in our calculations. However, we want to emphasise that it is not only a question of complexity being high enough. Too high complexity could also pose a problem, e.g. a highly complex ocean ecosystem model with several functional types would be more expensive to run in terms of computational cost and therefore less suitable for this study. cGENIE balances having enough complexity in the ocean carbon system with a suitable level of complexity in terms of ocean resolution.
The full sentence on p.7, lines 5-6: "cGENIE is higher in complexity than box models, but is still efficient enough to allow running a large ensemble to equilibrium for the carbon system, and has a level of detail for the carbon system that made it particularly suitable for this study." should be rephrased as follows: "cGENIE is higher in complexity than box models, but is still efficient enough to allow running a large ensemble to equilibrium for the carbon system. In terms of ocean carbon system tracers, the minimum required for this type of study is P, DIC, O2, ALK. cGENIE includes many additional tracers, out of which only some are used in this study. For example, particulate (POC) and dissolved organic carbon (DOC) are included in the calculations of model carbon inventory. Of particular importance for this study is the possibility to run with pre-formed tracers (Ppre, Cpre, O2pre, ALKpre)."

-- p. 8, line 25: When referring to Cdis, it would be useful to cite Ito and Follows (2013), GBC.
Response: The citation will be added in the updated manuscript.
→ citation added in the Introduction

* Pg 9 Methods: Are the ranges for vertical diffusivity, wind stress, horizontal diffusivity, etc that are used in the sensitivity experiments comparable to the range of values that are normally used to tune models? Would be useful to provide this information here, so that the reader can assess whether your sensitivity experiments represent values that might normally be used.
Response: For this study, our intention is for the ensemble to be representative of a wide range of plausible ocean circulation states. The chosen parameter ranges correspond to a halving and doubling of the values used in the control simulation. Our chosen values are within the parameter space explored for a predecessor to the GENIE-model by Edwards and Marsh (2005), except the low wind stress simulation (see below). Similar parameter ranges are also explored for GENIE by e.g. Marsh et al. (2013). For the most part, our selected values are within the parameter ranges that generate the subset Edwards and Marsh (2005) refer to as low-error simulations.
In the Bern3D model, with physics based on Edwards and Marsh (2005) and thus similar to GENIE, Müller et al. (2006) doubled the observed wind stress ($W = 2$) to get a more realistic gyre circulation. Marinov et al. (2008 a,b) used the Geophysical Fluid Dynamics Laboratory Modular Ocean Model version 3, which has the same default value for isopycnal diffusivity (1500 $m^2\ s^{-1}$) as our model. Marinov et al. (2008 a,b) explore a range of 1000-2000 $m^2\ s^{-1}$ (c.f. our range of 750-3000 $m^2\ s^{-1}$). When comparing with models that have different available tuning parameters, diagnostic variables such as temperature, salinity and AMOC volume transport can indicate whether our achieved states are within the common tuning range for ocean circulation.
We compare the temperature and salinity ranges in two selected grid points of the ensemble of pre-industrial control states (*PIC*) of PMPI2 and CMIP5/PMIP3 (IPCC; see Table B1) to

the corresponding grid cell ranges of our equilibrium states *SE1-SE12*. In these selected grid cells, we cover a similar span in salinity and an equally broad range in temperatures as the PMIP-ensemble, though the temperatures in our ensemble are higher (range shifted by ~1.5°C). According to Muglia and Schmittner (2015), the PMIP3 *PIC* AMOC range is 12.6-23.0 Sv (Table B1). If we exclude the combined simulation with halved wind stress and halved diapycnal (vertical) diffusivity (*SE12,* now denoted *WS/2_DD/2)*, which has a very weak AMOC (2.0 Sv), the AMOC range for our equilibrium states is 8.3-18.0 Sv (Table B1). Thus, there is a difference of ~8-9 Sv between highest and lowest value, which is also the case for the PMIP3 *PIC:s*, but our ensemble does not cover the two highest PMIP3 AMOC values.

Table B1 Diagnostic variables of the pre-industrial control states of PMIP2 and CMIP5/PMIP3 (temperature and salinity as read from Fig. 9.18. of WG1 in IPCC AR5 and AMOC as given in Table 1 in Muglia and Schmittner (2015)) compared to similar diagnostics for our ensemble *SE1*-SE12 and control state *PIES278*.

Variables	PMIP2 + CMIP5/PMIP3 pre-industrial control states	Ödalen et al. cGENIE *SE1-SE12* and *PIES278*
Potential temperature (°C), N.Atl.	2.9 – 6.4[1]	4.6 – 8.0[2]
Potential temperature (°C), S.Atl.	-1.6 – 2.0[3]	-0.3 – 3.7[4]
Salinity, N.Atl.	34.8 – 35.5[1]	35.3 – 35.6[2]
Salinity, S.Atl.	34.6 – 35.0[3]	34.9 – 35.1[4]
AMOC (1 Sv = 10^6 m^3 s^{-1})	12.64 – 23.02[5]	2.0 – 18.0[6]

[1] North Atlantic PMIP grid point: 55.5°N, 14.5°W, 2,184 m depth
[2] North Atlantic cGENIE closest corresponding grid cell: 51-56°N, 10-20°W, 1,738-2,100 m depth
[3] South Atlantic PMIP grid point: 50°S, 5°E, 3,636 m depth
[4] South Atlantic cGENIE closest corresponding grid cell: 46-51°S, 0-10°E, 3,008-3,576 m depth
[5] Muglia and Schmittner (2015), PMIP3 pre-industrial control ensemble AMOC at 25°N, average with interval of one standard deviation
[6] cGENIE maximum Atlantic overturning. The *SE* ensemble member with halved wind stress and low vertical (diapycnal) diffusivity has a collapsed AMOC circulation (2.0 Sv). The average of this variable for all other *SE*:s is 13.8 Sv (range 8.3 – 18.0 Sv).

→This full response has been added as a new subsection "Sensitivity experiment tuning parameters"

* Pg. 9 LN 13 – confusing – do you mean that you hold ALK and P constant in your experiments?
Response not given – corrected directly in manuscript
→ Clarification given: During the spin-up phase, pCO_2^{atm} is still restored to 278 ppm (Fig. 1) and the ocean reservoir of nutrients (in this case, PO_4) is the same as *PIES278*, though nutrients are redistributed. A_T has no external sources/sinks and is only affected by the biological pump, which means it is negligibly different between ensemble members.
.

* Pg 9 LN 14-20 – Upon first reading, it was unclear what delta (ïA¸Dˇ) represents. Please define specifically that you are comparing the carbon estimates from PIES278 with equilibrium values from SE(n).
Response not given – correct directly in manuscript
→ Clarified by changing the sentence at Pg. 9 LN19, which introduces the equation, to: "The change in the total carbon inventory, Δ{TC} [mol] between $PIES278$ and some equilibrium state $SE(n)$, where $n = (1, ..., 12)$, can be described by"

* Pg 9 and then again on Pg 10 – when you describe the experiments in which you have implemented artificially fast gas exchange to remove Cdis, please identify this experiment with its number listed in Table 1.
Response not given – correct directly in manuscript
→ The experiments with artificially fast gas exchange are no longer used, so this has been removed from the manuscript.

-- p. 10, lines 14-24: Another important reference is Ito et al. (2004), GRL.
Response: The citation will be added in the updated manuscript.
→ Reference added in the manuscript in the section about preformed nutrients, where the issue of oxygen disequilibrium is mentioned.

-- Section 3.3: Do you use the same parameterisation for preformed alkalinity in all simulations? Please specify the errors in Cres in the surface field.
Response: Yes, for comparability we were using the same parametrisation. Since we are now running with pre-formed tracers (including ALKpre), this question is no longer relevant for the updated manuscript.
→ Deleted

-- p. 12, lines 17-22: Again, please specify the size of the error introduced by making this approximation.
Response: First, we want to emphasise that the dissociation constants used to determine CO2 solubility in the model (Mehrbach et al., 1973) are only defined for temperatures between 2–35 °C. Since this restriction is applied in the model, we also apply it in the calculation of Csat throughout the manuscript. To make estimates of the error caused by the restriction, we must assume that the dissociation constants are valid for all temperatures and then make a new calculation of Csat without the restriction (henceforth we call this fullCsat). This assumption inevitably makes the error estimates approximate. However, the dissociation constants determined by Goyet and Poisson (1989) for artificial seawater between -1–40°C are similar to the constants given by Mehrbach et al. (1973). Thus, the assumption that the dissociation constants are applicable for a wider range of temperatures appears to be partly valid. When we calculate fullCsat, we find that this is larger than Csat in all ensemble members, by between 0.06 and 0.6% (clarification of line 20). When use the inventories of fullCsat to calculate DfullCsat (between the SEs and PIES278), we find that the contribution by temperature changes to DTC is on average underestimated by approximately 33 +/- 36% when the temperature restriction is applied. This hence strengthens our argument in Section 5.1. that the effects of the changes in the solubility pump should not be disregarded.
The paragraph on p. 12, lines 17-22 will be rephrased as follows:
"The dissociation constants used in the cGENIE calculations of solubility for CO2 in sea water follow Mehrbach et al. (1973), which are only defined for waters between 2–35 °C. Hence, the expression for CO2 solubility in the model is restricted so that all water below 2 °C has the same CO2 solubility (similarily for all water above 35°C). In the calculations of Csat, we use CO2SYS with this temperature restriction, to accurately represent the model behaviour. In order to estimate the error introduced by this restriction, we need to assume that the same dissociation constants can be used outside the given temperature interval. The validity of this assumption is supported by the results of Goyet and Poisson (1989), who find similar dissociation constants for the interval -1–40°C in a study on artificial seawater. When CO2SYS is run using model ocean temperatures without the temperature restriction, we find that the calculated inventory of Csat in the SEs is 0.06-0.6% larger than with the restriction. For PIES278 the inventory of Csat is 0.25% larger. In terms of DCsat, the unrestricted Csat inventories indicate that the contribution by temperature changes to DTC is on average underestimated by approximately 33 +/- 36% when the restriction is active. Since the restriction is used consistently, the error caused by the restriction being present in the model should not constitute a significant problem for our analysis. Nonetheless, the underestimation

of the effect of temperature changes should be heeded in the discussion of our results."
On p. 19, line 10, after the sentence ending with "…the dominant response", we add: "Due to the temperature restriction on the CO2 solubility constants (see Section 3.4), the effect of DCsat is likely to be underestimated by on average 33 +-/36 % in our results, further emphasising its importance."
→ added to Appendix B and Discussion

* Results section: The results section is similarly very wordy; it mixes methods, results, and discussion together; many points that take multiple paragraphs to make could be simplified to 1-2 sentences. I suggest a thorough attempt to go through this paper and streamline the writing.
→ We have made thorough changes to the Results section and separated methods, results and discussion (see List of relevant changes and marked up manuscript)

* The entire top of page 13 describes how figure 2 will be put together, with only two half-sentences (regarding ensemble range of pH and pCO2atm) that describe results.
→ replaced by actual results (ranges)

-- p. 14, lines 6-7: Isn't this relationship true per definition of Csoft?
Response: The text on line 6-7 on p. 14 does not mention Csoft. We assume the referee is in fact referring to the sentence starting on p. 15, line 6-7, which mentions the linear relationship between Csoft and P*. It is true that this linear relationship results from the definitions of Csoft and P*, which is also mentioned in the next sentence, starting with "P* is a direct measure…" on p. 15, line 7.
→ Sentence partially rephrased to clarify that the linearity is expected.

* p. 14 LN 12-17 – this section does not describe any results presented.
→ moved to Methods

* p. 14 LN 27 – here and throughout this discussion, the authors indicate that horizontal diffusivity affects Csat and Cres more than Csoft, but the more obvious result is the minimal impact on deltaTC overall. This is worth noting.
Response not given – correct directly in manuscript
→ note added

* p. 15 LN 28 – "In ensemble members in which horizontal diffusivity in the ocean is changed, _Csat is larger than _Csoft." When horizontal diffusivity is reduced or increased? Specify that it is larger whether horizontal diffusivity is increased or decreased. It is near impossible from Figure 2 to discern this.
Response not given – correct directly in manuscript
→ The paragraph is re-written according to the results of the calculations using preformed tracers.

* p. 15 ln 29-37 – estimating the implications of the relationship between Csat and aveT for the glacial ocean is a point for discussion, not results
Response not given – Correct directly in manuscript
→ Moved to subsection 'Solubility pump and disequilibrium' under Discussion

-- p. 15, lines 29-31: Please describe here the importance of the temperature limit on the calculation of Csat, if this is on a comparable order of magnitude.
Response: On line 28, after sentence ending "… larger that DCsoft.", we add:
"In addition, the temperature restriction on the dissociation constants (see Section 3.4) is

likely to cause DCsat to be underestimated by on average 33 +/- 36% in our ensemble."
→ added

Lines 29-31 are moved to Section 5.3, implications for glacial studies. After the sentence ending "…were likely larger than in our set of experiments.", we add: "Fig. 7 suggests that DCsat for a change in Tavg of -2.6°C c.f. pre-industrial would be approximately 2.6 * 1e16 mol (310 GtC), whereas DCsat for the coldest of our simulations is only 1.3 * 1e16 mol (160 GtC). If we account for a likely underestimation of DCsat of 30% (see Section 3.4) in Fig. 7, a simulation as cold as the LGM state suggested by Headly and Severinghaus (2007) would have an increase in strength of the solubility pump corresponding to ~400 GtC.
→ moved and added

*p. 15 LN 18-31 – the average global temperature of simulations has a range of 2.3-4.9_C, which results in a range in delta pCO2atm from Csat of -16 – +17 ppm or -13 to +12ppm (depending upon how the calculation is made). → Suggested shortening of the paragraph by the referee.
→ The suggested shortening removes some vital information that we want to include, especially the range in Csat. Also, we want to emphasise the usefulness of the Goodwin et al. equations and would prefer to keep the specific mention of it. Therefore, we suggest the following shortened paragraph:
"Csat,T is the contribution to Csat from water temperature. Global average temperature, Tavg, of the equilibrium states has a range of 2.3–4.9 °C (see Table 3), resulting in an interval of change in Csat;T of $-0.8*10^{16}$ – $+0.6*10^{16}$ mol (Fig. 2b, Fig. 6), or -96 – +72 GtC. Note that this includes a restriction on the solubility constants which prevents solubility from increasing with temperatures below 2°C, which weakens the close-to-linear relationship between Tavg and Csat;T (Fig. 6). This corresponds to a range in pCO^2atm of about -7 – +11 ppm (Figs. 2f and S1) when we solve the carbon system equations Appendix C). The simplified equation (Eq. C9) suggested by Goodwin et al. (2011) yields results for _ pCO2 that in general are 10 – 20 % lower compared to using the carbon system equation solver (Fig. S1). Changes in Csat caused by changes in preformed alkalinity (Csat;Apre) spans $-1.9 * 10^{16}$ – $1.8*10^{16}$ (Fig. 2b), which roughly corresponds to a range in pCO^2atm of -21 – +21 ppm (Fig. 2f)."
which spans approximately 8 lines in the updated manuscript (c.f. 13 lines in the discussion paper).

-- p. 17, lines 13-14: Have you done experiments to specifically examined he role of sea ice in determining Cdis? Quantitative results would be very interesting!
Response: We have done experiments to examine the differences in Cdis between simulations in a subset of the ensemble (as described in the manuscript). There is some sea ice output available from these simulations, but we have chosen not to include a deeper analysis of this output in this already long manuscript. We have not made separate simulations where we e.g. only vary the extent of the sea ice, but this could potentially be done for a future study.
→ No change

-- p. 17, line 15: Only 0.01%? This seems to be at odds with Fig. 2.
Response: The number should be 0.1% (the model carbon inventory is approximately 3* 1e18 mol and DeltaCdis is on the order of 1e16 mol). The calculation giving the number 0.01% used the difference between runs with normal and artificially fast gas exchange, which underestimated the signal of Cdis. We thank the referee for finding this error. The estimates of Fig. 2 agree better with the calculation of Cdis = Cpre – Csat, resulting from the new runs with pre-formed tracers (see new Fig. 9).
→ Changed to 0.1%, figures replaced

-- p. 18, line 15: Changes in the solubility due to ocean temperature changes don't seem "indirect"
Response: By indirect we mean secondary, as in a response that is the result of some other change. In this case, the primary change is to pCO2atm as the result of increased biological efficiency. As a response to the lower CO2, climate changes in terms of changed ocean circulation and ocean temperature occur. There is then a secondary, or rather additional, response of the ocean carbon system to these changes.
We will rephrase the sentence as follows: "There are also additional effects on pCOatm due to changes in ocean temperature caused by changes in radiative balance, circulation and disequilibrium.
→ "indirect" replaced by "additional"

<DISCUSSION>

-- p. 19, lines 31-32: Ito and Follows (2013), GBC also uses the same scheme to look specifically at this; please include this.
Response: The citation will be added in the updated manuscript.
→ citation added and discussed

* Pg 20 LN 17 – Technically the authors have not shown the role of "AMOC strength," which refers specifically to the Atlantic overturning limb. The plots calculate the difference between northern (Atlantic) and southern source components and thus combine the roles of the northern and southern overturning strengths. Changes in the southern source might mask changes in the AMOC alone. I suggest using a different phrase here.
→ Changed to overturning circulation strength, OVT, which is defined in the new Section 3.4 (see List of relevant changes)

-- p. 20, lines 23-24: Please specify what you mean by "an LGM-like circulation" and add appropriate citations
Response: By an LGM-like circulation we mainly mean that the boundary between North Atlantic Deep Water (NADW) and Antarctic Bottom Water (AABW) was substantially shallower during the LGM than today. This circulation pattern is supported by paleonutrient tracers (reviewed by Marchitto and Broecker, 2006). This will be added to the updated manuscript.
→ added description and citation

<CONCLUSIONS>

-- p. 22, line 27: Please cite the statement that "there may have been more, not less, preformed nutrients in the deep ocean during the last glacial"
Response: The reference is Homola et al. (2015), but the reference is located in the wrong part of the sentence.
→ This study is not yet published, but has been presented at AGU by Kira Homola and discussed in personal communication with Arthur Spivack. This has been clarified in the manuscript, where the sentence has been rewritten as: "However, on-going studies indicate that there may have been more, not less, preformed nutrients in the deep ocean during the last glacial \citep[][and Spivack, A. J. (P.C., 2015)]{HomolaEtAl2015}, which implies less efficient nutrient utilisation by biology."

<APPENDIX AND FIGURES>
-- p. 24, line 6: please specify if you mean the soft tissue pump and/or the carbonate pump
Response: We mean both pumps. There are alkalinity corrections that are associated with the carbonate system as well as with the formation and destruction of organic matter (related to

the nitrogen cycle).
→ clarification added

* Figure 2 summarizes all results, but its current presentation makes it very difficult to distill anything more than the general magnitudes. I suggest (1) providing the labels of the sensitivity experiments and sorting them somehow, perhaps by the anticipated magnitude of total effects, from largest to smallest; (2) separating this figure in to 3-4 panels: biological, residual, solubility, and total (indicating on the total plot the largest contributor to the total change).
Response: We have attempted to make the figure clearer by (1) providing the labels of the sensitivity experiment (note: the acronyms in the labels have changed from the submitted manuscript, to acronyms that should be easier to remember); (2) separating the figure in to the suggested panels; and 3) by re-sorting the simulations. We have chosen to keep the results sorted in pairs of high/low adjustments of circulation parameters (denoted x2 for doubled and /2 for halved, of which the doubled are always listed on top), and made this separation into pairs clearer, in order to make it easy to see the expected range of carbon storage differences within the span of the chosen parameter values. We have changed the order so that all the SEs with changes to atmospheric parameters come first, and put wind stress (WS) on top of atmospheric heat diffusivity (AD) because the wind effect is stronger. Then come the changes to the ocean diapycnal (DD, "vertical") and isopycnal (ID, "horizontal") diffusivities. Finally come the combined simulations, also re-ordered to have the simulations with larger DeltaTC come first. Sorting them by anticipated magnitude of total effects appears to be less useful, since the values of the explored parameters do not cover the full range of extreme values that could potentially be used in climate simulations (see response to point 3). The new version of the figure is attached to this response.
→ Figure updated accordingly

-- Fig. 8: Perhaps difference sections would be more useful?
Response: We wish to also show the structure of the water mass in the different states. Hence, we suggest adding difference sections as supplementary material, showing how SE5 and SE6 deviate from PIES278.
→ Difference sections added to supplementary material (Fig. S2)

-- Fig. 9: It would be more illustrative to zoom in with the colourbar.
Response: This figure will be updated to show Cpre – Csat, which improves the estimate of Cdis and shows that the previous method (calculating the difference between runs with normal and artificially fast gas exchange) did not fully reveal Cdis. See new, updated figure, which is attached to this response. When pre-formed tracers are available, the simulations with unrealistically fast gas exchange are no longer used for the analysis.
→ Figure updated

*** Fig. 10 showing the CO2 drawdown potential as a function of a change in the mean ocean temperature does not convey any messages. There seems no relationship between the two. Plus, if my reading is correct, water temperature does not control the strength/efficiency of the biological pump in the model. Therefore, there is no reason that the CO2 drawdown potential should be correlated with ocean temperature. Why don't the authors use other metrics such as the initial preformed PO4 as an X-axis instead, as was done in Marinov et al., 2008?
Response: The referee is correct in saying there is no direct relationship between mean ocean temperature and the efficiency of the biological pump. Any relationship between the two is indirect and due to the fact that the ocean circulation affects both variables. This is what we were trying to show with this figure. However, we agree with the referee that the figure is not crucially important for the story and it will therefore be removed. The figure described by the referee, which presents CO_2 drawdown potential and initial preformed PO_4, is present in the

manuscript, but in a slightly different format. Panel c in Figure 6 shows CO_2 drawdown potential on the Y-axis and global average P* on the X-axis. $P^* = P_{reg}/P$ and $P_{pre} = P - P_{reg}$ (see Eqs. 2 and 8), so the quantities of P* and P_{pre} are closely related. We therefore think an additional figure showing CO_2 drawdown potential vs. P_{pre} would be redundant.
→ Fig. 10 removed together with the paragraph where it was discussed.

-- Figures: Please make the font size larger, particularly in Fig. 7-10
Response: This will be corrected in the updated manuscript.
→ Figures updated

-- Table 3: Please give units for DC; why not include DCcarb?
Response: The table shows correlation coefficients between circulation strength and DC, not values of DC in different ocean basins. The order of magnitude of DC could be specified in the table caption. DCcarb will be included in the updated manuscript. The first sentence of the table caption will be rephrased as follows: "Correlations between the changes in carbon species and the changes in strength of the zonal average overturning streamfunction (PSImax - PSImin) below 556 m depth in different geographical regions."
→ After further revisions, the caption is rephrased to: "Correlation coefficients of the changes in OV T (see Section 3.4), sorted by geographical regions, and the anomaly in each carbon species for the SE-ensemble (relative to PIES278)."

List of relevant changes

- Abstract
  - The abstract has been clarified to better describe the manuscript's relevance.

- Introduction
  - The introduction has been restructured and clarified to better describe the manuscript's relevance.

- Framework and general concepts:
  - The section has been significantly shortened and now lacks subsections. The concepts are briefly introduced, while most of the explanations of Sections 2.1 ('The ocean carbon pumps') and 2.3 ('Nutrient utilisation efficiency') have been moved to Appendix A, sections A1 and A2 respectively.

- Methods
  - The general model description (Section 3.1) has been clarified according to specific requests of the referees and the text that was in Section 3.1.2 ('Remineralisation scheme') has been shortened incorporated into 3.1.
  - A new Section 3.1.2 on the use of preformed tracers in the model has been added to the updated manuscript.
  - Section 3.2 has been shortened and some explanations of concepts have been moved to Appendices A2, B and B1. Concept explanations have been updated to match the methods that make use of preformed model tracers.
  - Section 3.3-3.4 on methods concerning the separation of carbon species have been moved to Appendices B3 and B2 respectively. Methods have been updated for the use of preformed model tracers, e.g. the regression model for preformed alkalinity has been removed and we no longer use runs with artificially fast gas exchange in order to capture the effects of C_{dis}.
  - A new section 3.3 'Sensitivity experiment tuning parameters' has been added, in accordance with referee requests.
  - A new section 3.4 'Overturning' has been added to introduce the metric OVT, which was not properly described in the initial manuscript.

- Results
  - All results of the carbon separation have been updated according to the new methods, which make use of preformed model tracers.
  - Ensemble members have been given names (descriptive abbreviations).
  - In the initial manuscript, the Results section mixed methods, results and discussion. We have attempted to make a clearer separation between these and move each part to where they belong. We have also made an effort to streamline the writing. The updated Results section is therefore shorter.
  - We have shifted the order of the subsections 4.1.3 and 4.1.4 to match the subsection order with the order of the carbon species as listed in Eqs. 4 and 5.
  - Fig. 10 has been removed along with the associated discussion in the final paragraph of Section 4.2.

- Discussion
  - The discussion has been re-written according to the results obtained with the updated methods using preformed model tracers.
  - A new section 5.2 'Implications of changes in OVT in relation to changes in carbon' has been added. Some of the contents were previously in the Results section, but have been moved here to get a better structure for the manuscript.

- Conclusions
  - The conclusions have been updated to better describe the manuscript's relevance
  - In order to shorten the Conclusions section, the final paragraph has been moved to Section 5.4

- Appendices
  - The old Appendix A is now Appendix C
  - Some concepts and methods described in Sections 2 and 3 have been moved to the new appendices A and B.

- References
  - Several new references have been added, some requested by referees and some that are relevant to other updates in the manuscript (Brovkin et al., 2012; DeVries and Primeau, 2009; Eggelston and Galbraith, 2017; Goodwin et al., 2015; Goyet and Poisson, 1989; Heinze et al., 1991; Ito and Follows, 2013; Klockmann et al., 2016; Marchitto and Broecker, 2006; Martin, 1990; Marzocchi and Jansen, 2017; Mehrbach et al., 1973; Munhoven, 2002; Ridgwell, 2001; Sijp et al., 2014; Sime et al., 2016; Stocker, 2014; von der Heydt and Dijkstra, 2006)
  - References that are no longer relevant for the text in the updated version of the manuscript have been removed (Aumont et al., 2016; Broecker, 1974; Zeebe and Wolf-Gladrow, 2001)

- Figures
  - Relevant figures that show carbon components have been updated with results given by the new methods using preformed model tracers
  - Font size has been increased in most figures
  - Fig. 2 has been updated (requested by referee #1), and now shows subpanels for each of the carbon components. The ensemble members have been re-ordered to give a clearer structure to the results. All other figures that list the SEs in order have been updated according to the same structure.
  - Figs. 6-8 have been re-ordered to match the new structure of the text
  - Fig. 7 (Fig. 6 in the updated manuscript) has been updated with results from non-linear calculations of $C_{sat,T}$
  - Fig. 9 has changed significantly, because the new results for C_{dis} are given by the methods using preformed model tracers instead of subtraction of runs with artificially fast gas exchange.

- Tables
  - Tables have been updated with results given by the new methods using preformed model tracers
  - Tables have been re-ordered according to the new structure of SEs given in Fig. 2
  - A new Table 2 has been added, which compares diagnostic variables of the SE ensemble to PMIP/CMIP ensembles. The table is part of the new Section 3.3 on sensitivity experiments
  - Tables 2 and 3 have been re-numbered 3 and 4 respectively.

The influence of the ocean circulation state on ocean carbon storage and CO_2 drawdown potential in an Earth system model

Malin Ödalen[1], Jonas Nycander[1], Kevin I. C. Oliver[2], Laurent Brodeau[1,3], and Andy Ridgwell[4,5]

[1]Department of Meteorology, Stockholm University, 106 91 Stockholm, Sweden
[2]National Oceanography Centre, Southampton, University of Southampton, Southampton SO14 3ZH, United Kingdom
[3]Barcelona Supercomputer Center, Barcelona, Spain
[4]School of Geographical Sciences, Bristol University, Bristol, UK
[5]Department of Earth Sciences, University of California-Riverside, Riverside, CA, USA

Correspondence to: Malin Ödalen (malin.odalen@misu.su.se)

Abstract. During the four most recent glacial cycles, atmospheric CO_2 during glacial maxima has been lowered by about 90-100 ppm with respect to interglacials. There is widespread consensus that most of this carbon was partitioned in the ocean. It is however still debated which processes were dominant in achieving this increased carbon storage. In this paper, we use an Earth system model of intermediate complexity to constrain the range in ocean carbon storage for an ensemble of ocean circulation equilibrium states. We do a set of simulations where we run the model to pre-industrial equilibrium, but where we achieve different ocean circulation by changing forcing parameters such as wind stress, ocean diffusivity and atmospheric heat diffusivity. As a consequence, the ensemble members also have different ocean carbon reservoirs, global ocean average temperatures, biological pump efficiencies and conditions for air-sea CO_2 disequilibrium. We analyse changes in total ocean carbon storage and separate it into contributions by the solubility pump, the biological pump and the CO_2 disequilibrium component. We also relate these contributions to differences in strength of ocean overturning circulation. In cases with weaker circulation, we see that the ocean's capacity for carbon storage is larger. Depending on which ocean forcing parameter that is tuned, the origin of the change in carbon storage is different. When wind stress or ocean vertical diffusivity is changed, the response of the biological pump gives the most important effect on ocean carbon storage, whereas when atmospheric heat diffusivity or ocean horizontal diffusivity is changed, the solubility pump and the disequilibrium component are also important and sometimes dominant. Finally, we do a drawdown experiment, where we investigate the capacity for increased carbon storage by maximising the efficiency of the biological pump in our ensemble members. We conclude that different initial states for an ocean model result in different capacities for ocean carbon storage, due to differences in the ocean circulation state. This could explain why it is difficult to achieve comparable responses of the ocean carbon pumps in model intercomparison studies, where the initial states vary between models. The drawdown experiment highlights the importance of the strength of the biological pump in the control state for model studies of increased biological efficiency.

The influence of the ocean circulation state on ocean carbon storage and CO_2 drawdown potential in an Earth system model

Malin Ödalen[1], Jonas Nycander[1], Kevin I. C. Oliver[2], Laurent Brodeau[1,3], and Andy Ridgwell[4,5]

[1]Department of Meteorology, Stockholm University, 106 91 Stockholm, Sweden
[2]National Oceanography Centre, Southampton, University of Southampton, Southampton SO14 3ZH, United Kingdom
[3]Barcelona Supercomputer Center, Barcelona, Spain
[4]School of Geographical Sciences, Bristol University, Bristol, UK
[5]Department of Earth Sciences, University of California-Riverside, Riverside, CA, USA

Correspondence to: Malin Ödalen (malin.odalen@misu.su.se)

Abstract. During the four most recent glacial cycles, atmospheric CO_2 during glacial maxima has been lowered by about 90-100 ppm with respect to interglacials. There is widespread consensus that most of this carbon was partitioned in the ocean. It is however still debated which processes were dominant in achieving this increased carbon storage. In this paper, we use an Earth system model of intermediate complexity to explore the sensitivity of ocean carbon storage to ocean circulation state. We carry out a set of simulations where we run the model to pre-industrial equilibrium, but where we achieve different states of ocean circulation by changing forcing parameters such as wind stress, ocean diffusivity and atmospheric heat diffusivity. As a consequence, the ensemble members also have different ocean carbon reservoirs, global ocean average temperatures, biological pump efficiencies and conditions for air-sea CO_2 disequilibrium. We analyse changes in total ocean carbon storage and separate it into contributions by the solubility pump, the biological pump and the CO_2 disequilibrium component. We also relate these contributions to differences in strength of ocean overturning circulation. Depending on which ocean forcing parameter that is tuned, the origin of the change in carbon storage is different. When wind stress or ocean diapycnal diffusivity is changed, the response of the biological pump gives the most important effect on ocean carbon storage, whereas when atmospheric heat diffusivity or ocean isopycnal diffusivity is changed, the solubility pump and the disequilibrium component are also important and sometimes dominant. Despite this complexity, we obtain a negative linear relationship between total ocean carbon and the combined strength of the northern and southern overturning cells. This relationship is robust to different reservoirs dominating the response to different forcing mechanisms. Finally, we do a drawdown experiment, where we investigate the capacity for increased carbon storage by maximising the efficiency of the biological pump in our ensemble members. We conclude that different initial states for an ocean model result in different capacities for ocean carbon storage, due to differences in the ocean circulation state and the origin of the carbon in the initial ocean carbon reservoir. This could explain why it is difficult to achieve comparable responses of the ocean carbon pumps in model inter-comparison studies, where the initial states vary between models. We show that this effect of the initial state is quantifiable. The drawdown experiment highlights the importance of the strength of the biological pump in the control state for model studies of increased biological efficiency.

1 Introduction

When going from and interglacial toward a glacial maximum, atmospheric CO_2 is significantly lowered. During the last four glacial cycles (since ∼400000 years B.P.), the decrease has been about 1/3 and atmospheric pCO_2 at these glacial maxima (marine isotope stages 2, 6, 8 and 10) was approximately 180 ppm (see e.g. Petit et al. (1999); Lüthi et al. (2008) and references therein). The ocean's capacity for storing carbon is many times larger than its atmospheric and terrestrial (biosphere) counterparts. CO_2 reacts with water to form bicarbonate and carbonate ions, and because of this, a lot more CO_2 than expected (compared to e.g. O_2) is dissolved before chemical equilibrium is achieved. This leads to the ocean holding 50 times more carbon than the atmosphere (Williams and Follows, 2011; Falkowski et al., 2000) and over 13 times that of the terrestrial biosphere (Falkowski et al., 2000; IPCC, 2007). Due to this big difference in size between the carbon reservoirs, it is highly likely that most of the CO_2 that was taken out of the atmosphere during glacials was partitioned in the deep ocean rather than in the terrestrial biosphere (Kohfeld and Ridgwell, 2009).

That the oceanic carbon storage increased during glacials is a well established idea, and there are numerous studies of how and why this happened (e.g., Broecker, 1982; Sarmiento and Toggweiler, 1984; Archer et al., 2000a; Sigman and Boyle, 2000; Brovkin et al., 2007; Hain et al., 2010; Sigman et al., 2010). However, the relative effects of different processes contributing to this oceanic uptake have not yet been well constrained and, so far, there is a lack of consensus on which processes that were dominant (reviewed in Kohfeld and Ridgwell (2009)). Understanding these relative effects of oceanic CO_2 uptake mechanisms can also be important in other climate scenarios than glacial simulations.

To understand the oceanic uptake of CO_2 and the different processes involved, it is helpful to think about the different pathways that exist for carbon that is taken up in the surface layer to reach the deep ocean. These pathways are often referred to as the solubility pump and the biological pump (further described in Section 2.1). In this work, we focus on better constraining; 1) the effects of changes in global ocean mean temperature on the abiotic ocean-atmosphere CO_2 equilibrium and hence on the solubility pump; 2) the effect of changed CO_2 disequilibrium; and 3) the effects of increased efficiency of the biological pump. By performing ensemble runs using the Earth system model cGENIE (Ridgwell et al., 2007; Cao et al., 2009), we examine the changes in the carbon system that result from changes in ocean circulation.

Changes in ocean circulation, which can be due to climate change or other, independent physical processes (e.g. changes in bathymetry), will lead to changes in global ocean mean temperature, through e.g. redistribution and changes in formation rates of water masses. Firstly, if surface ocean temperature changes, this will have a direct effect on CO_2 solubility and hence on the atmosphere-ocean CO_2 equilibrium. Secondly, if the temperature, and thus the concentration of dissolved CO_2, in the deepwater formation areas changes, this will impact on the deep-ocean concentration of CO_2 (Goodwin et al., 2011). Ocean circulation changes will also affect the ocean carbon content by influencing nutrient distributions, biological efficiency and time scales for outgassing of CO_2 in upwelling areas.

Model studies of glacial climate generally start from pre-industrial atmospheric CO_2, that is prescribed, while the circulation model is tuned in order to achieve the target ocean fields of tracers such as salinity, temperature, and dissolved chemical compounds. However, the desired tracer fields can be achieved through multiple different combinations of the tuning parameters,

1 Introduction

The transition from interglacials to glacial maximums is associated by a substantial reduction in atmospheric CO_2 (henceforth, pCO_2^{atm}). During the last four glacial cycles (since ∼400,000 years B.P.), the decrease has been about 1/3 and atmospheric pCO_2 at these glacial maxima (marine isotope stages 2, 6, 8 and 10) was approximately 180 ppm (see e.g., Petit et al., 1999; Lüthi et al., 2008, and references therein). When CO_2 dissolves in water, most of the molecules react with the water to form bicarbonate and carbonate ions. To achieve equilibrium between the atmospheric and surface ocean partial pressures of CO_2, further dissolution is then required (c.f. e.g. O_2, which does not react with water). As a consequence, the ocean holds 50 times more carbon than the atmosphere (Williams and Follows, 2011; Falkowski et al., 2000) and over 13 times that of the terrestrial biosphere (Falkowski et al., 2000; IPCC, 2007). Due to this size difference between the carbon reservoirs, a larger fraction of the CO_2 that was missing from the atmosphere during glacials is likely to have been stored in the deep ocean than in the terrestrial biosphere (Kohfeld and Ridgwell, 2009).

That the oceanic carbon storage increased during glacials is a well established idea, and there are numerous studies of how and why this may have happened (e.g., Broecker, 1982; Sarmiento and Toggweiler, 1984; Archer et al., 2000a; Sigman and Boyle, 2000; Brovkin et al., 2007; Hain et al., 2010; Sigman et al., 2010). However, the relative effects of different processes contributing to this oceanic uptake have not yet been well constrained and, so far, there is a lack of consensus on which processes that were dominant (reviewed in Kohfeld and Ridgwell, 2009).

To understand the controls on oceanic storage of CO_2 and the different processes involved, it is helpful to think about the different pathways that exist for carbon that is taken up in the surface layer to reach the deep ocean. These pathways are often referred to as the solubility pump and the biological pump (further described in Section 2). In this work, we focus on better constraining: 1) the effects of changes in global ocean mean temperature on the abiotic ocean-atmosphere CO_2 equilibrium and hence on the solubility pump; 2) the effect of changed CO_2 disequilibrium; and 3) the effects of increased efficiency of the biological pump. By performing ensemble runs using the Earth system model cGENIE (Ridgwell et al., 2007; Cao et al., 2009), we examine the changes in the carbon system that result from changes in ocean circulation.

Changes in ocean circulation, which can be due to climate change or other independent physical processes (e.g. tectonic and ocean gateway changes, such as the opening of the Drake Passage, (e.g., von der Heydt and Dijkstra, 2006; Sijp et al., 2014)), will lead to changes in global ocean mean temperature, through e.g. changes in the locus and strength of deep water formation. Firstly, if surface ocean temperature changes, this will have a direct effect on CO_2 solubility and hence on the atmosphere-ocean CO_2 equilibrium. Secondly, if the temperature, and thus the concentration of dissolved CO_2, in the deepwater formation areas changes, this will impact on the deep-ocean concentration of CO_2 (Goodwin et al., 2011). Ocean circulation changes will also affect the ocean carbon content by influencing nutrient distributions, biological efficiency and time scales for outgassing of CO_2 in upwelling areas.

When studying glacial ocean CO_2 uptake, the most common modelling approach is to aim at reproducing a glacial climate by adjusting physical parameters, such as orbital parameters, pCO_2^{atm}, bathymetry, sea level, topography and/or ice sheets (e.g., Ganopolski et al., 2010; PMIP3), in ways that they may have changed during glacials. These changes influence the ocean

which means similar tracer fields can be achieved in different model states despite differences in their circulation. With this study, we aim to investigate the consequences of the circulation differences that result from this tuning: are there other aspects of the climate system, such as the strengths of the ocean carbon pumps, that become so significantly different that they can be crucial for the outcome of e.g. model intercomparison studies? As discussed in Zhang et al. (2013), overturning circulation differences in the initial glacial state can cause differences in results in model intercomparison studies of deglacial CO_2 rise.

Specifically, we aim to clarify how the ocean carbon storage, and in particular the CO_2 drawdown potential (DP, see Section 2.3, Eq. (3)), of a model depends on its equilibrium state. This will provide insight about why it is difficult to compare results from different model studies that have attempted to simulate and explain the lowering of atmospheric pCO_2 (henceforth, pCO_2^{atm}). One example of a model study where this dependence on the initial state may have been key is Archer et al. (2000b). They investigated the abiotic chemical equilibrium in a few different models and showed that there was a consistent difference between box models and general circulation models (GCMs). They attributed this to differences in complexity. However, they also found a significant difference in behaviour between different GCMs, which they were unable to explain. We hypothesize, and show, that such differences could instead be due to differences in the initial state, where differences in circulation are causing the strengths of the carbon pumps, and thus model carbon inventories, to be different.

When studying glacial ocean CO_2 uptake, the most common modelling approach is to aim at reproducing a glacial climate by adjusting physical parameters, such as orbital parameters, pCO_2^{atm}, bathymetry, sea level, topography and/or ice sheets (e.g., Ganopolski et al., 2010; PMIP3), in ways that they may have changed during glacials. These, in turn influence the ocean circulation by affecting e.g. climate (temperature), tidal dissipation (Schmittner et al., 2015) and wind stress (Sime et al., 2013). In the first step of this modelling study, we instead do a process study where we change physical parameters in the model, one or two at a time, while restoring pCO_2^{atm} to the pre-industrial value. The parameters we change are common tuning parameters in climate models, such as wind stress intensity and ocean diffusivity. This approach allows us to see how the ocean circulation changes that follow from tuning each of these parameters affect the ocean carbon storage. We are particularly interested in the relative importance of the changes in the solubility pump, the biological pump and in CO_2 disequilibrium.

Through the first step of the modelling, we will show that the effect of changes in ocean circulation on global ocean mean temperature, and thus on the solubility pump, is significant and in some cases of similar importance as the effect on the biological pump. This first step will also allow us to discuss how specific changes to circulation parameters will influence the total carbon uptake in model simulations of e.g. glacial scenarios. In particular, we will focus on the influence of the strength of the global and basin scale overturning circulation.

In the second step, we enforce 100 % nutrient utilisation efficiency (see Section 2.3) in the different circulation patterns of the ensemble. This allows us to measure the difference in drawdown potential for CO_2 between different ocean circulation states. A new equilibrium in CO_2 between atmosphere and ocean will be established, and thus also pCO_2^{atm}, will be different depending on the ocean circulation. This will illustrate how the initial state of a model can be important for the outcome of a glacial CO_2 drawdown experiment and highlight the importance of differences in the initial states of models in intercomparison studies. Our theoretical approach is similar to those taken by Marinov et al. (2008a, b); Kwon et al. (2011). However, these studies all focus mainly on the contributions to ocean dissolved inorganic carbon (DIC) by the biological pump. In this study,

circulation by affecting e.g. climate (temperature), tidal dissipation (Schmittner et al., 2015) and wind stress (Sime et al., 2013). Model studies of glacial climate are generally based on a pre-industrial control state, where pCO_2^{atm} is prescribed, while the circulation model is tuned in order to achieve the target ocean fields of tracers such as salinity, temperature, and dissolved chemical compounds (e.g. Heinze et al., 1991; Brovkin et al., 2007; PMIP3). However, the desired tracer fields can be achieved through multiple different combinations of the tuning parameters, which means that similar tracer fields can be achieved in different model states despite differences in their circulation. In this study, we aim to investigate the consequences of the initial state circulation differences that result from this tuning: are there other aspects of the climate system, such as the strengths of the ocean carbon pumps, that become so significantly different that they can be crucial for the outcome of e.g. model inter-comparison studies of glacial CO_2 drawdown? As discussed in Zhang et al. (2013), overturning circulation differences in an initial glacial state could similarily cause differences in results in model inter-comparison studies of deglacial CO_2 rise.

Specifically, we aim to clarify how the initial equilibrium state, not only in terms of ocean circulation, but in terms of ocean carbon inventory and the origin of the already stored carbon (e.g. biological or solubility pump), is crucial for the outcome of a study investigating increased efficiency of the biological pump. This will provide insight about why it is difficult to compare results from different model studies that have attempted to simulate and explain the glacial lowering of pCO_2^{atm}. One example of a model study where this dependence on the initial state may have been key is Archer et al. (2000b). They investigated the abiotic chemical equilibrium in a few different models and showed that there was a consistent difference between box models and general circulation models (GCMs). They attributed this to differences in complexity, although Ridgwell (2001) found that the box vs. GCM differences could be explained by inappropriately low ocean surface temperature assumptions in the original box model descriptions. However,Archer et al. (2000b) also found a significant difference in behaviour between different GCMs, which they were unable to explain. We show that such differences could instead be due to differences in the initial state, where differences in circulation are causing the strengths of the carbon pumps, and thus model carbon inventories, to be different. More importantly, we highlight that this effect of the initial state is quantifiable.

In this study, we do not attempt to reproduce glacial climate. In the first step of the modelling, we instead carry out a process study where we change physical parameters in the model, one or two at a time, while restoring pCO_2^{atm} to the pre-industrial value. The parameters we change are common tuning parameters in climate models, such as wind stress intensity and ocean diffusivity. This approach allows us to see how the ocean circulation changes that follow from tuning each of these parameters affect the ocean carbon storage. We are particularly interested in the relative importance of the changes in the solubility pump, the biological pump and the CO_2 disequilibrium. Through the first step, we will show that the effect of changes in ocean circulation on global ocean mean temperature, and thus on the solubility pump, is non-negligible and in some cases of similar importance as the effect on the biological pump. We will also show that the relative contributions by the biological pump, the solubility pump and by CO_2 disequilibrium to the ocean carbon inventory in the initial equilibrium state depends on the model tuning strategy, yet these combine in a manner to give a response in total carbon that is more straightforwardly related to the circulation than any of the individual components. This first step will also allow us to discuss how specific changes to circulation parameters will influence the total carbon uptake in model simulations of e.g. glacial scenarios. In particular, we will focus on the influence of the strength of the global and basin scale overturning circulation.

we give equal attention to the perspective of the solubility pump and disequilibrium contributions to the total ocean carbon storage in a similar set of simulations.

Some general concepts and the framework we have used are introduced in Section 2. Theory and methods are described in Section 3. We then present the model ensemble output in Section 4. These results are discussed and put into perspective in Section 5.

2 Framework and general concepts

2.1 The carbon pumps

CO_2 that is dissolved in the ocean surface layer is often described as being able to reach the deep ocean via two pathways – the solubility pump and the biological pump. These pathways are thouroughly described in Volk and Hoffert (1985) and later in Williams and Follows (2011).

The abiotic (non-biological), physical patwhay, or *the solubility pump*, begins with air-sea gas exchange, which acts to achieve a chemical equilibrium between the atmosphere and the surface ocean. This equilibrium depends on temperature. Colder surface water can dissolve more CO_2 which can then be transported (or pumped) down into the deep ocean with the ocean circulation. This carbon is also referred to as *preformed* carbon. Due to the fact that deep water forms in cold regions, the sinking water is enriched in carbon compared to surface waters in warmer regions. Since this cold water fills up the deep ocean everywhere, there will be a close link between the global ocean averages of temperature and preformed carbon.

The biological pathway, or *the biological pump*, begins with biological production in the surface ocean. Carbon is incorporated into soft-tissue organic compounds. Some of this material then reaches the deep ocean, either by being advected in currents or by simply falling out of the surface layer. When the organic material is decomposed, inorganic carbon (CO_2) comes back into dissolution in the water. This fraction of DIC is referred to as *regenerated* carbon. Carbon is also incorporated into hard-tissue (shells) in the form of $CaCO_3$ which can be dissolved in the deep ocean. This dissolution influences deep ocean alkalinity (Section 2.2).

Due to the difference in the chemical role of soft-tissue and hard tissue carbon, the biological pump is more correctly referred to as being two separate pumps; the soft-tissue pump and the carbonate (hard-tissue) pump. The soft-tissue pump acts to increase deep ocean DIC, whereas the hard-tissue pump has a counter effect (Section 2.2), but net effect of the biological pump is to enhance the deep ocean concentration of DIC.

In the massive ocean carbon reservoir, about 90 % is expected to be preformed carbon and the remaining 10 % organic or regenerated carbon. (Williams and Follows, 2011). If the capacity of one or all of the carbon pumps to redistribute carbon from the surface to the deep ocean increased, this would act to decrease pCO_2^{atm}.

In the second step, we enforce 100 % nutrient utilisation efficiency (see Section 2) in the different circulation patterns of the ensemble. This allows us to measure the difference in drawdown potential for CO_2 between different ocean circulation states. A new equilibrium in CO_2 between atmosphere and ocean will be established, and thus also pCO_2^{atm}, will be different depending on the ocean circulation. This will illustrate how the initial state of a model can be important for the outcome of a glacial CO_2 drawdown experiment and highlight the importance of differences in the initial states of models in inter-comparison studies. The effect of the solubility pump on pCO_2^{atm} has previously been studied by e.g. DeVries and Primeau (2009). The effect of air-sea disequilibrium of CO_2 and its connection with biological carbon sequestration was studied by Ito and Follows (2013) and in recent work by Eggleston and Galbraith (2017) (in review). Our theoretical approach is similar to those taken by Marinov et al. (2008a), Marinov et al. (2008b) and Kwon et al. (2011). However, these studies all focus mainly on the contributions to ocean dissolved inorganic carbon (DIC) by the biological pump. In this study, we aim to determine a robust relationship between a model's initial-state and its drawdown potential that accounts for the biological pump, the solubility pump and disequilibrium contributions. Such a relationship, if it is sufficiently simple, will be useful in assessing the effect of model biases on the sensitivity of the carbon cycle to climate perturbations.

2 Framework and general concepts

CO_2 that is dissolved in the ocean surface layer is often described as being able to reach the deep ocean via two pathways – the solubility pump and the biological pump. These pathways are thouroughly described in Volk and Hoffert (1985) and later in Williams and Follows (2011). More details are given in Appendix A1. Our separation of DIC into its different sources of origin (see Section 3.2), which is related to the two carbon pumps, will largely follow the framework of Ito and Follows (2005). This framework has been widely applied (e.g., Williams and Follows, 2011; Marinov et al., 2008b; Kwon et al., 2011; Lauderdale et al., 2013).

Of the total ocean carbon reservoir, about 90 % is expected to be preformed carbon, i.e. from the solubility pump, and the remaining 10 % organic or regenerated carbon, i.e. from the biological pump (Williams and Follows, 2011). If the net capacity of the carbon pumps increased, this would act to decrease pCO_2^{atm}. For instance, increased efficiency of the biological pump is a frequently proposed explanation for the glacial CO_2 drawdown (e.g. Sarmiento and Toggweiler, 1984; Martin, 1990; Sigman and Boyle, 2000). By "increased efficiency" we mean that more of the available nutrients in the surface layer are used for biological production before the water is subducted into the deep ocean. When the nutrient utilisation efficiency (NUE) is increased, the biological pump gets stronger and transfers more carbon to the deep ocean. As a result, the air-sea equilibrium of CO_2 is shifted and more CO_2 is drawn from the atmosphere into the surface layer of the ocean, reducing pCO_2^{atm}.

As described in the framework of Ito and Follows (2005), NUE can be described in terms of the parameter $\overline{P^*}$, which is the global average ratio of regenerated to total nutrients in the deep ocean (see Appendix A2). In Earth system models, how much CO_2 that can be removed from the atmosphere by increasing the NUE depends on $\overline{P^*}$, which can differ between models and between different climate states achieved in the same model (Marinov et al., 2008b). The difference between pCO_2^{atm} in the

2.2 Alkalinity

An important player in the oceanic carbon cycle is alkalinity. It describes the buffer capacity of the ocean; hence, the ocean's capacity to resist a change in pH despite the addition of an acid, such as CO_2. Sea water total alkalinity is the number of moles of H^+ equivalent to the excess of proton accepting ions (bases), mainly CO_3^{2-} and $HCO3^-$, over proton donors (acids). If there is an excess of proton acceptors, the addition of an acid to the sea water will only weakly affect the pH (Zeebe and Wolf-Gladrow, 2001). The main external source of alkalinity to the ocean is weathering of carbonates on land and the main sinks are precipitation of $CaCO_3$ by marine organisms, such as microorganisms and reef building corals, and burial of these carbonates in both shallow and deep sea sediments (Sarmiento and Gruber, 2006).

Biological production affects the vertical distribution of ocean alkalinity, due to the hard-tissue pump. In the surface ocean, some microorganisms such as coccolithophores and foraminifera surround their cells with a shell consisting of $CaCO_3$. Since CO_3^{2-} is one of the H^+-accepting ions that contribute to ocean alkalinity, the formation of shells will decrease the alkalinity of the surface ocean. This leads to a reduction of the surface ocean capacity to dissolve CO_2. Hence, this will act to increase pCO_2^{atm}. Due to this, the hard-tissue pump is sometimes called the 'carbonate counter pump' (Kohfeld and Ridgwell, 2009).

When the shells are exported to the deep ocean and dissolved, alkalinity is returned to solution. Hence, some of the alkalinity in the deep ocean is of biological, or regenerated, origin. This part of the alkalinity, we will denote A_{reg}. The rest of the alkalinity in the deep ocean was set at the surface and then brought into the deep ocean by the circulation; this is preformed alkalinity, A_{pre}. Unlike CO_2, A_{pre} does not have a typical, expected value, set by processes in the surface ocean. However, sea surface salinity and oxygen concentration are correlated with surface alkalinity and can therefore be used to estimate A_{pre} (see section 3.3).

Total alkalinity, A_T, is

$$A_T = A_{pre} + A_{reg} \quad (1)$$

This partitioning of alkalinity will be useful for understanding the relative importance of the hard-tissue biological pump in oceanic carbon storage.

It is likely that ocean alkalinity increased during glacials due to ice formation and associated sinking sea levels, causing e.g. more weathering of carbonates. This may have contributed to the substantial drawdown of CO_2 into the ocean that happened during glacials (see e.g. Sigman and Boyle (2000) and references therein).

In order to model the effect of alkalinity changes on pCO_2^{atm}, we would need an open ocean-atmosphere system with river supply and sedimentation of alkalinity. This would require a different type of modelling than we do here and our analysis is restricted to the ocean-atmosphere system, excluding sediment feedbacks.

2.3 Nutrient utilisation efficiency

Increased efficiency of the biological pump is a frequently proposed explanation for the glacial CO_2 drawdown (eg. Sarmiento and Toggweiler (1984); Sigman and Boyle (2000). By "increased efficiency" we mean that more of the available nutrients in

initial equilibirum state, pCO_2^{eq}, and the lowest pCO_2^{atm} that can be achieved by increased NUE, pCO_2^{min} (achieved when $\overline{P^*} = 1$), will be referred to as the CO_2 *drawdown potential* of a model, DP:

$$DP = pCO_2^{eq} - pCO_2^{min} \quad (1)$$

When the biological pump is working at maximum efficiency (when $\overline{P^*} = 1$), we can assume that a specific amount of carbon proportional to the total amount of nutrients in the ocean will be trapped in the deep ocean at all times, assuming fixed stoichiometric ratios (see Section 3.1.1). This carbon will not participate in the chemical equilibrium between atmosphere and ocean which decides the pCO_2^{atm}.

An important component of the oceanic carbon cycle is alkalinity. It is related to the buffer capacity of the ocean; hence, the ocean's capacity to resist a change in pH despite the addition of an acid, such as CO_2. Biological production affects the vertical distribution of ocean alkalinity through the hard-tissue pump. When the $CaCO_3$ shells of micro-organisms are exported to the deep ocean and dissolved, alkalinity is returned to solution. Hence, some of the alkalinity in the deep ocean is of biological, or regenerated, origin. This part of the alkalinity, we will denote A_{reg}. The rest of the alkalinity in the deep ocean was set at the surface and then brought into the deep ocean by the circulation; this is preformed alkalinity, A_{pre}. Total alkalinity, A_T, is

$$A_T = A_{pre} + A_{reg} \quad (2)$$

This partitioning of alkalinity will be useful for understanding the relative importance of the hard-tissue biological pump in oceanic carbon storage.

It is likely that ocean alkalinity increased during glacials due to more weathering of carbonates caused by lower sea levels (e.g., Munhoven, 2002; Brovkin et al., 2012). This may have contributed to the substantial drawdown of CO_2 into the ocean that happened during glacials (see e.g. Sigman and Boyle, 2000, and references therein). In order to model the effect of alkalinity changes on pCO_2^{atm}, we would need an open ocean-atmosphere system with river supply and sedimentation of alkalinity. This would require a different type of modelling than we do here. Our analysis is restricted to the ocean-atmosphere system, excluding sediment feedbacks. A_T thus has no external sources/sinks and is only affected by the biological pump.

3 Methods

3.1 Model

We use the model cGENIE, an Earth System Model of Intermediate Complexity (EMIC), which is a computationally efficient model developed for studying the ocean carbon cycle on timescales of 100–100,000 years. cGENIE is higher in complexity than box models, but is still efficient enough to allow running a large ensemble to equilibrium for the carbon system. In terms of ocean carbon system tracers, the minimum required for this type of study is P, DIC, O_2 and A_T. cGENIE includes many additional tracers, out of which only some are used in this study. For example, particulate (POC) and dissolved organic carbon

the surface layer are used for biological production before the water is subducted into the deep ocean. The remaining, unused, nutrients are brought with the circulation into the deep ocean, where no new production is possible. In the same way as carbon and alkalinity, the inorganic nutrients in the deep ocean can be separated into a preformed and a regenerated contribution; preformed nutrients are the unused nutrients subducted during deepwater formation (the physical pathway), whereas regenerated nutrients have been transported to the deep via the biological pump (Ito and Follows, 2005).

When the nutrient utilisation efficiency is increased, the concentration of preformed nutrients, P_{pre}, decreases and the concentration of regenerated nutrients, P_{reg}, increases. This means that the biological pump gets stronger and transfers more carbon to the deep ocean. The air-sea equilibrium of CO_2 is shifted and more CO_2 is drawn from the atmosphere into the surface layer of the ocean, reducing pCO_2^{atm}.

As described in the framework introduced by Ito and Follows (2005), the global average of P_{reg} relative to the overall global average concentration of inorganic nutrients (denoted by P) is a measure of nutrient utilisation efficiency. This can be described using the parameter P^*,

$$\overline{P^*} = \frac{\overline{P_{reg}}}{\overline{P}}. \quad (2)$$

Here, the overbars mark that we are using the global average of a quantity. If $\overline{P^*}$ is 1, all available nutrients in the deep ocean were brought there by the biological pump. In other words, the deep ocean is ventilated by surface waters that have had all nutrients removed, hence (at steady state,) the ocean interior will have no preformed nutrients.

In Earth system models, how much CO_2 that can be removed from the atmosphere by increasing the nutrient utilisation efficiency depends on $\overline{P^*}$, which can differ between models and between different climate states achieved in the same model (Marinov et al., 2008b). The difference between pCO_2^{atm} in the initial equilibirum state, pCO_2^{eq}, and the lowest pCO_2^{atm} that can be achieved by increased nutrient utilisation efficiency, pCO_2^{min} (achieved when $\overline{P^*} = 1$), will be referred to as the CO_2 *drawdown potential* of a model, DP:

$$DP = pCO_2^{eq} - pCO_2^{min} \quad (3)$$

When the biological pump is working at maximum efficiency (when $\overline{P^*} = 1$), we can assume that a specific amount of carbon proportional to the total amount of nutrients in the ocean will be trapped in the deep ocean at all times, assuming fixed stoichiometric ratios (see Section 3.1.1). This carbon will not participate in the chemical equilibrium between atmosphere and ocean which decides the pCO_2^{atm}.

3 Methods

3.1 Model

We use the model cGENIE, an Earth System Model of Intermediate Complexity (EMIC), which is a computationally efficient model developed for studying the ocean carbon cycle on timescales of $\sim 100 - 100{,}000$ years. cGENIE is higher in complexity than box models, but is still efficient enough to allow running a large ensemble to equilibrium for the carbon system, and has a level of detail for the carbon system that made it particularly suitable for this study. Model characteristics are described in Edwards and Marsh (2005) and Ridgwell et al. (2007).

The physical ocean is modeled using a frictional-geostrophic 3D model on a 36x36 equal area grid in the horizontal and 16 depth levels. The atmospheric model is an Energy Moisture Balance Model (EMBM) with prescribed, climatological wind-fields. Ocean biogeochemistry and atmospheric chemistry are treated by separate modules that are coupled to the physical models and to each other. The biogeochemical module is based on a phosphate-only nutrient scheme. Hence, phosphate (P) is the limiting nutrient. The nitrogen (N) cycle is not modelled, but the effect of N on alkalinity during production and remineralisation of organic matter is represented. In those cases, N is assumed to have a fixed stoichiometric relationship with P (see Section 3.1.1).

As our control state, we use the pre-industrial equilibrium state described in Cao et al. (2009). During the spin-up (10,000 years) to this equilibrium state, pCO_2^{atm} is restored to 278 μatm ($\approx$ 278 ppm), while the inventory of carbon in the model is allowed to change. Henceforth, this pre-industrial equilibrium state will be referred to as $PIES278$.

3.1.1 Stoichiometry

The stoichimoetric relationships in cGENIE is based on Redfield (1963). As such, there is, on average, a fixed relationship between the number of moles of the elements that are taken up (or released) in organic processes in the ocean. This relationship is $N : P : C : O_2 = 16 : 1 : 106 : -138$; for each 1 mole of P used in biological production, 16 moles of N and 106 moles of C are also used, but 138 moles of O_2 are released. The same relationship applies to the decomposition of organic material, which releases N, P and C, but consumes O_2. Any stoichiometric ratio involving oxygen is negative, e.g. the ratio between C and O_2 is $R_{C:O_2} = 106/-138 \approx -0.768$.

Adjustments to the stoichiometric ratios given in Redfield (1963) have been proposed by e.g. Takahashi et al. (1985) and Anderson and Sarmiento (1994), but the classic Redfield ratios are still widely accepted and used. The choice of constants is not crucial for the outcome of the study, and we have hence stayed with the default model setup of the official release of cGENIE.

More recently, the stoichiometry of production of new organic material has been shown to be highly variable, between species but also within the same species while living under different conditions, such as nutrient availability (e.g., Quere et al., 2005; Galbraith and Martiny, 2015). While this does not contradict that the ratios are on average similar to the results by Redfield (1963), this *in-situ* variability in stoichiometric ratios could potentially be important in a glacial scenario. However, evaluating the influence of such variability is beyond the scope of the present study.

(DOC) are included in the calculations of model carbon inventory (see Appendix B). Of particular importance for this study is the possibility to run with preformed tracers ($P_{pre}, C_{pre}, O_{2_{pre}}, A_{pre}$, see Section 3.1.2). Model characteristics are described in Edwards and Marsh (2005); Ridgwell et al. (2007) and Cao et al. (2009).

The physical ocean is modeled using a frictional-geostrophic 3D model on a 36x36 equal area grid in the horizontal and 16 depth levels. The atmospheric model is an Energy Moisture Balance Model (EMBM) with prescribed, climatological wind-fields (Cao et al., 2009). Ocean biogeochemistry and atmospheric chemistry are treated by separate modules that are coupled to the physical models and to each other (Ridgwell et al., 2007). The biogeochemical module is based on a phosphate-only nutrient scheme. Hence, phosphate (P) is the limiting nutrient. The model description of export flux of organic matter is based on available surface nutrients (see Ridgwell et al., 2007, Eqs. 1-4), and instead of having a "standing plankton biomass" in the model, the export of particulate organic matter is derived directly from uptake of P. Remineralisation in cGENIE primarily depends on oxygen availability (Ridgwell et al., 2007). POC is modelled as two fractions: one more easily degradable (labile) fraction, which undergoes an exponential decay with depth, and one fraction that is more resistant to degradation, which remineralises at the ocean floor. In the drawdown experiment (Section 3.2), the length scale of the exponential decay is adjusted. The remineralisation of $CaCO_3$ in the water column is treated in a similar manner to POC. The carbonate precipitation rate is thermodynamically-based and relates export flux of $CaCO_3$ to the flux of POC (see Ridgwell et al., 2007, Eq. 8). As investigation of carbonate system feedbacks are not the purpose of this study, interactive sediments are not used, and in terms of carbon cycling, the atmosphere-ocean is studied as a closed system.

As our control state, we use the pre-industrial equilibrium state described in Cao et al. (2009). During the spin-up (10,000 years) to this equilibrium state, pCO_2^{atm} is restored to 278 μatm ($\approx$ 278 ppm), while the inventory of carbon in the model is allowed to change. Henceforth, this pre-industrial equilibrium state will be referred to as $PIES278$.

3.1.1 Stoichiometry

The stoichimoetric relationships in cGENIE is based on Redfield (1963). Thus, when organic material is formed, the elements are taken up in the proportions $N : P : C : O_2 = 16 : 1 : 106 : -138$. For example, 138 moles of O_2 are released for every mole of phosphorus that is taken up. The same relationship applies to the decomposition of organic material, which releases N, P and C, but consumes O_2. The nitrogen (N) cycle is not modelled, but the effect of N on alkalinity during production and remineralisation of organic matter is represented, based on the fixed stoichiometric relationship with P. Adjustments to the stoichiometric ratios given in Redfield (1963) have been proposed by e.g. Takahashi et al. (1985) and Anderson and Sarmiento (1994), but the classic Redfield ratios are still widely accepted and used. The choice of constants is not crucial for the outcome of the study, and we have hence stayed with the default model setup of the official release of cGENIE.

More recently, the stoichiometry of production of new organic material has been shown to be highly variable, between species but also within the same species while living under different conditions, such as nutrient availability (e.g., Quere et al., 2005; Galbraith and Martiny, 2015). While this does not contradict that the ratios are on average similar to the results by Redfield (1963), this *in-situ* variability in stoichiometric ratios could potentially be important in a glacial scenario. However, evaluating the influence of such variability is beyond the scope of the present study.

3.1.2 Remineralisation scheme

Remineralisation in cGENIE primarily depends on oxygen availability, but if O_2 is depleted and NO_3 is selected as an active tracer, denitrification will allow for remineralisation to continue. When NO_3 is depleted, sulphate reduction can also occur if SO_4^{2-} is an active tracer. When supply of oxidants is exhausted, remineralisation is inhibited.

In cGENIE, POC is modelled as two fractions: one more easily degradable (labile) fraction and one fraction that is more resistant to degradation. In terms of remineralisation, this means the labile fraction undergoes an exponential decay with depth, whereas the other fraction is remineralised at the ocean floor. The remineralisation scheme is described in detail in Ridgwell et al. (2007).

To further improve the representation of carbon fluxes to the deep ocean, a more explicit approach with several different types of particulate organic matter with different reactivity can be used (Aumont et al., 2016).

3.2 Theory and experimental setup

The inventory of total carbon, TC [mol], in the equilibrium state can be described by

$$TC = M_a\, pCO_2^{atm} + M_o(\overline{C_{sat}} + \overline{C_{soft}} + \overline{C_{carb}} + \overline{C_{res}}) \quad (4)$$

Equation (4) sums the contributions to TC. The atmospheric carbon content, which in this model is limited to its content of CO_2, is given by the partial pressure of CO_2 times the number of moles of gas in the atmosphere, M_a. Assuming an atmospheric thickness of 7,777 m, M_a is given to $1.7692 \cdot 10^{20}$ mol. In this case 1 ppm of CO_2 corresponds to 2.123 PgC, which is consistent with the OCMIP recommendation. M_o is the mass of the ocean [kg], which in our ensemble of simulations is kept constant at $1.34 \cdot 10^{21}$ kg. Implications of changes in volume are further discussed in Section 5.3. For one individual water parcel, C_{sat} corresponds to the concentration [mol kg^{-1}] of carbon the water parcel would have had if it would have been in equilibrium with the atmosphere, taking into account its temperature, salinity, alkalinity and also the minor effect of the concentration of PO_4 in the absence of biology. C_{soft} corresponds to the carbon that has been added to the water parcel through the remineralisation of the soft tissue of biogenic material that has entered the water parcel. The biogenic material also carries hard tissue and the carbon contained in this tissue is denoted C_{carb}. C_{res} is the residual needed to get the actual carbon concentration in the water parcel. C_{res} contains three components; 1) The first, and most interesting, contribution to C_{res} is the disequilibrium component C_{dis}. This is the part of the water parcel carbon concentration which results from the water parcel not being in perfect equilibrium with the atmosphere at the time when it left the surface. Hence, the concentration of carbon of abiotic origin (preformed carbon) in the water parcel consists of $C_{sat} + C_{dis}$. 2) The second contribution to C_{res} is the presence of carbon in the form of particulate and dissolved organic matter. At any one model time step, the concentration of such carbon is very small compared to the other terms in the equation (<1 %, $\sim 1 \cdot 10^{15}$ mol) and this is therefore not considered separately. 3) The third contribution to C_{res} consists of the errors associated with any imperfect assumptions in the theory used for calculating C_{sat}, C_{soft} and C_{carb}. To allow us to distinguish between the components 1 and 3, we will make

3.1.2 Preformed tracers

In cGENIE, we also employ a set of preformed nutrients, carbon, oxygen and alkalinity (P_{pre}, DIC_{pre}, O_{2pre} and A_{pre}). The initial concentrations of the preformed tracers are set in the surface ocean, where they are set equal to the concentration of the corresponding active tracers. After the surface water is submerged, they are passively advected and mixed in the interior ocean. We use these tracers to calculate e.g. $\overline{P^*}$ (see Appendix A2), apparent oxygen utilisation (AOU, see Appendix B2) and for separating ocean DIC into categories of different origin (see Appendices B1 and B2).

Preformed tracers are a recent addition to the model, which have only been used to a limited extent in previous studies (Goodwin et al., 2015). Studies using other models have shown the usefulness of e.g. P_{pre}, DIC_{pre}, A_{pre} as explicit model tracers (e.g., Marinov et al., 2008b; Duteil et al., 2012; Bernardello et al., 2014; Eggleston and Galbraith, 2017), but in this case we expand this by using as many as four preformed tracers simultaneously. This eliminates errors that would result from using a linear regression for A_{pre} (Lauderdale et al., 2013; Eggleston and Galbraith, 2017), or from the presence of oxygen disequilibrium in the calculation of AOU (Eq. B3), as discussed by Ito et al. (2004). Consequently, there is no need to make simulations with infinitely fast gas exchange, which is a common approach to remove errors due to O_2 disequilibrium (e.g., Marinov et al., 2008b). Concerns as those raised by Bernardello et al. (2014), regarding the 'back-tracking' methods of the Ito and Follows framework and the errors introduced by oxygen disequilibrium, are hence not an issue here. P_{pre} allows direct determination of nutrient utilisation efficiency, eliminating any sources of error that could be associated with indirect methods of determination. Finally, DIC_{pre} allows us to estimate the errors associated with the carbon species separation (see e.g. Section 4.1.4).

3.2 Theory and experimental setup

The inventory of total carbon, TC [mol], in the equilibrium state can be described by

$$TC = M_a\, pCO_2^{atm} + M_o(\overline{C_{sat}} + \overline{C_{soft}} + \overline{C_{carb}} + \overline{C_{res}}) \quad (3)$$

Equation (3) sums the contributions to TC. The atmospheric carbon content is given by the partial pressure of CO_2 times the number of moles of gas in the atmosphere, M_a. M_o is the mass of the ocean [kg]. C_{sat} is the concentration [mol kg^{-1}] of carbon an individual water parcel would have had if it were in equilibrium with the atmosphere at the ambient temperature, salinity, alkalinity and concentration of PO_4. C_{soft} originates from remineralisation of the soft tissue of biogenic material that has entered the water parcel. Carbon from biogenic hard tissue is denoted C_{carb}. C_{res} is the residual needed to get the actual carbon concentration in the water parcel. C_{res} contains three components; 1) The disequilibrium component C_{dis}, which we will quantify in Section 4.1.5. 2) Carbon in the form of particulate and dissolved organic matter. 3) Errors associated with any imperfect assumptions in the theory used for calculating C_{sat}, C_{soft} and C_{carb}. The overbars represent global averages. The concentration C_{pre} in the water parcel consists of $C_{sat} + C_{dis}$, whereas $C_{soft} + C_{carb}$ gives regenerated carbon, C_{reg}. We calculate the contributions to Eq. 3 and and any changes to this inventory (see Eq. 4) using methods of Kwon et al. (2011) and

simulations with artificially fast gas exchange to remove as much of C_{dis} as possible. These simulations are further described at the end of this section. The overbars represent global averages. In the deep ocean overall, C_{sat} and C_{res} together constitute the concentration of preformed carbon plus any calculation errors, whereas adding C_{soft} and C_{carb} gives regenerated carbon.

Initialising from our pre-industrial equilibrium state $PIES278$, we perform 12 different spin-ups in which one or two physical parameters have been changed compared to the control (Fig. 1, Table 1). They are run for 10,000 years, which is enough to reach a new equilibrium state. These sensitivity experiment equilibrium states are denoted $SE1-SE12$. The physical parameters that we change are atmospheric heat diffusivity, wind stress and ocean vertical and horizontal diffusivity. They are selected because they are common tuning parameters (e.g., Müller et al., 2006; Marsh et al., 2013), which influence the ocean circulation.

These modifications of physical parameters will cause the ocean circulation to change c.f. $PIES278$; the circulation gets weaker/stronger, overturning cells change their latitudinal extent etc. During the spin-up phase, pCO_2^{atm} is still restored to 278 ppm (Fig. 1) and the ocean reservoir of nutrients (in this case, PO_4) and alkalinity is the same as in $PIES278$. Hence, the atmospheric carbon inventory is identical in all ensemble members and in $PIES278$, but the ocean carbon inventory, as well as the TC of these 12 ensemble members will be different than in $PIES278$. We aim at comparing the drawdown potential of models that have the same pCO_2^{atm}, but different oceanic carbon distributions and inventories, which is usually the case in model intercomparison projects. For example, the instructions for the LGM simulations within the framework of the current PMIP3-CMIP5 project specify the LGM pCO_2^{atm} to be set to 185 ppm, whereas there are no specifications for the ocean carbon inventory (see https://pmip3.lsce.ipsl.fr/).

The change in the total carbon inventory, ΔTC [mol] can be described by

$$\Delta TC = M_o(\Delta\overline{C_{sat}} + \Delta\overline{C_{soft}} + \Delta\overline{C_{carb}} + \Delta\overline{C_{res}}) \quad (5)$$

The theoretically determined contributions by C_{soft}, C_{carb} and C_{sat} to this observed change in TC in Eq. (5) are then evaluated as described in the subsections 3.3 and 3.4, excluding the change in C_{res}. The change in C_{res} will simply be the residual between the observed change in TC and sum of the theoretically determined contributions by C_{soft}, C_{carb} and C_{sat}.

The changes in inventories of TC, C_{sat}, C_{soft}, C_{carb} and C_{res} are translated into the equivalent change in pCO_2^{atm} that would occur if we were not restoring it to pre-industrial levels. This translation is performed as described in detail in Appendix A. This translation allows us to test the validity of the equation describing the effect on global ocean mean temperature effect on pCO_2^{atm} suggested by Goodwin et al. (2011) (see Appendix A)

Finally, starting from each of $SE1-SE12$ as well as from $PIES278$, we run experiments where the nutrient utilisation efficiency of biology is maximised (100 % efficiency) (Fig. 1) and again allow the model to run for 10,000 years to new equilibrium states ($DE1-DE12$). This reveals the differences in drawdown potential between ensemble members with different ocean circulation characteristics. Maximum nutrient utilisation efficiency, i.e. $\overline{P^*}=1$ (see Eq. (2)), is achieved by changing the remineralisation length scale in the model. It is made deep enough (10,000 m) for any carbon that is taken up in organic material to be highly efficiently trapped in the deep ocean and not undergo any significant remineralisation. The concentration

Lauderdale et al. (2013), when necessary solving the carbon system equations using the solver of Lewis et al. (1998). More details about the calculations of the contributions to TC are given in Appendix B.

Initialising from our pre-industrial equilibrium state $PIES278$, we perform 12 different equilibrium experiments in which one or two physical tuning parameters have been changed compared to the control (Fig. 1). The parameters and their ranges are further described in Section 3.3 and listed in Table 1. The experiments are run for 10,000 years, which is enough to reach a new equilibrium state. These 12 sensitivity experiment equilibrium states ($SE1$–$SE12$) are given descriptive notations listed in Table 1. These modifications of physical tuning parameters will cause the ocean circulation to change c.f. $PIES278$; the circulation gets weaker/stronger, overturning cells change their latitudinal extent etc. During the spin-up phase, pCO_2^{atm} is still restored to 278 μatm (Fig. 1). The ocean reservoir of nutrients (in this case, PO_4) is the same as in $PIES278$, but the partitioning between P_{reg} and P_{pre} is changed, and thereby the strength of the biological pump. Likewise, the mean temperature of the ocean changes, and thereby the strength of the solubility pump. Hence, while the atmospheric carbon inventory is identical in all ensemble members and in $PIES278$, but the ocean carbon inventory, as well as the TC of these 12 ensemble members will be different. We aim at comparing the drawdown potential of models that have the same pCO_2^{atm} in their initial equilibrium state, but different oceanic carbon distributions and inventories, which is usually the case in model inter-comparison projects. For example, the instructions for the LGM simulations within the framework of the current PMIP3-CMIP5 project specify the LGM pCO_2^{atm} to be set to 185 ppm, whereas there are no specifications for the ocean carbon inventory (see https://pmip3.lsce.ipsl.fr/).

The change in the total carbon inventory, ΔTC [mol] between $PIES278$ and some equilibrium state $SE(n)$, where $n=(1,...,12)$, can be described by

$$\Delta TC = M_o(\Delta\overline{C_{sat}} + \Delta\overline{C_{soft}} + \Delta\overline{C_{carb}} + \Delta\overline{C_{res}}) \quad (4)$$

The theoretically determined contributions by C_{soft}, C_{carb} and C_{sat} to this observed change in TC in Eq. (4) are then evaluated as described in the subsections B2 and B1, excluding the change in C_{res}. The change in C_{res} will simply be the residual between the observed change in TC and sum of the theoretically determined contributions by C_{soft}, C_{carb} and C_{sat}. pCO_2^{atm} is restored and thus the atmospheric carbon reservoir does not contribute to ΔTC.

The changes in inventories of TC, C_{sat}, C_{soft}, C_{carb} and C_{res} are translated into the equivalent change in pCO_2^{atm} that would occur if we were not restoring it to pre-industrial levels, but instead kept TC constant in the ensemble (cf. methods of Marinov et al., 2008a, b). This translation is performed as described in detail in Appendix C. This translation allows us to test the validity of the equation describing the effect on global ocean mean temperature effect on pCO_2^{atm} suggested by Goodwin et al. (2011) (see Appendix C).

Finally, starting from each of $SE1$–$SE12$ as well as from $PIES278$, we run experiments where the NUE of biology is maximised (100 % efficiency) (Fig. 1) and again allow the model to run for 10,000 years to new equilibrium states ($DE1-DE12$). This reveals the differences in drawdown potential between ensemble members with different ocean circulation characteristics. Note that in this step, pCO_2^{atm} is not restored, thus TC is held constant between SE(n) and DE(n) and carbon is only redis-

of dissolved P (at the surface, and on a global annual mean) being reduced by two orders of magnitude in all DE:s, due to P being bound in organic material, confirms that this effect is achieved.

To calculate $\overline{P^*}$ according to the framework by Ito and Follows (2005) (Section 2.3), we need to know $\overline{P_{reg}}$, the concentration of dissolved phosphate in the deep ocean that is of regenerated origin. $\overline{P_{reg}}$ is derived from global average apparent oxygen utilisation, $\overline{AOU}$, using the Redfield ratio of phosphate to oxygen, $R_{P:O_2}$, as shown below in Eqs. 6-7. By removing $\overline{P_{reg}}$ from the overall global average concentration of phosphate, $\overline{P}$, we get the global average concentration of preformed phosphate, $\overline{P_{pre}}$ (see Eq. (8)).

$$\overline{P_{reg}} = -R_{P:O_2} \cdot \overline{AOU} \quad (6)$$

$$AOU = O_{2_{sat}} - O_2 \quad (7)$$

$$\overline{P_{pre}} = \overline{P} - \overline{P_{reg}} \quad (8)$$

As seen in Eq. (7), AOU is the difference between the saturation concentration of oxygen, $O_{2_{sat}}$, which is the concentration that would be present if the water were at saturation at the ambient potential temperature and salinity, and the actual concentration of oxygen, O_2, that is registered in the water. It is assumed that most of this difference is due to decomposition of organic soft-tissue material, which consumes oxygen. According to Williams and Follows (2011), this is a valid assumption since the equilibration time with the atmosphere of oxygen at the ocean surface is only a few days. Hence, oxygen disequilibrium is likely to be small and O_2 at the surface is very close to $O_{2_{sat}}$. Therefore, AOU can be used to 'back-track' the amount of nutrients or carbon that was brought into the deep ocean trapped in organic material and which has then been remineralised.

The Ito and Follows framework has been widely applied, e.g. by Williams and Follows (2011); Marinov et al. (2008b); Kwon et al. (2011); Lauderdale et al. (2013). However, the validity of using this framework has been questioned (Bernardello et al., 2014). In the real ocean, oxygen disequilibrium is negative and though it is small, it is not negligible. The result is that P_{reg} and C_{soft} are overestimated when calculated with the 'back-tracking' method. This overestimation may not be critical when looking at the total global ocean inventory of carbon, but in the present study that looks at small changes in this inventory, the error is significant and of the same order of magnitude as the observed changes in C_{soft}. Hence, Bernardello et al. (2014) are right in their critisism. We have therefore made sure to eliminate this issue by running the model with artificially fast gas exchange for O_2, which rules out any disequilibirum effects on C_{soft}.

For CO_2, we have run the model with both fast and normal gas exchange, because we are interested in effects of C_{dis}. By applying fast gas exchange we are theoretically able to remove C_{dis} and can thus get an indication of how large the contributions of C_{dis} is to C_{res} in each simulation. To achieve artificially fast gas exchange we have multiplied the scaling constant (k = 0.31, following Wanninkhof (1992)) used in the calculation of the gas exchange coefficient by 100 (higher numbers did not achieve any significant difference) and removed the physical barrier effect of sea-ice on air-sea gas exchange.

tributed between reservoirs (see Eq. 3). Eq. 4 is not applicable in this step, because it assumes constant pCO_2^{atm}. Maximum NUE, i.e. $\overline{P^*} = 1$ (see Eq. (A1)), is achieved by changing the remineralisation length scale in the model (Section 3.1). It is made deep enough (10,000 m) for any carbon that is taken up in organic material to be highly efficiently trapped in the deep ocean and not undergo any significant remineralisation. The concentration of dissolved P (at the surface, and on a global annual mean) being reduced by two orders of magnitude in all DEs, due to P being bound in organic material, confirms that this effect is achieved. However, due to convection, mixing and local remineralisation of dissolved organic matter, the surface concentration of P does not go to zero. Note that the contribution of organic material to the carbon inventory TC is substatial in this step. Thus, quantifying ΔC_{soft} and ΔC_{carb} for this step is not useful unless the carbon contained in organic material is also considererd to contribute to these reservoirs. However, the very deep remineralisation length scale is a highly hypothetical case and we therefore choose not to separate the contributions by the different carbon reservoirs to the drawdown of pCO_2^{atm}.

3.3 Sensitivity experiment tuning parameters

The physical tuning parameters that we change are atmospheric heat diffusivity, wind stress and ocean vertical and isopycnal diffusivity. They are selected because they are common tuning parameters (e.g., Müller et al., 2006; Marsh et al., 2013), which influence the ocean circulation.

For this study, our intention is for the ensemble to be representative of a wide range of plausible ocean circulation states. The chosen parameter ranges correspond to a halving and doubling of the values used in the control simulation. Our chosen values are within the parameter space explored for a predecessor to the GENIE-model by Edwards and Marsh (2005), except the low wind stress simulation (see below). Similar parameter ranges are also explored for GENIE by e.g. Marsh et al. (2013). For the most part, our selected values are within the parameter ranges that generate the subset Edwards and Marsh (2005) refer to as low-error simulations. In the Bern3D model, with physics based on Edwards and Marsh (2005) and thus similar to GENIE, Müller et al. (2006) doubled the observed wind stress (W = 2) to get a more realistic gyre circulation. Marinov et al. (2008a, b) used the Geophysical Fluid Dynamics Laboratory Modular Ocean Model version 3, which has the same default value for isopycnal diffusivity (1500 $m^2 s^{-1}$) as our model. Marinov et al. (2008a, b) explore a range of 1000-2000 $m^2 s^{-1}$ (cf. our range of 750-3000 $m^2 s^{-1}$).

When comparing with models that have different available tuning parameters, diagnostic variables such as temperature, salinity and AMOC volume transport can indicate whether our achieved states are within the common tuning range for ocean circulation. The IPCC AR5 WG1 report (Stocker, 2014) shows temperature and salinity ranges in two selected deep ocean grid points, in the North and South Atlantic respectively, of the ensemble of pre-industrial control states (PIC) of PMPI2 and CMIP5/PMIP3 (see grid point positions and data in Table 2). We compare those ranges to the corresponding grid cell ranges of our equilibrium states $SE1$–$SE12$. In these selected grid cells, we cover a similar span in salinity and an equally broad range in temperatures as the PMIP-ensemble, though the temperatures in our ensemble are higher (range shifted by 1.5°C). According to Muglia and Schmittner (2015), the PMIP3 PIC AMOC range is 12.6-23.0 Sv (Table 2). If we exclude the combined simulation with halved wind stress and halved diapycnal (vertical) diffusivity ($WS/2\_DD/2$), which has a very weak AMOC (2.0 Sv), the AMOC range for our equilibrium states is 8.3-18.0 Sv (Table 2). Thus, there is a difference of 8-9

3.3 Contribution by the biological pumps

The calculations in this section largely follow the Appendix in Lauderdale et al. (2013), who studied the correlation between wind-driven changes of the residual circulation in the Southern Ocean and changes in ocean carbon reservoirs and atmospheric CO_2. All stoichiometric ratios for organic material are based on Redfield (1963) (see Section 3.1.1).

The ocean global average of C_{soft} is calculated from apparent oxygen utilisation, AOU, as

$$\overline{C_{soft}} = -R_{C:O_2} \cdot \overline{AOU}, \quad (9)$$

where $R_{C:O_2}$ is the stoichiometric ratio of carbon to oxygen of $-106/138 \approx -0.768$. Here, we make use of the assumption that AOU is due to decomposition of organic soft-tissue material (see also Section 3.2).

To calculate the ocean inventory of C_{carb}, we need to know the preformed alkalinity, A_{pre}, of each grid cell. For this, we make a linear regression from model control state surface ocean data of salinity, oxygen and phosphate, similar to the regression made in Lauderdale et al. (2013). Note that the regression model is adapted for concentrations given in mmol L^{-1} to be comparable to the regression made by Lauderdale et al. (2013).

$$A_{pre} = 0.0339 + 0.0642 \cdot S + 0.1777 \cdot PO \quad (10)$$

where

$$PO = O_2 - R_{P:O_2} \cdot P. \quad (11)$$

Here, S is salinity and the second term represents the effect on alkalinity due to dilution. The third term represents alterations of alkalinity due to biological activity. PO is oxygen distribution with alterations due to respiration and remineralisation removed Broecker (1974), O_2 is the oxygen concentration, P is the phosphate concentration and $R_{P:O_2}$ is the stoichiometric ratio of phosphorus to oxygen of 1:-138 ($\approx -7.25 \cdot 10^{-3}$). This means that with a stronger biological pump, surface alkalinity is reduced by a factor corresponding to this ratio.

We can now calculate the grid cell concentration of C_{carb} as

$$C_{carb} = \frac{1}{2}(A_T - A_{pre} - R_{N:O_2} \cdot AOU) \quad (12)$$

where A_{tot} is the grid cell alkalinity and $R_{N:O_2}$ is the stoichiometric ratio of nitrogen to oxygen of 16:-138 (≈ -0.116). We can then calculate the volume-weighted global average of C_{carb}.

Sv between highest and lowest value, which is also the case for the PMIP3 PICs, but our ensemble does not cover the two highest PMIP3 AMOC values.

3.4 Overturning

In a coarse-resolution model like cGENIE, the overturning circulation, which transports carbon to the deep ocean and back up to the surface again (Eriksson and Welander, 1956), is one of the most sensitive cirulation components. We diagnose an overturning circulation strength (henceforth denoted OVT) by taking the difference between the maximum and minimum (i.e. the maximum of the negative overturning cell) of the zonal average overturning streamfunction, ψ, below 556 m depth (excluding the uppermost five gridboxes), as shown in Eq. 5. The subscript gr in Eq. 5 denotes the geographical region. OVT is diagnosed for the Atlantic basin and the Pacific basin separately. A global measure of OVT is calculated by taking the difference between the Northern hemisphere maximum and the Southern hemisphere minimum of ψ below 556 m depth.

$$OVT = \psi_{max_{gr}} - \psi_{min_{gr}} \quad (5)$$

The OVT measures the amount of flushing of the deep water, which is important for the carbon storage (Eggleston and Galbraith, 2017). Another important factor influencing the carbon pools is which overturning cell is dominating in terms of volume (Eggleston and Galbraith, 2017); the northern cell (producing North Atlantic Deepwater, NADW) or the southern cell (producing Antarctic Bottom Water, AABW, and Circumpolar Deep Water, CPDW). Since these water masses are of different origin, they will differ in properties, such as water temperature and nutrients, and will therefore have different capacities for holding C_{sat}, C_{soft} and C_{dis}. However, the inter-member differences in this aspect are difficult to discern and we have therefore chosen to focus on the impact of OVT described above, which are more clearly identifiable.

4 Results

We use a two-step modelling approach, as explained in Section 3.2; the first step is where we change the ocean circulation by changing physical parameters as listed in Table 1, and the second is where we force the biological pump to become 100 % efficient. The results from this two-step approach are described in Sections 4.1 and 4.2.

4.1 Step 1 - The effects of ocean circulation changes

In this first step, we achieve a set of pre-industrial equilibrium states — all with pre-industrial pCO_2^{atm} of 278 ppm — where, as a result of ocean circulation differences, the ensemble members have different carbon reservoirs.

In $PIES278$ and $SE1$–$SE12$, global average salinity, total alkalinity and PO_4 are 34.90, 2363 $\mu molkg^{-1}$ and 2.15 $\mu molkg^{-1}$ respectively. These properties are conserved, but redistributed, which gives some very small differences in the global averages between ensemble members. Global average temperature, $T_{avg} = 3.58$°C in $PIES278$, which is close to the modern day observational estimate 3.49°C (Locarnini et al., 2013)). In the SEs, T_{avg} ranges between 2.31–4.91°C. Sea-ice

3.4 Contribution by the solubility pump

Since pCO_2^{atm} is constant and the global ocean mean salinity is similar in all ensemble members $SE1-SE12$, any changes in global average C_{sat} between $PIES278$ and the SE:s will be due to changes in ocean temperature or alkalinity:

$$\overline{\Delta C_{sat}} = \overline{\Delta T \frac{\partial C_{sat}}{\partial T}\Big|_{pCO_2,S,A_{pre}}} + \overline{\Delta A_{pre} \frac{\partial C_{sat}}{\partial A_{pre}}\Big|_{pCO_2,S,T}} \quad (13)$$

Note: Salinity is conserved, but re-distributed. Hence, when using Eq. (13) at the local scale, the term dependent on ΔS must be included. It only disappears after global integration, assuming that $\frac{\partial C_{sat}}{\partial S} \simeq constant$, which is done here.

We calculate the first term in Eq. (13) in a non-linear way, based on the changes in temperature in each grid cell of each ensemble member SE_n (n = 1 – 12) compared to $PIES278$, while keeping salinity and alkalinity constant using the $PIES278$ grid cell salinity and A_{pre}. We calculate the global average of grid cell $C_{sat}(T_{SE_n}) - C_{sat}(T_{PIES278})$ solving the carbon system equations using the solver CO2SYS (Lewis et al., 1998). The constants used in the scheme do not match exactly with those used in the model, but the differences are minor, which makes it relevant to assume that this is an acceptable choice.

The partial derivative in the second term on the right hand side of Eq. (13) is also calculated by solving the carbon system equations using CO2SYS. While keeping T constant we change grid cell A_{pre} by 1 % to get $\frac{\partial C_{sat}}{\partial A_{pre}}$. To get the full contribution to ΔC_{sat} by changes in A_{pre}, we then multiply by grid cell ΔA_{pre} before averaging globally. Because the change in alkalinity is small between the different ensemble members, the contribution to the change in C_{sat} by the second term in Eq. (13) is much smaller, and even negligible, compared to the contribution by changes in temperature (the first term).

In cGENIE, there is a restriction of the solubility coefficients for CO_2 which are only defined for waters between 2–35 °C. Hence, all water below 2 °C has the same CO_2 solubility in the model. In the calculations of C_{sat}, we use CO2SYS with this temperature limitation. The difference in global average C_{sat} between the case when this restriction is used with CO2SYS compared to when it is not used is smaller than 0.6 % for all ensemble members, including the control state. Since the restriction is used consistently, the error caused by the restriction being present in the model should not constitute a significant problem for our analysis.

4 Results

We use a two-step modelling approach, as explained in Section 3.2; the first step is where we change the ocean circulation by changing physical parameters as listed in Table 1, and the second is where we force the biology to become 100 % efficient. The results from this two-step approach is described in Sections 4.1 and 4.2.

4.1 Step 1 - The effects of ocean circulation changes

In this first step, we achieve a set of pre-industrial equilibrium states — all with pre-industrial pCO_2^{atm} of 278 μatm — where, as a result of ocean circulation differences, the ensemble members have different carbon reservoirs. We use this set of equilibrium states to investigate what controls these differences in reservoirs.

To allow for comparison between the control equilibrium state $PIES278$ and the ensemble members $SE1 - SE12$, Table 2 lists important diagnostic variables; global ocean averages of temperature (T_{avg}) and pH (pH_{avg}), surface ocean average pH (pH_{surf}), global percentage of sea ice cover, global average nutrient utilisation efficiency (in terms of $\overline{P^*}$) and a measure of the strength of the global ocean overturning circulation. For reference, the table also includes observational estimates (Locarnini et al., 2013; Comiso, 2008; Ito and Follows, 2005; Raven et al., 2005). In $PIES278$ and $SE1 - SE12$, global average salinity, alkalinity and PO_4 are 34.90, 2363 $\mu molkg^{-1}$ and 2.15 $\mu molkg^{-1}$ respectively. These properties are conserved, but redistributed, which gives some very small differences in the global averages between ensemble members.

The changes in model total carbon inventory, ΔTC, in the biological and the solubility pumps and the contributions from C_{res} (Eq. (5)) in the ensemble — which are effects of the changes in ocean circulation — are presented and compared in Fig. 2a. The control $PIES278$ model TC inventory is $3 \cdot 10^{18}$ mol ($\sim 36,000$ Pg C), so the changes are of the magnitude of a few percent. This corresponds to a range in pH_{avg} between 7.79 and 7.97 (Table 2), while pH_{surf} stays close to the observational estimate (~ 8.2, see Raven et al. (2005)).

For reference, we have also added a second panel (Fig. 2b), showing the changes in TC expressed as changes in pCO_2^{atm} (see Appendix A). Hence, if we were not restoring pCO_2^{atm} to pre-industrial conditions, but instead kept TC constant, this is how much pCO_2^{atm} would approximately have changed due to the changes in physical characteristics of the system. In this ensemble, these changes in pCO_2^{atm} stay between ± 50 ppm.

The methods we use to convert our carbon inventory changes to changes in pCO_2^{atm} assume that the changes are small (Appendix A). Hence, the methods become less valid, and the estimates of the corresponding changes in CO_2 become less reliable for ensemble members with greater changes, e.g. $SE4$ and $SE12$. This should be kept in mind when examining Fig. 2b. However, this is not considered a major issue, since these calculations are only made to give an idea of the order of magnitude of the effects on pCO_2^{atm} rather than exact numbers.

4.1.1 Sensitivity of overturning streamfunction

In a coarse-resolution model like cGENIE, the overturning circulation, which transports carbon to the deep ocean and back up to the surface again (Eriksson and Welander, 1956), is one of the most sensitive cirulation components.

The overturning circulation strength (henceforth denoted OVT) is diagnosed by taking the difference between the maximum and minimum (i.e. the maximum of the negative overturning cell) of the zonal average overturning streamfunction, ψ, below 556 m depth (excluding the uppermost five gridboxes). ψ for different ocean basins are shown in Table S.1.

Figure 3 suggests a linear relationship between the OVT and the total carbon inventory TC, in this case represented by ΔTC, in the ensemble members. The relationship is clearer for the Atlantic and the global measure (Fig. 3a and 3c) than for the Pacific (Fig. 3b). The correlation coefficients indicate that as much as 90 % of the variance in TC can be explained by changes in the OVT (Table 3).

For the different carbon pumps, the correlation with OVT is most clear for C_{soft} (see Fig. 4), where 73 – 79 % of the variance can be explained by the OVT (Table 3). Note that since no biogeochemical manipulations have been made in this step, the remaining variance (21 – 27 %) is also due to physical perturbations. For C_{sat} and C_{res}, the correlation is weak (26 – 49

cover ranges from 0.0–10.6% in the SEs, with $PIES278$ in the centre of the interval (c.f. observational estimates of sea-ice cover, which range between 3-6% due to seasonal variability (Comiso, 2008)). Diagnostic variables for all the individual SEs are given in (Table 3).

The control $PIES278$ model total carbon inventory, TC, is $3 \cdot 10^{18}$ mol ($\sim 36,000$ Pg C). ΔTC, and the contributions to ΔTC by the biological and the solubility pump and by C_{res} (Eq. (4)) in the SEs — which are effects of the changes in ocean circulation — are of the magnitude of a few percent ($\sim 10^{16}$ mol, Fig. 2a–d). This corresponds to a range in pH_{avg} between 7.79 and 7.97 (Table 3), while pH_{surf} stays close to the observational estimate (~ 8.2, see Raven et al., 2005). For reference, Fig. 2e–h show the approximate differences in pCO_2^{atm} that would have occurred in the SEs, if we were not restoring it to 278 ppm (see Section 3.2 and Appendix C). In this ensemble, these differences in pCO_2^{atm} stay between ± 50 ppm (Fig. 2e), because of cancellation between the effects of the different carbon pumps. Note that the methods of Appendix C Fig. 2e-h are based on the assumption that changes in pCO_2^{atm} are small and are therefore less reliable for SEs with large changes, e.g. $WSx2$ and $WS/2\_DD/2$. Because the computed changes in pCO_2^{atm} are approximate, the sum of the contributions from the different pumps do not exactly equal the ΔpCO_2^{atm} corresponding to ΔTC.

4.1.1 Sensitivity of overturning streamfunction

The range of OVT (see Eq. 5) resulting from the differences in zonal average overturning stream function (ψ, Table S1), is 10.1–32.6 Sv for the global measure (Table 3). The range of Atlantic OVT is 4.1–19.5 Sv (see Figs. 3a and 4a). Note that OVT is not the same as $AMOC$ strength, which ranges between 2.0-18.0 Sv for the SEs (Table 2), though the $AMOC$ is a large part of the OVT in the Atlantic. The zonal average overturning streamfunction, ψ, for a typical weak ($DD/2$ with $OVT = 17.4$ Sv) and strong ($DDx2$ with $OVT = 32.6$ Sv) circulation SE in Fig. 5a-b show that the overturning circulation patterns in comparison to the control $PIES278$ ($OVT = 20.4$ Sv) are similar, with no major changes in extent of the overturning cells.

Figure 3 suggests a linear relationship between OVT (Eq. 5) and the total carbon inventory TC, in this case represented by ΔTC, in the SEs. The relationship is clearer for the Atlantic and the global measure (Fig. 3a and 3c) than for the Pacific (Fig. 3b). The correlation coefficients indicate that as much as 90 % of the variance in TC can be explained by changes in OVT (Table 4). For the different carbon pumps, the correlation with OVT is most clear for C_{soft} (see Fig. 4), where 75–80 % of the variance can be explained by the OVT (Table 4). Note that since no biogeochemical manipulations have been made in this step, the remaining variance (20–25 %) is also due to physical perturbations. For C_{sat} and C_{res}, the correlation is weak (40–57 % and 25–30 % respectively, Table 4), but statistically significant. If we add C_{soft} and C_{res} and correlate with the OVT, the correlation gets stronger than it is for C_{soft} alone. In experiments with stronger OVT (global and/or basin scale), the relative importance of ΔC_{soft} (negative, see Table 4), ΔC_{sat} (positive for total, negative for temperature contribution and positive for alkalinity contribution) and ΔC_{res} (negative) will determine the sign of ΔTC. In our ensemble, stronger OVT (global and basin scale) leads to a decreased storage of carbon in the ocean compared to $PIES278$ (Figure 3).

% and 40 – 48 % respectively, Table 3), but statistically significant, especially for the Atlantic basin. If we add C_{soft} and C_{res} and correlate with the OVT, the correlation gets stronger than it is for C_{soft} alone.

In experiments with stronger OVT (global and basin scale) than in $PIES278$, e.g. $SE6$ (see Figs. 5b, 2 and 8b), a water parcel will, on average, stay near the ocean surface for a shorter amount of time than if the OVT is weaker (e.g $SE5$, see Figs. 5a, 2 and 8a). Hence, biology will have less time to use the nutrients available and ΔC_{soft} will be negative. Meanwhile, there will be more mixing, leading to a deepening of the thermocline, and T_{avg} will increase. Thus, ΔC_{sat} will also be negative. However, ΔC_{res} will be more likely to be positive, due to changes in the temperature gradient (especially important in the North Atlantic), sea ice and outgassing (dominant in the Southern Ocean). These effects on C_{res} are further discussed in 4.1.5.

In experiments with stronger OVT (global and/or basin scale), the relative importance of ΔC_{soft} (negative, see Table 3), ΔC_{sat} (negative) and ΔC_{res} (positive) will determine the sign of ΔTC. In our ensemble, stronger OVT (global and basin scale) leads to a decreased storage of carbon in the ocean compared to $PIES278$ (Figure 3).

Another important factor influencing the carbon pools is which overturning cell is dominating in terms of volume; the northern cell (producing North Atlantic Deepwater, NADW) or the southern cell (producing Antarctic Bottom Water, AABW, and Circumpolar Deep Water, CPDW). Since these water masses are of different origin, they will differ in properties, such as water temperature and nutrients, and will therefore have different capacities for holding C_{sat}, C_{soft} and C_{res}. However, the inter-member differences in this aspect are difficult to discern and we have therefore chosen to focus on the impact of OVT described above, which are more clearly identifiable.

4.1.2 Sensitivity of total carbon inventory

The relative contributions of the carbon pumps to ΔTC are very different depending on the modified physical characteristics (Fig. 2). In experiments in which the modified atmospheric heat diffusivity is partly driving the circulation (and temperature) changes ($SE1$, $SE2$ and $SE11$), the contributions by changes in the three components C_{soft}, C_{sat} and C_{res} are of similar magnitude and are all important for the change in TC. This is also the case for some ensemble members with changes in ocean diffusivity ($SE7$ and $SE9$).

In other experiments (e.g. with altered wind stress intensity, SE:s 3, 4 and 12) or in most cases where vertical diffusivity has been changed (SE:s 5, 6, 10)), the change in C_{soft} is dominant. In such experiments, ΔC_{carb} can be as significant as ΔC_{sat} and δC_{res}, whereas it, in most other experiments, plays a minor role. In experiments where only the horizontal diffusivity has been changed (SE:a 7 and 8), the contributions by C_{sat} and C_{res} are larger than the contribution from C_{soft}.

This shows that no contributing terms can be considered negligible relative to the other terms. The importance of a given term for ΔTC depends on the mechanism and the origin of the circulation change (Section 4.1.1).

In the following subsections, some results for each of the contributing terms are analysed.

4.1.3 Sensitivity of biogenic carbon

Changes in C_{soft} and C_{carb} always have the same sign, but the effect of C_{carb} has a smaller magnitude (Fig. 2). The ratio $\Delta C_{carb}/\Delta C_{soft}$ spans between 0.23 and 0.42 for SE:a 7 and 8 (halved and doubled horizontal ocean diffusivity respectively),

4.1.2 Sensitivity of total carbon inventory

Although the total carbon inventory is strongly correlated with OVT (Fig. 3), the relative contributions of the carbon pumps to ΔTC are very different depending on the modified physical characteristics (Fig. 2). They combine in a way to make ΔTC be more closely correlated with OVT than any of the individual components (Table 4). Altered wind stress (WS) intensity (SEs 1, 2 and 9), and diapycnal diffusivity (DD, SEs 5, 6, 8), has a large impact on TC, dominated by changes in C_{soft}. Here, ΔC_{carb} can be as significant as ΔC_{sat} and δC_{res}, whereas it in most other experiments plays a minor role. The overall impact on TC from changing isopycnal diffusivity ($IDx2$ and $ID/2$ ($SE7--8$) is small, with larger contributions by C_{sat} and C_{res} than from C_{soft}. For SEs 3, 4 and 10, in which the modified atmospheric heat diffusivity (AD) is partly driving the circulation (and temperature) changes, the contributions by changes in C_{soft} and C_{sat} are of similar magnitude and equally important for the change in TC. This is also the case for some SEs with changes in ocean diffusivity ($ID/2$ and $DD/2\_IDx2$). Overall, no contributing terms can be considered negligible relative to the other terms, though $\Delta C_{sat,A}$ and ΔC_{carb} partly cancel each other. The importance of a given term for ΔTC depends on the mechanism and the origin of the circulation change (Section 4.1.1).

In the following subsections, we analyze each of the contributing terms.

4.1.3 Sensitivity of temperature and saturation carbon

$C_{sat,T}$ is the contribution to C_{sat} from water temperature. Global average temperature, T_{avg}, of the equilibrium states has a range of 2.3–4.9 °C (see Table 3), resulting in an interval of change in $C_{sat,T}$ of -0.8 $\cdot 10^{16}$ – +0.6 $\cdot 10^{16}$ mol (Fig. 2b, Fig. 6), or -96 – +72 GtC. Note that this includes a restriction on the solubility constants which prevents solubility from increasing with temperatures below 2°C, which weakens the close-to-linear relationship between T_{avg} and $C_{sat,T}$ (Fig. 6). This corresponds to a range in ΔpCO_2^{atm} of about -7 – +11 ppm (Figs. 2f and S1) when we solve the carbon system equations (Appendix C). The simplified equation (Eq. C9) suggested by Goodwin et al. (2011) yields results for ΔpCO_2 that in general are 10 – 20 % lower compared to using the carbon system equation solver (Fig. S1). Changes in $\overline{C_{sat}}$ caused by changes in preformed alkalinity ($\Delta\overline{C_{sat,A_{prc}}}$) spans -1.9 $\cdot 10^{16}$ – 1.8 $\cdot 10^{16}$ (Fig. 2b), which roughly corresponds to a range in ΔpCO_2^{atm} of -21 – +21 ppm (Fig. 2f).

Fig. 2a–e stresses that, in some SEs the contribution by $\Delta C_{sat,T}$ to ΔTC, and hence to changes in pCO_2^{atm}, is nearly as important as (e.g. $ADx2$, $ADx2\_DDx2$, $DD/2\_IDx2$, $ID/2$) or even more important than ($IDx2$) the changes in C_{soft}. Further, the temperature restriction on the CO_2 dissociation constants (see Appendix B1) is likely to cause an underestimation of the effect of ΔC_{sat} by on average 56 ±67% in our results.

In the ensemble, simulations with a weaker OVT than $PIES278$ tend to have a lower T_{avg} (thus larger $C_{sat,T}$) and a larger ocean storage of TC (SEs 4, 6, 7, 9 and 12 in Table 3 and in Fig. 3). The correlation between $C_{sat,T}$ and OVT (see Table 4) is -0.63 globally. The temperature sections in Fig. 7 show that when increased mixing is achieved by higher diapycnal diffusivity ($DDx2$), this causes the stratification to be less sharp between warm surface water and cold deepwater, because the warmer waters are mixed deeper, and T_{avg} increases while $C_{sat,T}$ decreases. The colder, and more stratified simulation ($DD/2$) is

and spans 0.15 and 0.20 in other ensemble members. The effects that the changes in C_{soft} and C_{carb} have on pCO_2^{atm} are of opposite signs due to the effect of the carbonate pump on preformed alkalinity (Goodwin et al., 2008) (Fig. 2b).

Globally, about 75 % of the variance in C_{soft} is explained by the strength of the OVT (Fig. 4 and Table 3). This correlation is strongest over the Atlantic basin. The rest of the variance is likely explained by e.g. redistribution of nutrients, light limitation regions or similar.

Fig. 6 b, suggests a tight, linear relationship between the inventory of C_{soft} and nutrient utilisation efficiency (here in terms of $\overline{P^*}$, Eq. (2)). P^* is a direct measure of the efficiency of the biological pump, and the linear relationship is expected from its definition (Eqs. 2, 6 and 7). Since the ratio between ΔC_{carb} and ΔC_{soft} is similar across ensemble members, the relationship between C_{carb} and $\overline{P^*}$ is also fairly linear.

The relationship between TC and $\overline{P^*}$ (Fig. 6 a) is quite linear too and is presumably dominated by C_{soft} and C_{carb} together (compare Figs. 6a and 6b). Deviations from a perfect straight line are caused by changes in the other carbon species. The influence of ΔC_{sat} and ΔC_{res} on ΔTC can be fairly small compared to the influence of biogenic carbon (see Fig. 2, e.g. SE:s 3, 5, 6, 12) or fairly large but of opposite sign (see Fig. 2, e.g. SE:a 2, 4, 11), thus cancelling each other out to some extent, resulting in biogenic carbon "passing on" its linear relationship with $\overline{P^*}$ to ΔTC.

$\overline{P^*}$ is important for the drawdown potential of a model (Fig. 6c), which is examined in the second step of the modelling (Section 4.2).

4.1.4 Sensitivity of temperature and saturation carbon

In the ensemble, global average temperature, T_{avg}, spans 2.3 and 4.9 °C, and in $PIES278$ it is 3.6 °C (see Table 2). This corresponds to an interval of change in ocean carbon storage of -1.4 $\cdot 10^{16}$ – +1.3 $\cdot 10^{16}$ mol (Fig. 2 a). Solving the carbon system equations (Appendix A), indicates that this is equivalent to an interval of about -16 – +17 ppm in terms of pCO_2^{atm} change (ΔpCO_2, Fig. 2 b.). The response in pCO_2^{atm} to changes in temperature is very close to linear; about 12.9 ppm °C^{-1} (12.5–13.1 ppm °C^{-1}, Fig. S1).

Calculating ΔpCO_2 for the temperature range of the ensemble using the simplified equation (A9) suggested by Goodwin et al. (2011), which is based directly on T_{avg} (Appendix A), gives an interval of -12 – +13 ppm. In this case, the linear fit gives changes of 9.8 ppm °C^{-1} (9.1–11.1 ppm °C^{-1}, Fig. S1). For this ensemble, using the simplified equation yields results for ΔpCO_2 that in general differ by $\sim$ 20–25 % compared to using the carbon system equation solver.

Fig. 2 stresses that the contribution by ΔC_{sat} to ΔTC, and hence to changes in pCO_2^{atm}, is nearly as important as the changes in C_{soft}. In ensemble members in which horizontal diffusivity in the ocean is changed, ΔC_{sat} is larger than ΔC_{soft}.

According to Headly and Severinghaus (2007), the global average temperature of the glacial ocean was 2.6 ± 0.6 °C colder than the modern day ocean. Since the ensemble member with the coldest ocean is only 1.3 °C colder than $PIES278$, the variations in C_{sat} during the past glacial cycles were likely larger than in our set of experiments.

The relationship between the changes in T_{avg} andΔC_{sat} is linear (Fig. 7), indicating that the changes in C_{sat} brought about by changes in alkalinity are insignificant in our model ensemble. The slope of the line is $\frac{\partial C_{sat}}{\partial T} = -1.02 \cdot 10^{16}$ mol °C^{-1}. If the global ocean cooled by $\sim$ 2.6 °C, as expected in a glacial state, the slope of the line suggests the excursion in C_{sat} would be

$\sim 2.7 \cdot 10^{16}$ mol. In the context of a 2.6 °C cooling, the carbon system equations (see Appendix A) yield that this corresponds to a decrease of about 30 ppm in pCO_2^{atm}. Here, we cannot use the simplified Eq. (A9), because the buffered carbon inventory is unknown in this hypothetical case.

The temperature sections in Fig. 8 show that when increased mixing is achieved by higher vertical diffusivity, this causes the stratification to be less sharp between warm surface water and cold deepwater, because the warmer waters are mixed deeper. Thus, T_{avg} increases because of increasing vertical diffusivity. The colder, and more stratified simulation is also the simulation with the weakest OVT (Fig. 5a, Fig. 8a). Note: the deepest water in the Pacific Ocean is actually warmer in this simulation, but the effect of the shallower thermocline compensates for this and the net effect is a decreased T_{avg}. In the ensemble, simulations with a weaker OVT than $PIES278$ tend to have a lower T_{avg} and a larger ocean storage of TC (SE:s 1, 5, 8, 9 and 12 in Table 2 and in Fig. 3). Despite this, the correlation between C_{sat} and the strength of the OVT (see Table 3) is weak. This is because the ocean cooling and the OVT are also influenced by other factors; as such they are not linearly related.

4.1.5 Sensitivity of residual carbon

The global inventory of C_{res} in the initial equilibrium states is slightly negative in all cases and of the magnitude 10^{16} mol (c.f. global TC inventory of $\sim 3 \cdot 10^{18}$ mol). Hence, when we look at Fig. 2 and we see a positive contribution from C_{res}, keeping in mind that the global inventories of C_{res} are negative in all ensemble members, this actually means it has only become less negative.

Comparing to observations described in Williams and Follows (2011), it seems like the inventory of C_{res} would be slightly positive or close to zero in the modern ocean (see the patterns in Fig. 11.21 and 11.22, where the Atlantic interior is slightly negative, but the surface and the Pacific are positive). Though Williams and Follows (2011) do not state a number for the global inventory, they mention that the magnitude is close to the uncertainties in the analysis. Hence, it is possible, and even likely, that our global inventory of C_{res} is slightly negative due to these uncertainties.

When looking at C_{res}, we are mainly interested in the contribution by C_{dis}. The experiments with artificially fast gas exchange for CO_2 indicate that the contribution to C_{res} by calculation errors (see Section 3.2) is in some cases of the same magnitude as the contribution by C_{dis}. This makes it difficult to constrain the effect of changes in C_{dis} in the ensemble by looking at C_{res}. However, when the model is run with artificially fast gas exchange, noticable changes in local DIC concentrations occur (examples shown in Fig. 9). These changes in DIC can be directly attributed to removing the contribution from C_{dis}. The changes are of the magnitude 10–20 μmol kg^{-1}, which is on the order of 0.5–1 % of the grid cell DIC concentration. Hence, an ocean circulation change that drastically changes C_{dis} in the deep ocean will potentially see a significant contribution to ΔTC from this component.

The processes influencing C_{dis} will be different in the deepwater formation areas in the Northern and Southern hemispheres (Toggweiler et al., 2003; Ito and Follows, 2005; Lauderdale et al., 2013). In the deepwater formation areas in the North Atlantic, C_{dis} is mainly a result of the temperature gradient. If a water parcel cools too fast before it sinks, there is not enough time to equilibrate with the atmosphere and the result will be a negative C_{dis}. This is seen as a negative signal in the upper half of the sections in Figure 9c. In a warmer global ocean, the temperature gradient between the equator and the poles will be

also the simulation with the weaker OVT (Fig. 5b, Fig. 7b). Note: the Pacific Ocean deep water is warmer in $DD/2$ than in $DDx2$, but the shallower thermocline has a compensating effect and the net result is a decreased T_{avg} (Fig. S2).

4.1.4 Sensitivity of biogenic carbon

Theoretical ($C_{soft} + C_{carb}$) underestimates C_{reg}, c.f. the model tracer ($DIC_{reg} = DIC - DIC_{pre}$), by 1-3%. Because this error is consistent, the contribution to ΔC_{res} (Section 4.1.5) is negligible. Changes in C_{soft} and C_{carb} always have the same sign, but the effect of C_{carb} has a smaller magnitude (excepted $IDx2$, Fig. 2 c). The effects of ΔC_{soft} and ΔC_{carb} on pCO_2^{atm} are of opposite signs (Fig. 2 g) as expected due to the effect of the carbonate pump on preformed alkalinity (Goodwin et al., 2008). Globally, 75–80 % of the variance in C_{soft} is explained by the OVT (Fig. 4, Table 4). This correlation is strongest over the Atlantic basin.

$\overline{P^*}$ in the SEs ranges between 0.32–0.59 (Table 3), while $\overline{P^*} = 0.43$ in $PIES278$. For reference, the observational estimate for $\overline{P^*}$ of the modern ocean is 0.36 (Ito and Follows, 2005). The tight, linear relationship between the inventory of C_{soft} and $\overline{P^*}$ (Fig. 8b) is expected from the definition of $\overline{P^*}$ (Eqs. A1 and B3), since it is a direct measure of the efficiency of the biological pump. The relationship between TC and $\overline{P^*}$ (Fig. 8 a) is also close to linear and appears dominated by biogenic carbon (compare Figs. 8a and 8b). Deviations from a perfect straight line are caused by ΔC_{carb}, ΔC_{sat} and ΔC_{res}. Their influence on ΔTC can be small compared to the influence of biogenic carbon (see Fig. 2, e.g. SEs 2, 6, 9) or large but partly cancelling each other (see Fig. 2, SEs 1, 3, 5, 10, 11), thus resulting in biogenic carbon "passing on" its linear relationship with $\overline{P^*}$ to ΔTC. $\overline{P^*}$ is important for the drawdown potential of a model (Fig. 8c), which is examined in the second step of the modelling (Section 4.2).

4.1.5 Sensitivity of residual and disequilibrium carbon

The global inventory of C_{res} in the SEs ranges between $-3.7 \cdot 10^{15} - 2.3 \cdot 10^{16}$ (c.f. global TC inventory of $\sim 3 \cdot 10^{18}$ mol). The contribution from ΔC_{res} to ΔTC ((Fig. 2 d)) is generally of the order $\sim 1 \cdot 10^{15}$, and the inventory of ΔC_{res} in the SEs changes c.f. $PIES278$ by 0–30 %.

When looking at ΔC_{res} (Fig. 2 d), we are mainly interested in the contribution by C_{dis}. We have previously confirmed that the contribution to ΔC_{res} by errors in calculations of biogenic carbon are negligible (Section 4.1.4), and we find that the ΔC_{res} given by Eqs. 4, B1 and B5-B6 corresponds closely to $\Delta\overline{DIC_{pre}} - C_{sat}$, where DIC_{pre} is preformed carbon from the model. Thus, ΔC_{res} is representative of ΔC_{dis}.

The processes influencing C_{dis} will be different in the deepwater formation areas in the Northern and Southern hemispheres (Toggweiler et al., 2003; Ito and Follows, 2005; Lauderdale et al., 2013). In the deepwater formation areas in the North Atlantic, C_{dis} is mainly a result of the temperature gradient. If a water parcel cools too fast before it sinks, there is not enough time to equilibrate with the atmosphere and the result will be a negative C_{dis}. This is seen as a negative signal in the NADW in Figure 9a–c. In a warmer global ocean, the temperature gradient between the equator and the poles is smaller. This makes it easier for a parcel travelling north in the Atlantic to reach equilibrium with the atmosphere before deepwater forms, since the parcel does not have to cool as much as in a colder simulation. In a warmer ocean, there is also less sea ice preventing

smaller. This makes it easier for a parcel travelling north in the Atlantic to reach equilibrium with the atmosphere before deepwater forms, since the parcel does not have to cool as much as in a colder simulation. In a warmer ocean, there is also less sea ice preventing exchange with the atmosphere. However, a warmer global ocean is often associated with faster circulation (see Section 4.1.1), and if the circulation becomes faster at the same time, the negative effect of the shorter time available for equilibration will compete with the positive effect of a smaller temperature gradient and less sea ice. In some cases, but not all, the warmer high latitude temperatures can compensate for the speed up of the circulation.

In the Southern Ocean there will also be less time for the surface water to equilibrate its gas concentrations with the atmosphere. Here, oversaturated deepwater coming back to the surface in this area may not have the time to release its carbon to the atmosphere before the water sinks back into the deep, producing positive C_{dis}. This appears as a positive signal in the lower half of the sections in Figure 9c. In a case with faster circulation, the contribution of positive C_{dis} will be even larger. This effect dominates over the temperature gradient effect in this area, because the waters being brought back to the surface are already very cold. However, in this model, the effect of sea ice on C_{dis} can also be very pronounced in this area, if it caps the upwelling area and prevents outgassing.

As we have seen in Figure 9, the local effects of C_{dis} for the simulations with artificially fast gas exchange are noticable. Despite this, the net effect on global ocean TC by the changes in C_{dis} is very small (on the order of 0.01 %). This is due to the fact that both the northern and the southern sinking are affected simultaneously; since they are of opposite signs they cancel each other. In a case with changes in ocean circulation, both sinking branches are not necessarily affected to equal amounts. As we will see below, this means the net effect on C_{dis}, and thus on TC, can still be significant.

Figure 9a shows the indication of C_{dis} in $SE1$ (halved atmospheric heat diffusivity), given by the runs with fast gas exchange for CO_2. We see a signal of positive C_{dis} originating in the Southern Ocean that is much more pronounced in $SE1$ compared to the control $PIES278$ (Fig 9c). $SE1$ is by far the coldest state and the global percentage of sea ice cover is doubled compared to $PIES278$ (for reference, in the second coldest state the sea ice cover has increased by less than 40 % compared to $PIES278$, see Table 2). It is likely that the extensive sea ice in $SE1$, to a larger extent than in the control, prevents the oversaturated deepwater from equilibrating with the atmosphere before sinking again. For $SE1$, the analysis of the run with artificially fast gas exchange reveals that the contribution of C_{dis} to C_{res} is large enough in this case to be critical for the sign of ΔTC (see $SE1$ in Figure 2); it shifts from being +0.64 $\cdot 10^{16}$ mol with normal gas exchange to being -0.43 $\cdot 10^{16}$ mol when the gas exchange is artificially fast.

Comparing panels b and c in Figure 9, we see that the differences are more difficult to attribute to one single process. The overturning circulation in $SE4$ is stronger than in $PIES278$. This makes the global ocean warmer, reduces sea ice, but also shortens the time for equilibration with the atmosphere in the North Atlantic branch. In this particular case of stronger circulation, the shorter time for equilibration dominates over the reduced temperature gradient and causes more negative disequilibrium in the North Atlantic deepwater formation area compared to the control in panel c. In the Southern Ocean, there is less sea ice, which allows more direct contact between the ocean and the atmosphere. However, due to the faster overturning, the deep waters that upwell here will quickly sink again. This is particularly seen in the Pacific sector, as a band of positive

exchange with the atmosphere. However, a warmer global ocean is often associated with faster circulation (see Section 4.1.1), and if the circulation becomes faster at the same time, the negative effect of the shorter time available for equilibration will compete with the positive effect of a smaller temperature gradient and less sea ice. In some cases, but not all, the warmer high latitude temperatures can compensate for the speed up of the circulation. In the Southern Ocean there will also be less time for the surface water to equilibrate its gas concentrations with the atmosphere. Here, oversaturated deepwater coming back to the surface in this area may not have the time to release its carbon to the atmosphere before the water sinks back into the deep, producing positive C_{dis}. This appears as a positive signal in the lower half of the sections in Figure 9c. In a case with faster circulation, the contribution of positive C_{dis} will be even larger. This effect dominates over the temperature gradient effect in this area, because the waters being brought back to the surface are already very cold. However, in this model, the effect of sea ice on C_{dis} can also be very pronounced in this area, if it caps the upwelling area and prevents outgassing. This effect is evident in $AD/2$, which has, by far, both the largest sea ice cover (10.6 %, Table 3) and the largest inventory of C_{dis} ($2.1 \cdot 10^{16}$ mol). The competing effects described above result in significant correlations betwen C_{res} (and similarily C_{dis}) and global OVT (Table 4), T_{avg} and sea ice cover (%) of -0.30, -0.65 and 0.50 respectively.

Comparing panels a and c in Figure 9, we see that the differences are difficult to attribute to one single process. The overturning circulation in $WSx2$ is stronger than in $PIES278$. This makes the global ocean warmer, reduces sea ice, but also shortens the time for equilibration with the atmosphere in the North Atlantic branch. In this particular case of stronger circulation, the shorter time for equilibration dominates over the reduced temperature gradient and causes more negative disequilibrium in the North Atlantic deepwater formation area compared to the control case in panel c. In the Southern Ocean, there is less sea ice, which allows more direct contact between the ocean and the atmosphere. However, due to the faster overturning, the deep waters that upwell here will quickly sink again. This is particularly seen in the Atlantic sector, as a band of positive C_{dis} extending from the surface and down, whereas in the control, the positive C_{dis} is more confined to just below the sea ice area.

In $AD/2$ (Fig. 9b), we see a signal of positive C_{dis} originating in the Southern Ocean that is much more pronounced compared to the control $PIES278$ (Fig. 9c). $AD/2$ is by far the coldest state and the global percentage of sea ice cover is doubled compared to $PIES278$ (for reference, in the second coldest state the sea ice cover has increased by less than 40 % compared to $PIES278$, see Table 3). It is likely that the extensive sea ice in $AD/2$, to a larger extent than in the control, prevents the oversaturated deepwater from equilibrating with the atmosphere before sinking again. For $AD/2$, the contribution of C_{dis} to C_{res} is large enough to be critical for the sign of ΔTC (see $AD/2$ in Figure 2).

4.2 Step 2 - Drawdown potential

In this step, we use the set of equilibrium states (SEs and the control $PIES278$) from step 1 as initial states for determining the drawdown potential, DP (Fig. 1). This reveals the dependence of the resulting equilibrium state $DE1--DE12$ on differences in the initial states $SE1$–$SE12$. The control drawdown equilibrium is denoted CDE. DP is computed as the difference in pCO_2^{atm} between 278 ppm and the drawdown equilibrium states.

The DP varies strongly between the ensemble members and is close to linearly related to the biological efficiency, in terms of $\overline{P^*}$, of the initial equilibrium state (Fig. 8 c). The near linear relationship between DP and $\overline{P^*}$ of the initial SE is expected

C_{dis} extending from the surface and down, whereas in the control, the positive C_{dis} is more confined to just below the sea ice area.

4.2 Step 2 - Drawdown potential

In this step, we use the set of equilibrium states (SE:s and the control $PIES278$) from step 1 as initial states for determining the drawdown potential, DP (Fig. 1). This reveals the dependence of the resulting equilibrium state $DE1 - DE12$ on differences in the initial states $SE1 - SE12$. The control drawdown equilibrium is denoted CDE. DP is computed as the difference in pCO_2^{atm} between 278 ppm and the drawdown equilibrium states.

The DP varies strongly between the ensemble members. We see that DP is close to linearly related to the biological efficiency, in terms of $\overline{P^*}$, of the initial equilibrium state (Fig. 6 c). The near linear relationship between DP and $\overline{P^*}$ of the initial SE is expected (see e.g. Marinov et al. (2008a)). If the biological efficiency in the SE is small, there is a larger pool of unused nutrients that can be used to capture carbon when biological efficiency is increased to 100 %. In this ensemble, an increase in biological efficiency manifested by an increase in $\overline{P^*}$ of 0.1, corresponds to a drawdown of CO_2 from the atmosphere of about 20-30 ppm. This is similar to the theoretical prediction by Ito and Follows (2005) of ~ 30 ppm.

However, the drawdown of atmospheric CO_2 achieved during the drawdown experiments is not purely due to biology. There are also indirect effects on pCO_2^{atm} due to changes in ocean temperature caused by changes in radiative balance, circulation and disequilibrium. Hence, we can not expect the model results to correspond exactly to the theoretical prediction in this case. The most prominent example is $SE1$, which has a low initial $\overline{P^*}$, but still has a low DP. This is the coldest of all initial states, with very high ocean sea ice cover (Table 2) compared to the other SE:a, and the cold conditions are likely to be affecting the conditions for biological production. Another example is that the near-linear relationship between $\overline{P^*}$ and DP does not predict DP to be exactly zero for $\overline{P^*} = 1$, as would have to be the case.

There is a tendency that those experiments that have a lower T_{avg} (thus a larger inventory of C_{sat}) compared to $PIES278$ have a smaller DP than those with higher temperatures (Fig. 10). This has to do with circulation changes acting in a predictable way. The circulation change that is causing a colder temperature is also causing the OVT to be weaker, and at the same time causing a more efficient biological pump (more C_{soft} and higher $\overline{P^*}$) and hence a smaller DP (Fig. 10). When OVT is weaker, there is more time for biology to take up nutrients and there is hence less preformed nutrients left at the surface, which means the DP will be smaller.

When compared to the CDE, there are two exceptions to the rule of colder temperatures in the initial state being associated with a smaller DP and warmer temperatures being associated with a larger DP; 1) $DE3$ (cyan star in Fig. 10), where the circulation in the initial state $SE3$ is slightly weaker than the control $PIES278$ (see Table S1 and Fig. 4). In this experiment, the Southern Ocean cell retreats while the NADW-cell expands. Since temperatures in the North Atlantic are higher, T_{avg} increases. In this case, DP is smaller, as expected for a case with weaker circulation. 2) $DE10$ (yellow square in Fig. 10), where the circulation in the initial state $SE10$ is stronger, but the global ocean temperature is in fact lower, than in the control $PIES278$, due to the expansion of the Southern Ocean cell. However, DP is still larger, as expected in a case with stronger circulation.

(see e.g. Marinov et al., 2008a). If the biological efficiency in the SE is small, there is a larger pool of unused nutrients that can be used to capture carbon when biological efficiency is increased to 100 %. In this ensemble, an increase in biological efficiency manifested by an increase in $\overline{P^*}$ of 0.1, corresponds to a drawdown of CO_2 from the atmosphere of about 20-30 ppm. This is similar to the theoretical prediction by Ito and Follows (2005) of ~ 30 ppm. However, the drawdown of atmospheric CO_2 achieved during the drawdown experiments is not purely due to biology. There are also additional effects on pCO_2^{atm} due to changes in ocean temperature (caused by changes in radiative balance), circulation and disequilibrium, and due to the climatic conditions of the initial state. Thus, the model results do not correspond exactly to the theoretical prediction in this case. The most prominent example is $AD/2$, which has a low initial $\overline{P^*}$, but still has a low DP. This is the coldest of all initial states, with very high ocean sea ice cover (Table 3) compared to the other SEs, and the cold conditions are likely to be affecting the conditions for biological production and disequilibrium. Note also that the near-linear relationship between $\overline{P^*}$ and DP does not predict DP to be exactly zero for $\overline{P^*} = 1$, as would have to be the case. When all climatic changes caused by the drawdown experiment itself are removed, DP is reduced by 4 – 7 ppm. This shows that the biological component is highly dominant in the total drawdown. However, the climatic differences between the initial states will still not allow the theoretical prediction to be exact.

Those experiments that have a lower T_{avg} (thus a larger inventory of C_{sat}) compared to $PIES278$) tend to have a smaller DP than those with higher temperatures, which is due to circulation changes acting in a predictable way. The circulation change that is causing a colder temperature is also causing the OVT to be weaker (Table 3), and at the same time causing a more efficient biological pump (more C_{soft}) (Fig. 4), because there is more time for biology to take up nutrients. Hence, there is less preformed nutrients left at the surface, which means $\overline{P^*}$ is higher and the DP is smaller.

5 Discussion

5.1 Solubility pump and disequilibrium

The effect on pCO_2^{atm} of a change in the solubility pump is approximately quantifyable from the change in global ocean average temperature, ΔT_{avg}, between two simulations, as described by Eq. (C9) suggested by Goodwin et al. (2011). According to this equation, the span of ΔT_{avg} in our ensemble would correspond to 10.5 $\pm$0.2 °C^{-1}. Solving the carbon system for the same span of ΔT_{avg} yields 12.8 $\pm$0.1 ppm °C^{-1}. The error in using the simplified equation seems to be on the order of 20 %. Depending on which process is causing the change in ocean circulation, the impact of changes in the solubility pump on pCO_2^{atm} can be almost as important as the impact of changes in the biological CO_2 efficiency of carbon uptake. For changes in ocean isopycnal diffusivity, the solubility pump effect is even the dominant response. Due to the temperature restriction on the CO_2 solubility constants (see Appendix B1), the effect of ΔC_{sat} is likely to be underestimated by on average 56 $\pm$67% in our results, further emphasising its importance. In previous studies, this has to some extent been disregarded, when the response of the biological pump has been assumed to be the dominant response to the applied changes in circulation (e.g., Archer et al., 2000a; Kwon et al., 2011).

5 Discussion

5.1 Solubility pump and disequilibrium

The effect on pCO_2^{atm} of a change in the solubility pump is approximately quantifyable from the change in global ocean average temperature, ΔT_{avg}, between two simulations, as described by Eq. (A9) suggested by Goodwin et al. (2011). According to this equation, the span of ΔT_{avg} in our ensemble would correspond to 9.1–11.1 ppm °C^{-1} (linear fit: 9.8 ppm °C^{-1}). Solving the carbon system for the same span of ΔT_{avg} yields 12.5–13.1 ppm °C (linear fit: 12.9 ppm °C^{-1}). The error in using the simplified equation seems to be on the order of 20 %. Depending on which process is causing the change in ocean circulation, the impact of changes in the solubility pump on pCO_2^{atm} can be almost as important as the impact of changes in the biological CO_2 efficiency of carbon uptake. For changes in ocean horizontal diffusivity, the solubility pump effect is even the dominant response. In previous studies, this has to some extent been disregarded, when the response of the biological pump has been assumed to be the dominant response to the applied changes in circulation (e.g., Archer et al., 2000a; Kwon et al., 2011).

It has been more difficult to quantify the effects of CO_2 disequilibirum, but in this model it appears to be particularily important in simulations with a lot of sea ice (e.g. $SE1$). This leads us to the conclusion that it may also be of importance in glacial simulations. A caveat to this finding is cGENIE's coarse resolution at high latitudes, and its simplified representation of sea ice as a complete barrier to gas exchange. If we assume that calculation errors are small, and thus that ΔC_{res} is mainly due to ΔC_{dis}, the circulation changes we impose would contribute $\sim$ 10–30 ppm of atmospheric CO_2, which is comparable to the results of Marinov et al. (2008a).

5.2 Implications for model validation

When comparing model studies, it is important to recognize differences in biological efficiency in their control states. The pre-industrial $\overline{P^*}$ of a model will determine its pre-industrial inventory of C_{soft} but also its drawdown potential. If the pre-industrial $\overline{P^*}$ is incorrect, the total carbon inventory in the model will adjust to compensate this error, in order to achieve equilibirum with pre-industrial pCO_2^{atm}. Hence, failing to tune the models for pre-industrial $\overline{P^*}$ will mean that they start from a non-representative state of the carbon system. Thus, models with different initial $\overline{P^*}$ will have different ΔpCO_2 in response to similar circulation changes. This point was mentioned in Marinov et al. (2008a), but does not seem to have been picked up in the model intercomparison community and, still, models are not tuned for $\overline{P^*}$. The range of $\overline{P^*}$ in our pre-industrial ensemble ($SE1 - SE12$) is 0.34–0.62. This range includes the current estimate for the global ocean, which according to Ito and Follows (2005) is 0.36. Our range in initial state $\overline{P^*}$ corresponds to a range in drawdown potential of 94–139 ppm. While using a different model, but a similar approach, we confirm the conclusion of Marinov et al. (2008a) and want to stress the importance of a similar initial efficiency of the biological pump in model intercomparison studies where CO_2 drawdown is diagnosed.

Few studies have simultaneously diagnosed the individual contributions by the solubility and biological pumps and the effect of surface CO_2 disequilibrium. Studies by Lauderdale et al. (2013) and Bernardello et al. (2014) use a similar separation of the carbon storage processes as we do. For increases in wind stress, the sign of ΔTC (and thus of ΔpCO_2^{tm}) and the

The relationship between the changes in T_{avg} and$\Delta C_{sat,T}$ is close to linear (Fig. 6). Any deviation from a perfect, straight line is caused by the temperature restriction on the solubility equation (Appendix B1) The slope of the line is $\overline{\frac{\partial C_{sat}}{\partial T}} = -0.59 \cdot 10^{16}$ mol °C^{-1}. If the global ocean cooled by $\sim$ 2.6 °C, as expected in a glacial state (Headly and Severinghaus, 2007), the slope of the line suggests the excursion in C_{sat} would be $\sim 1.5 \cdot 10^{16}$ mol. Note that this excursion is underestimated due to the restriction on the solubility equation. In the context of a 2.6 °C cooling, the carbon system equations (see Appendix C) yield a corresponding decrease of about 30 ppm in pCO_2^{atm}. Here, we cannot use the simplified Eq. (C9), because the buffered carbon inventory is unknown in this hypothetical case.

In a set of idealised GCM simulations, Eggleston and Galbraith (2017) show that CO_2 disequilibirum can be as important as C_{soft}. In this ensemble, the effects of C_{dis} appear to be particularily important in simulations with a lot of sea ice (e.g. $AD/2$, see Fig. 2d,h). This leads us to the conclusion that it may also be of importance in glacial simulations. A caveat to this finding is cGENIE's coarse resolution at high latitudes, and its simplified representation of sea ice as a complete barrier to gas exchange. Assuming that ΔC_{res} is mainly due to ΔC_{dis}, the circulation changes we impose correspond to a change in pCO_2^{atm} of $\sim -30 - -+10$ ppm due to ΔC_{dis}. This is comparable to the results of Marinov et al. (2008a), while Eggleston and Galbraith (2017) suggest as much as $\sim 40 - -70$ ppm drawdown of CO_2 due to increased C_{dis} in glacial like simulations. This emphasises the need for further studies on the role of C_{dis} in glacial as well as other climate scenarios with changes in ocean cirulation.

5.2 Implications of changes in OVT in relation to changes in carbon

In experiments with stronger OVT (global and basin scale) than in $PIES278$, e.g. $DDx2$ (Figs. 5a and 7a), a water parcel will, on average, stay near the ocean surface for a shorter time than if the OVT is weaker (e.g $DD/2$, see Figs. 5b and 7b). Hence, biology will have less time to use the available nutrients and this will give less C_{soft}, thus ΔC_{soft} has a strong negative correlation with OVT (Fig. 4, Table 4). Changes in OVT explains 75-80% of the variance in C_{soft} in the SE ensemble, while the rest of the variance is likely explained by e.g. redistribution of nutrients, light limitation regions or similar. Meanwhile, with stronger OVT there will be more mixing, leading to a deepening of the thermocline, and T_{avg} will increase (Fig. 7a, Tables 3 and 4). Thus, the correlation with $\Delta C_{sat,T}$ will also be negative, though weaker (43–64 %). The response of ΔC_{dis} is more difficult to predict from the OVT, due to competing changes in the temperature gradient (especially important in the North Atlantic), sea ice and outgassing (dominant in the Southern Ocean) resulting from a change in OVT. Interestingly, the total carbon inventory TC shows a closer correlation with the OVT than any of the individual ocean carbon components (Figs. 3 and 4, Table 4). Thus, the inventories of the individual DIC components are affected by the choice of model tuning strategy, whereas the total carbon inventory is mainly a result of the strength of the circulation i.e. the ventilation of the deepwater. Similar results are found for C_{soft} and C_{dis} by Eggleston and Galbraith (2017), who describe the changes in ocean ventilation using an ideal age tracer. Here, we show that the correlation with ocean ventilation holds even stronger for total carbon and is also present for C_{sat}.

individual contributions by the carbon pumps and C_{dis} agree with those found by Lauderdale et al. (2013). Compared to the scenario-specific results of Bernardello et al. (2014), our results could be used more generally as a way of anticipating the model behaviour, based on in which way the ocean circulation changes in a model study. Depending on in which way we have changed the ocean forcing, and what the resulting effect on ocean circulation is, the origin of the change in ocean carbon storage is different. When wind stress or ocean vertical diffusivity is changed, the response of the biological pump gives the most important effect on ocean carbon storage, whereas when atmospheric heat diffusivity or ocean horizontal diffusivity is changed, the solubility pump and the disequilibrium component are also important and sometimes dominant. Our results give a first approximation of the effect of these ocean circulation changes on the ocean carbon storage, but it is important to keep in mind that the results of changes in individual parameters do not always combine linearly. For example, in the case of halved winds combined with low ocean vertical diffusivity ($SE12$), we see that the response of the biological pump in the combined case is more or less a linear combination of the cases where these changes were made individually (SE:s 3 and 5 respectively). However, the solubility pump behaves in the same way as in the case with low ocean vertical diffusivity and control state winds ($SE5$). This is because the low ocean vertical diffusivity is more important for the global ocean mean temperature, and thus for the solubility pump, than the surface wind stress.

5.3 Implications for glacial studies

We have shown that, when comparing model simulations with the same pCO_2^{atm}, but with differences in ocean circulation and AMOC strength, the compared simulations will have different carbon inventories, and different strengths of the ocean carbon pumps. In the PMIP3 intercomparison project, where glacial simulations with different models are compared, the models are forced with glacial pCO_2^{atm} to achieve the LGM state (https://pmip3.lsce.ipsl.fr/). The ocean circulation state is however not specified. Otto-Bliesner et al. (2007) showed that model simulations in the PMIP2 project developed very different LGM ocean circulation patterns and specifically large differences in AMOC strength, despite displaying similar ocean circulation patterns in pre-industrial simulations. Most models in the studied ensemble had been initiated with pre-industrial circulation and LGM boundary conditions according to the PMIP2 protocol. When run to quasi-equilibrium, some models would develop an LGM-like circulation (when compared to proxy data) and some would keep a more pre-industrial like simulation. Since the ocean circulation patterns differ, the ocean carbon storage and thus the model carbon inventories of the compared PMIP-simulations also differ. This will be important when comparing e.g. deglacial scenarios run with these different models (e.g., Zhang et al., 2013).

When attempting to simulate the glacial CO_2 drawdown, it is crucial to critically evaluate the changes in forcing that need to be applied to achieve a glacial state in the model. We should ask ourselves whether these changes agree with what we believe actually happened in the climate system during a glacial.

When applying PMIP3 boundary conditions for the LGM, the height of the ice sheet in the northern hemisphere will tend to intensify both the wind stress over the North Atlantic basin and as a result the AMOC-circulation (Muglia and Schmittner, 2015). Similar effects on the wind fields due to the Laurentide ice sheet are seen in e.g. Löfverström et al. (2014). Sime et al. (2013) suggest that Southern Hemisphere winds will also be stronger when applying LGM boundary conditions, though they

5.3 Implications for model validation

When comparing model studies, it is important to recognize differences in biological efficiency in their control states. The pre-industrial $\overline{P^*}$ of a model will determine its pre-industrial inventory of C_{soft} but also its drawdown potential. If the pre-industrial $\overline{P^*}$ is incorrect, the total carbon inventory in the model will adjust to compensate this error, in order to achieve equilibirum with pre-industrial pCO_2^{atm}. Hence, failing to tune the models for pre-industrial $\overline{P^*}$ will mean that they start from a non-representative state of the carbon system. Thus, models with different initial $\overline{P^*}$ will have different ΔpCO_2 in response to similar circulation changes. This point was mentioned in Marinov et al. (2008a) and emphasised by Duteil et al. (2012), but does not seem to have been recognised in the model inter-comparison community and, still, models are not tuned for $\overline{P^*}$. The range of $\overline{P^*}$ in our pre-industrial ensemble ($SE1$–$SE12$) is 0.32–0.59. This range includes the current estimate for the global ocean, which according to Ito and Follows (2005) is 0.36. Our range in initial state $\overline{P^*}$ corresponds to a range in drawdown potential of 94–139 ppm. While using a different model, but a similar approach, we confirm the conclusion of Marinov et al. (2008a) and want to stress the importance of a similar initial efficiency of the biological pump in model inter-comparison studies where CO_2 drawdown is diagnosed.

Few studies have simultaneously diagnosed the individual contributions by the solubility and biological pumps and the effect of surface CO_2 disequilibrium. Studies by Ito and Follows (2013), Lauderdale et al. (2013), Bernardello et al. (2014) and Eggleston and Galbraith (2017) use a similar separation of the carbon storage processes as we do. For increases in wind stress, the sign of ΔTC (and thus of ΔpCO_2^{atm}) and the individual contributions by the carbon pumps and C_{dis} agree with those found by Lauderdale et al. (2013). In our ensemble, the anomalies in C_{soft} and $C_{sat,A}$ in the equilibrium states, resulting from differences in circulation between ensemble members, tend to be partially compensating each other. Thus, ΔTC does not fully reveal the magnitude of the differences in the individual carbon pumps between ensemble members. We show that the differences in equilibrium state efficiency of the biological pump between SEs manifests itself as as differences in model sensitivity to the perturbation in biological pump efficiency, as predicted by Ito and Follows (2013). Our result can be important for future model inter-comparison studies, in explanations of results, but also in planning for common tuning strategies and experimental design. Compared to the scenario-specific results of Bernardello et al. (2014), our results could be used more generally as a way of anticipating the model behaviour, based on in which way the ocean circulation changes in a model study. Depending on in which way we have changed the ocean forcing, and what the resulting effect on ocean circulation is, the origin of the change in ocean carbon storage is different. When wind stress (WS) or ocean diapycnal diffusivity (DD) is changed, the response of the biological pump gives the most important effect on ocean carbon storage, whereas when atmospheric heat diffusivity (AD) or ocean isopycnal diffusivity (ID) is changed, the solubility pump and the disequilibrium component are also important and sometimes dominant. Our results give a first approximation of the effect of these ocean circulation changes on the ocean carbon storage, but it is important to keep in mind that the results of changes in individual parameters do not always combine linearly. For example, with doubled atmospheric heat diffusivity ($ADx2$) and doubled ocean diapycnal diffusivity ($DDx2$), the response of the solubility pump is very similar in both simulations. In the combined simulation ($ADx2\_DDx2$), the response of the solubility pump is larger, but far from doubled, and the response of the soft tissue pump is smaller than

in $DDx2$ alone. In this particular case, it is difficult to discern which of these two parameters has the strongest impact on the system.

The four different preformed model tracers (P_{pre}, DIC_{pre} ,O_{2pre}, A_{pre}) are shown to be useful for accurate determination of the initial state carbon partitioning and nutrient utilisation efficiency, of which we demonstrate the importance for model drawdown potential. They eliminate errors associated with indirect methods used to determine AOU and A_{pre} (as described by e.g., Ito et al., 2004; Bernardello et al., 2014; Eggleston and Galbraith, 2017), and facilitate error estimates for the carbon partitioning methods. Some useful applications of preformed tracers have previously been presented by e.g. Marinov et al. (2008b), Bernardello et al. (2014) and Eggleston and Galbraith (2017), but such extensive use of preformed tracers is, to our knowledge, unprecedented in studies of the ocean carbon system.

5.4 Implications for glacial studies

We have shown that, when comparing model simulations with the same pCO_2^{atm}, but with differences in ocean circulation and overturning circulation strength (OVT, see Section 3.4), the compared simulations will have different carbon inventories, and different strengths of the ocean carbon pumps. In the PMIP3 inter-comparison project, where glacial simulations with different models are compared, the models are forced with glacial pCO_2^{atm} to achieve the LGM state (https://pmip3.lsce.ipsl.fr/). The ocean circulation state is however not specified. Otto-Bliesner et al. (2007) showed that model simulations in the PMIP2 project developed very different LGM ocean circulation patterns and specifically large differences in AMOC strength, despite displaying similar ocean circulation patterns in pre-industrial simulations. Most models in the studied ensemble had been initiated with pre-industrial circulation and LGM boundary conditions according to the PMIP2 protocol. When run to quasi-equilibrium, some models would develop an LGM-like circulation, with a shallower boundary between NADW and AABW than today, as indicated by paleonutrient tracers (see e.g., Marchitto and Broecker, 2006), and some would keep a more pre-industrial like circulation. Since the ocean circulation patterns differ, the ocean carbon storage and thus the model carbon inventories of the compared PMIP-simulations also differ. This will be important when comparing e.g. deglacial scenarios run with these different models (e.g., Zhang et al., 2013).

When attempting to simulate the glacial CO_2 drawdown, it is crucial to critically evaluate the changes in forcing that need to be applied to achieve a glacial state in the model. We should ask ourselves whether these changes agree with what we believe actually happened in the climate system during a glacial. When applying PMIP3 boundary conditions for the LGM, the height of the ice sheet in the northern hemisphere will tend to intensify both the wind stress over the North Atlantic basin and as a result the AMOC-circulation, (Muglia and Schmittner, 2015; Klockmann et al., 2016). In a full glacial state, the associated deepening of the AMOC is however counteracted by the decrease in pCO_2^{atm} (Klockmann et al., 2016). Similar effects on the wind fields due to the Laurentide ice sheet are seen in e.g. Löfverström et al. (2014). Sime et al. (2013) and Sime et al. (2016) suggest that Southern Hemisphere winds will also be stronger when applying LGM boundary conditions, though they emphasise that results from different palaeoproxies and models disagree on this. In our simulation, we intensify the wind stress in both hemispheres and this leads to decreased capacity of both the biological and the solubility pump, and effectively an increase in pCO_2^{atm}. Lauderdale et al. (2013) showed similar results, but for increased Southern Ocean winds. Hence, the

emphasise that results from different palaeoproxies and models disagree on this. In our simulation, we intensify the wind stress in both hemispheres and this leads to decreased capacity of both the biological and the solubility pump, and effectively an increase in pCO_2^{atm}. Lauderdale et al. (2013) showed similar results, but for increased Southern Ocean winds. Hence, the changes in wind fields achieved by the applied LGM boundary conditions in models may be contributing to the difficulties in simulating the glacial decrease in pCO_2^{atm}.

In those of our ensemble members where ocean vertical diffusivity is halved, we achieve some glacial-like ocean characteristics; the circulation is weaker, the global ocean temperature is colder and the biological pump is stronger. However, it has been shown by Schmittner et al. (2015) that open ocean mixing is likely to have been intensified during glacials, when lower sea level made shelf areas decrease and tidal mixing was shifted to the deep ocean. In their model, global ocean mean vertical diffusivity increased by more than a factor of 3, leading to an intensification of ocean overturning. In our experiments, a doubling of vertical diffusivity leads to a decrease in ocean carbon storage corresponding to an increase of pCO_2^{atm} of more than 20 ppm (see $SE6$ in Figure 2). Hence, in a full glacial scenario, processes causing increased ocean carbon storage would have to offset this effect before causing any net decrease in pCO_2^{atm}. Other effects on glacial pCO_2^{atm} linked to lower sea level (reduced ocean volme) during glacials, caused by higher salinity, and higher concentration of DIC, alkalinity and nutrients, have been constrained to +12–16 ppm (Köhler and Fischer, 2006; Brovkin et al., 2007; Kohfeld and Ridgwell, 2009). In this process study we are not aiming to reproduce LGM conditions in the model and such effects of changes in ocean volume are beyond the scope of our investigations. Ocean volume, and global averages of salinity, alkalinity and phosphate have thus been kept constant in our simulations.

Since numerous studies of proxy data indicate that the global ocean was in fact less ventilated during glacials (e.g., Broecker et al., 1990; Sikes et al., 2000; Keigwin and Schlegel, 2002; Skinner et al., 2010, 2015), it seems possible that the effect of increased mixing was indeed offset by some other process. One such factor could be that the global ocean was saltier and more stratified (Ballarotta et al., 2014). In our simulations, weaker overturning circulation is also connected to colder temperatures. These cold simulations show a tendency towards lower drawdown potentials. It is likely that the more sluggish circulation is already allowing a more efficient biological pump, leading to a higher $\overline{P^*}$ and thus a smaller drawdown potential.

6 Conclusions

In this paper, we have studied three mechanisms for ocean carbon storage — the biological pump, the solubility pump and the contribution from air-sea CO_2 disequilibrium — and quantified the response of these mechanisms to differences in the equilibrium ocean circulation state. For a given set of equilibrium states in the model cGENIE, we have constrained the response of the carbon storage associated with the first two mechanisms reasonably well and diagnosed their influence on pCO_2^{atm}. We have also seen some response related to ocean CO_2 disequilibrium.

We have obtained different states of equilibrium ocean circulation by varying forcings and model parameters (listed in Table 1) in a model ensemble. This was not done with the aim to achieve a glacial-like circulation, but to study how the ocean carbon storage responds to changes in a wide range of circulation processes. We change forcing parameters such as wind stress, ocean

changes in wind fields achieved by the applied LGM boundary conditions in models may be contributing to the difficulties in simulating the glacial decrease in pCO_2^{atm}.

In those of our ensemble members where ocean diapycnal (i.e. near vertical) diffusivity is halved, we achieve some glacial-like ocean characteristics; the circulation is weaker, the global ocean temperature is colder and the biological pump is stronger. However, it has been shown by Schmittner et al. (2015) that open ocean mixing is likely to have been intensified during glacials, when lower sea level made shelf areas decrease and tidal mixing was shifted to the deep ocean. In their model, global ocean mean vertical diffusivy increased by more than a factor of 3, leading to an intensification of ocean overturning. In our experiments, a doubling of diapycnal diffusivity leads to a decrease in ocean carbon storage corresponding to an increase of pCO_2^{atm} of more than 20 ppm (see $DDx2$ in Figure 2e). Hence, in a full glacial scenario, processes causing increased ocean carbon storage would have to offset this effect before causing any net decrease in pCO_2^{atm}. Other effects on glacial pCO_2^{atm} linked to lower sea level (reduced ocean volme) during glacials, caused by higher salinity, and higher concentration of DIC, alkalinity and nutrients, have been constrained to +12–16 ppm (Köhler and Fischer, 2006; Brovkin et al., 2007; Kohfeld and Ridgwell, 2009). In this process study we are not aiming to reproduce LGM conditions in the model and such effects of changes in ocean volume are beyond the scope of our investigations. Ocean volume, and global averages of salinity, alkalinity and phosphate have thus been kept constant in our simulations.

Since numerous studies of proxy data indicate that the global ocean was in fact less ventilated during glacials (e.g., Broecker et al., 1990; Sikes et al., 2000; Keigwin and Schlegel, 2002; Skinner et al., 2010, 2015), it seems possible that the effect of increased mixing was indeed offset by some other process. One such factor could be that the global ocean was saltier and more stratified (Ballarotta et al., 2014). In our simulations, weaker overturning circulation is also connected to colder temperatures. These cold simulations show a tendency towards lower drawdown potentials. It is likely that the more sluggish circulation is already allowing a more efficient biological pump, leading to a higher $\overline{P^*}$ and thus a smaller drawdown potential. According to Headly and Severinghaus (2007), the global average temperature of the glacial ocean was 2.6 ± 0.6 °C colder than the modern day ocean. Since the ensemble member with the coldest ocean is only 1.3 °C colder than $PIES278$, the variations in C_{sat} during the past glacial cycles were likely larger than in our set of experiments, allowing for a larger contribution by the solubility pump. Hence, the colder temperatures could play an important role in offsetting the effect of increased mixing. Fig. 7 suggests that ΔC_{sat} for a change in T_{avg} of -2.6°C c.f. pre-industrial would be approximately $1.5 \cdot 10^{16}$ mol (180 GtC), whereas ΔC_{sat} for the coldest of our simulations is only $0.58 \cdot 10^{16}$ mol (70 GtC). If we account for a likely underestimation of ΔC_{sat} of ~ 50 % (see Section 4.1.3 and Appendix B1) in Fig. 6, a simulation as cold as the LGM state suggested by Headly and Severinghaus (2007) would have an increase in strength of the solubility pump corresponding to ~ 300 GtC. Another important mechanism for the global glacial deep ocean circulation is surface buoyancy loss around Antarctica driven by the brine rejection associated with sea ice formation (Klockmann et al., 2016; Marzocchi and Jansen, 2017). This effect is not explored in our simulations.

In our ensemble of simulations, 100 % nutrient utilisation efficiency (NUE) causes more drawdown than is necessary to reach glacial values. Future efforts need to deduce how big an increase in NUE we could expect for a glacial, when using proxy data of e.g. iron fertilisation (e.g., Petit et al., 1999) and water mass properties (e.g., Elderfield and Rickaby, 2000) as

diffusivity and atmospheric heat diffusivity and run the model to equilibrium while keeping atmospheric CO_2 constant. We study the response of the three mechanisms for ocean carbon storage and relate it to differences in ocean circulation strength. In cases with weaker circulation, we see that the ocean's capacity for carbon storage is larger. The contributions to the change in carbon storage by the solubility pump, the biological pump or CO_2 disequilibrium are different depending on the origin of the ocean circulation change. When wind stress or ocean vertical diffusivity is changed, the response of the biological pump has the strongest impact on ocean carbon storage. In contrast, when atmospheric heat diffusivity or ocean horizontal diffusivity is changed, the solubility pump and the disequilibrium component also give important, and sometimes dominant, contributions to the change in ocean carbon storage.

Finally, to constrain the biological pump, we used the SE ensemble members (Fig. 1) as initial states to see how their pCO_2^{atm} responded when the model was forced into a state with 100 % efficient biology. We applied similar adjustments to circulation parameters as those tested in Marinov et al. (2008b), in order to allow some direct comparison of our results with their study. In agreement with Marinov et al. (2008b), we find that the drawdown potential of an ensemble member is a direct result of its biological efficiency, as measured by the ratio between global average regenerated ($\overline{P_{reg}}$) and total ($\overline{P}$) phosphorus, denoted $\overline{P^*}$, in its initial equilibirum state.

This study shows that, a model's control pre-industrial state will determine the sensitivity of the mechanisms for ocean carbon storage to changes in biological efficiency. Often, a model with stronger circulation will have a higher global ocean mean temperature, thus a weaker solubility pump, and lower biological efficiency, thus also a weaker biological pump. This leads to that model having a smaller ocean carbon inventory in the control state, but a larger drawdown potential for CO_2, compared to a model with weaker circulation. Hence, when different models are used to simulate a glacial scenario, it is likely that a significant part of the difference in their CO_2 drawdown potentials results from differences that are already present, but not directly visible, in their control states. This has potentially important implications for model intercomparison studies.

In our entire ensemble of simulations, 100 % nutrient utilisation efficiency causes more drawdown than necessary to reach glacial values. Future efforts need to deduce how big an increase in nutrient utilisation we could expect for a glacial, when using proxy data of e.g. iron fertilisation (e.g., Petit et al., 1999) and water mass properties (e.g. Elderfield and Rickaby, 2000) as a constraint. By understanding how ocean circulation changes during the glacials may have contributed to altering the ocean nutrient utilisation efficiency, it will be easier to quantify how much it may have increased due to e.g. fertilisation by deposition of iron from dust. However, recent studies have shown that there may have been more, not less, preformed nutrients in the deep ocean during the last glacial, which implies less efficient nutrient utilisation by biology Homola et al. (2015). One aspect that could explain how more carbon could still be trapped by biology in such a case is if the stoichiometric ratios in a glacial scenario no longer follow the averages described by Redfield (1963). In most climate models, this is currently not taken into account. Implementation of variable stoichiometry in models could however bring interesting insights in the future.

a constraint. By understanding how ocean circulation changes during the glacials may have contributed to altering the ocean NUE, it will be easier to quantify how much it may have increased due to e.g. fertilisation by deposition of iron from dust. However, on-going studies indicate that there may have been more, not less, preformed nutrients in the deep ocean during the last glacial (Homola et al., 2015, and Spivack, A. J. (P.C., 2015)), which implies less efficient nutrient utilisation by biology. One aspect that could explain how more carbon could still be trapped by biology in such a case is if the stoichiometric ratios in a glacial scenario no longer follow the averages described by Redfield (1963). In most climate models, this is currently not taken into account. Implementation of variable stoichiometry in models could however bring interesting insights in the future.

6 Conclusions

In this paper, we have studied three mechanisms for ocean carbon storage — the biological pump, the solubility pump and the contribution from air-sea CO_2 disequilibrium — and quantified the response of these mechanisms to differences in the equilibrium ocean circulation state. For a given set of equilibrium states in the model cGENIE, we have constrained the response of the carbon storage associated with the first two mechanisms reasonably well and diagnosed their influence on pCO_2^{atm}. We have also seen some response related to ocean CO_2 disequilibrium.

We have obtained different states of equilibrium ocean circulation by varying forcings and model parameters (listed in Table 1) in a model ensemble, while keeping atmospheric CO_2 constant. This was not done with the aim to achieve a glacial-like circulation, but to study how the ocean carbon storage responds to changes in a wide range of circulation processes and relate the response of the three mechanisms for ocean carbon storage to differences in ocean circulation strength. The contributions to the change in carbon storage by the solubility pump, the biological pump or CO_2 disequilibrium are different depending on the origin of the ocean circulation change, i.e. the model tuning strategy. When wind stress or ocean diapycnal diffusivity is changed, the response of the biological pump has the strongest impact on ocean carbon storage. In contrast, when atmospheric heat diffusivity or ocean isopycnal diffusivity is changed, the solubility pump and the disequilibrium component also give important, and sometimes dominant, contributions to the change in ocean carbon storage. Despite this complexity, we obtain a negative linear relationship between total ocean carbon and the combined strength of the northern and southern overturning cells. This relationship is robust to different reservoirs dominating the response to different forcing mechanisms. We show that the individual carbon components are all to some extent correlated with the strength of the circulation, but they combine in a way that makes the response in total carbon inventory be nearly fully explained by changes in circulation strength.

Finally, to constrain the biological pump, we used the SE ensemble members (Fig. 1) as initial states to see how their pCO_2^{atm} responded when the model was forced into a state with 100 % efficient biology. We applied similar adjustments to circulation parameters as those tested in Marinov et al. (2008b), in order to allow some direct comparison of our results with their study. In agreement with Marinov et al. (2008b), we find that the drawdown potential of an ensemble member is a direct result of its biological efficiency, as measured by the ratio between global average regenerated ($\overline{P_{reg}}$) and total ($\overline{P}$) phosphorus, denoted $\overline{P^*}$, in its initial equilibirum state. We show that it is possible to quantify, from theory, the effect of biases in the carbon inventory of a model's control state on its sensitivity to changes in the biological pump. We test a wide range of changes to the

forcing in order to demonstrate that the result is robust. This result should be of value in understanding the biases of individual models, in model inter-comparison studies, and potentially for choosing tuning criteria. Often, a model with stronger circulation will have a higher global ocean mean temperature, thus a weaker solubility pump, and lower biological efficiency, thus also a weaker biological pump. This leads to that model having a smaller ocean carbon inventory in the control state, but a larger drawdown potential for CO_2, compared to a model with weaker circulation. Hence, when different models are used to simulate a glacial scenario, it is likely that a significant part of the difference in their CO_2 drawdown potentials results from differences that are already present, but not directly visible, in their control states.

Code and data availability. The source code for cGENIE is publically available at http://www.seao2.info/mycgenie.html. Data is available upon request (e-mail to the corresponding author).

Appendix A: The ocean carbon system

A1 The ocean carbon pumps

The abiotic, physical pathway, or *the solubility pump*, begins with air-sea gas exchange, which acts to achieve a chemical equilibrium between the atmosphere and the surface ocean. This equilibrium depends on temperature. The ocean circulation then advects both the temperature and the dissolved carbon into the deep ocean. This carbon is also referred to as *preformed* carbon. Since the solubility of CO_2 is larger in colder water, the sinking cold water is enriched in carbon compared to surface waters in warmer regions.

The biological pathway, or *the biological pump*, begins with biological production in the surface ocean. Carbon is incorporated into soft-tissue organic compounds. Some of this material then reaches the deep ocean, either by being advected in currents or by falling out of the surface layer. When the organic material is decomposed, inorganic carbon (CO_2) comes back into dissolution in the water. This fraction of DIC is referred to as *regenerated* carbon. Carbon is also incorporated into hard tissue (shells) in the form of $CaCO_3$ which can be dissolved in the deep ocean. This dissolution influences deep ocean alkalinity (Section 2).

Due to the difference in the chemical role of soft-tissue and hard-tissue carbon, the biological pump is more correctly referred to as being two separate pumps; the soft-tissue pump and the carbonate (hard-tissue) pump (e.g., Sarmiento and Gruber, 2006; Kohfeld and Ridgwell, 2009). The soft-tissue pump acts to increase deep ocean DIC. The carbonate pump has a counter effect, because uptake of $CaCO_3$ for shell formation reduces alkalinity and the capacity to dissolve CO_2 in the surface ocean. The soft-tissue pump is stronger than the carbonate pump. Therefore, the net effect of the biological pump is to enhance the deep ocean concentration of DIC.

A2 Nutrient utilisation efficiency and P^*

Biology in the surface ocean uses a fraction of the available nutrients to produce new organic material and binds CO_2 in the process. The remaining, unused (or preformed), nutrients, denoted P_{pre}, are brought with the circulation (the physical pathway) into the deep ocean, where no new production is possible. The nutrients transported to the deep ocean via the biological pump are called regenerated nutrients, P_{reg}. If the biology becomes more efficient at using the nutrients in the surface ocean, the fraction of P_{reg} in the deep ocean increases and P_{pre} decreases.

As described in the framework introduced by Ito and Follows (2005), the global average of P_{reg} relative to the overall global average concentration of inorganic nutrients (denoted by P) is a measure of nutrient utilisation efficiency, NUE. This can be described using the parameter P^*,

$$\overline{P^*} = \frac{\overline{P_{reg}}}{\overline{P}}. \quad \text{(A1)}$$

Here, the overbars mark that we are using the global average of a quantity. If $\overline{P^*}$ is 1, all available nutrients in the deep ocean were brought there by the biological pump. In other words, the deep ocean is ventilated by surface waters that have had all nutrients removed, hence (at steady state,) the ocean interior will have no P_{pre}.

To calculate $\overline{P^*}$ (Eq. A1), we need to know $\overline{P_{reg}}$, the concentration of dissolved phosphate in the deep ocean that is of regenerated origin. We get P_{reg} by removing P_{pre} from the concentration of total phosphate, P.

Appendix B: Separation of carbon species

In this section, the calculations of the total carbon inventory described by Eq. 3 are described in detail.

The atmospheric carbon content, which in this model is limited to its content of CO_2, is given by the partial pressure of CO_2 times the number of moles of gas in the atmosphere, M_a. Assuming an atmospheric thickness of 7,777 m, M_a is given to $1.7692 \cdot 10^{20}$ mol. In this case 1 ppm of CO_2 corresponds to 2.123 PgC, which is consistent with the OCMIP recommendation. M_o is the mass of the ocean [kg], which in our ensemble of simulations is kept constant at $1.34 \cdot 10^{21}$ kg. Implications of changes in volume are further discussed in Section 5.4. Calculations of C_{sat}, C_{soft} and C_{carb} are described in Sections B1-B2. C_{res} is the residual between the sum of the calculated C_{sat}, C_{soft} and C_{carb} and the actual carbon concentration in the water parcel, which includes DIC and organic matter (POC and DOC). C_{res} contains three components; 1) The first, and most interesting, contribution to C_{res} is the disequilibrium component C_{dis}. This is the part of the water parcel carbon concentration which results from the water parcel not being in perfect equilibrium with the atmosphere at the time when it left the surface. Hence, the concentration of carbon of abiotic origin (preformed carbon) in the water parcel consists of $C_{sat} + C_{dis}$. We can therefore use the relation $C_{dis} = C_{pre} - C_{sat}$ to estimate this component of C_{res}, though we need to keep in mind that it there are calculation errors associated with C_{sat} that will affect this estimate (see point 3 below). 2) The second contribution to C_{res} is the presence of carbon in the form of particulate and dissolved organic matter. At any one model time step, the concentration of such carbon is very small compared to the other terms in the equation (<1 %, $\sim 1 \cdot 10^{15}$ mol) and this is therefore not

considered separately. It is however included when model TC is quantified. 3) The third contribution to C_{res} consists of the errors associated with any imperfect assumptions in the theory used for calculating C_{sat}, C_{soft} and C_{carb}. These are further discussed in Sections B1-B2.

B1 Contribution by the solubility pump

For one individual water parcel, C_{sat} corresponds to the concentration [mol kg^{-1}] of carbon the water parcel would have had if it would have been in equilibrium with the atmosphere, taking into account its temperature, salinity, alkalinity and also the minor effect of the concentration of PO_4 in the absence of biology. We calculate the global average of grid cell $C_{sat}(T_{SE_n}) - C_{sat}(T_{PIES278})$ solving the carbon system equations using the solver CO2SYS (Lewis et al., 1998). The constants used in the scheme do not exactly match those used in the model, but the differences are minor.

The dissociation constants used in the cGENIE calculations of solubility for CO_2 in sea water follow Mehrbach et al. (1973), which are only defined for waters between 2–35 °C. Hence, the expression for CO_2 solubility in the model is restricted so that all water below 2 °C has the same CO_2 solubility (similarily for all water above 35°C). In the calculations of C_{sat}, we use CO2SYS with this temperature restriction, to accurately represent the model behaviour. In order to estimate the error introduced by this restriction, we need to assume that the same dissociation constants can be used outside the given temperature interval. The validity of this assumption is supported by the results of Goyet and Poisson (1989), who find similar dissociation constants for the interval -1–40°C in a study on artificial seawater. When CO2SYS is run using model ocean temperatures without the temperature restriction, we find that the calculated inventory of C_{sat} in the SEs is 0.06-0.5% larger than with the restriction. For $PIES278$ the inventory of C_{sat} is 0.25% larger. In terms of ΔC_{sat}, the unrestricted C_{sat} inventories indicate that the contribution by temperature changes to ΔTC is on average underestimated by approximately 56 $\pm$67% when the restriction is active. Since the restriction is used consistently, the error caused by the restriction being present in the model should not constitute a significant problem for our analysis. Nonetheless, the underestimation of the effect of temperature changes should be heeded in the discussion of our results.

Since pCO_2^{atm} is constant and the global ocean mean salinity is similar in all ensemble members $SE1$–$SE12$, any changes in global average C_{sat} between $PIES278$ and the SEs will be due to changes in ocean temperature or alkalinity:

$$\overline{\Delta C_{sat}} = \overline{\Delta T \frac{\partial C_{sat}}{\partial T}\Big|_{pCO_2,S,A_{pre}}} + \overline{\Delta A_{pre} \frac{\partial C_{sat}}{\partial A_{pre}}\Big|_{pCO_2,S,T}} \quad \text{(B1)}$$

Note: Salinity is conserved, but re-distributed. Hence, when using Eq. (B1) at the local scale, the term dependent on ΔS must be included. It only disappears after global integration, assuming that $\frac{\partial C_{sat}}{\partial S} \simeq constant$, which is done here.

We calculate the first term on the right hand side in Eq. (B1) on the local scale, by solving the carbon system equations using CO2SYS and taking the global average of the grid cell difference $C_{sat}(T_{SE(n)}) - C_{sat}(T_{PIES278})$ for each ensemble member, while keeping salinity and alkalinity constant using the $PIES278$ grid cell salinity and A_{pre}. Similarily, the second term on the right hand side is calculated as the global average of grid cell $C_{sat}(A_{pre,SE(n)}) - C_{sat}(A_{pre,PIES278})$ for each ensemble member, using T and S of $PIES278$.

Code and data availability. The source code for cGENIE is publically available at http://www.seao2.info/ mycgenie.html. For this work, modifications have been made to the gas exchange code in the file biogem_box.f90 and the modified version is provided for download with this manuscript. Data is available upon request (e-mail to the corresponding author).

Appendix A: Corresponding changes in pCO_2^{atm}

To achieve the equilibirium states of our ensemble ($SE1 - SE12$), we have been restoring pCO_2^{atm} to 278 µatm (µatm ≈ ppm). This means that the changes in carbon cycling caused by the imposed circulation changes are only seen as changes in ocean carbon storage. In the real world, we would also get an effect on the air-sea equilibirum and on pCO_2^{atm}.

In this section, we translate the observed changes in the ocean TC, C_{sat}, C_{soft}, C_{carb}, and C_{res} to the effect on pCO_2^{atm} that would have been seen if it had not been restored. The fact that we are indeed changing the total carbon inventory of the system means that these translations are approximate, since they assume the inventory to be constant. However, the changes in inventory are small compared to the size of the total inventory and therefore these calculations are still reasonably correct.

First, we need to know the Revelle buffer factor, R_C, for the control equilibrium, where R_C is

$$R_C = \frac{\Delta[CO_2]}{[CO_2]} \Big/ \frac{\Delta[DIC]}{[DIC]} \approx \frac{\Delta[CO_2]}{[CO_2]} \Big/ \frac{\Delta[TC]}{[TC]} \tag{A1}$$

where $[CO_2]$ and $[DIC]$ are the concentrations of dissolved CO_2 and DIC in the surface ocean. The difference between $[TC]$ and $[DIC]$ is very small and is due to the carbon trapped in organic molecules. This difference is small enough to be negligible in these calculations, and henceforth we consider DIC and TC to be directly interchangeable in all equations.

R_C is calculated by using the carbon system equation solver CO2SYS (Lewis et al., 1998). As input we use the control equilibirum global averages of temperature, salinity and concentrations of A_{pre} and PO_4, which are 3.58 °C, 34.90, 2296 µmol kg^{-1}, 2.15 µmol kg^{-1} respectively. R_C is given as output from CO2SYS. Given the control pCO_2^{atm} of 278 ppm, R_C is 12.4, which we then use as R_C in the rest of our calculations. From the equation solver, we also get the global average ocean concentration of DIC that corresponds to the given conditions. We call this concentration DIC_{ref} and it is 2100 µmol kg^{-1}.

DIC_{ref} is used as input when we next prepare to calculate the alkalinity factor, R_A, of the system. This factor is used to calculate the effect of a change in alkalinity on pCO_2^{atm}. R_A is given by

$$R_A = \frac{\Delta[CO_2]}{[CO_2]} \Big/ \frac{\Delta[A_{pre}]}{[A_{pre}]} \tag{A2}$$

Again, we use CO2SYS, with the same control state equilibrium parameters as before, but now giving DIC_{ref} instead of pCO_2^{atm}. This time we get a value for pCO_2^{atm} as output. We will denote this output $pCO_{2_{alk}}$. We also let CO2SYS calculate pCO_2^{atm} for a 1 % increase in $\overline{A_{pre}}$. $pCO_{2_{alk}}$ is 278 ppm in the case with all control values and 248 ppm in the case with increased A_{pre}. We take the average of these two calculations, 263 ppm, as $\overline{pCO_{2_{alk}}}$ and $\Delta pCO_{2_{alk}} = 278 - 248 = 30$ ppm. With these values, Eq. (A2) gives $R_A = -11.4$.

B2 Contribution by the biological pumps

The calculations in this section largely follow the Appendix in Lauderdale et al. (2013), who studied the correlation between wind-driven changes of the residual circulation in the Southern Ocean and changes in ocean carbon reservoirs and atmospheric CO_2. In contrast to Lauderdale et al. (2013), our model computes A_{pre} and $O_{2_{pre}}$, which reduces the sources of error in Eqs. B2 and B4. All stoichiometric ratios for organic material are based on Redfield (1963).

C_{soft} corresponds to the carbon that has been added to the water parcel through the remineralisation of the soft tissue of biogenic material that has entered the water parcel. The global ocean average of C_{soft} is calculated as

$$\overline{C_{soft}} = -R_{C:O_2} \cdot \overline{AOU} \tag{B2}$$

$$AOU = O_{2_{pre}} - O_2 \tag{B3}$$

where $R_{C:O_2}$ is the stoichiometric ratio of carbon to oxygen of $-106/138 \approx -0.768$ and AOU is the apparent oxygen utilisation. As seen in Eq. (B3), we calculate AOU as the difference between the preformed concentration of oxygen, $O_{2_{pre}}$, which is the concentration that the water had at the surface before it was subducted, and the actual concentration of oxygen, O_2, that is registered in the water. This difference is due to decomposition of organic soft-tissue material, which consumes oxygen. Therefore, AOU can be used to 'back-track' the amount of nutrients or carbon that was brought into the deep ocean trapped in organic material, which has then been remineralised. When $O_{2_{pre}}$ is not an available quantity, it is commonly assumed that oxygen is at equilibrium at the ocean surface. AOU is then calculated by replacing $O_{2_{pre}}$ with the saturation concentration for oxygen at the ambient temperature and salinity. In the real ocean, oxygen disequilibrium is negative and though it is small, it is not negligible. Hence, using $O_{2_{pre}}$ gives a more reliable result for AOU.

The biogenic material also carries hard tissue, and the carbon dissolved from this tissue is denoted C_{carb}. We calculate the grid cell concentration of C_{carb} as

$$C_{carb} = \frac{1}{2}(A_{tot} - A_{pre} - R_{N:O_2} \cdot AOU) \tag{B4}$$

where A_{tot} is the grid cell alkalinity and $R_{N:O_2}$ is the stoichiometric ratio of nitrogen to oxygen of 16:-138 (≈ -0.116). We can then calculate the volume-weighted global average of C_{carb}.

Finally, ΔC_{soft} and ΔC_{carb} for each $SE(n)$, where $n = (1,..,12)$, are given by the difference between the global average concentration in the SE and in $PIES278$, as

$$\Delta\overline{C_{soft}} = \overline{C_{soft_{SE(n)}}} - \overline{C_{soft_{PIES278}}} \tag{B5}$$

$$\Delta\overline{C_{carb}} = \overline{C_{carb_{SE(n)}}} - \overline{C_{carb_{PIES278}}} \tag{B6}$$

(B7)

B3 Contribution by residual and desiquilibrium carbon

Residual carbon, C_{res}, is TC minus the contributions from the computed C_{sat}, C_{soft} and C_{res}. The residual will mainly consist of desiquilibrium carbon, C_{dis}. Since C_{dis} is determined at the surface, before water sinks, by definition $C_{dis} = C_{pre} - C_{sat}$. Assuming the methods described in Section B1 give a good approximation of C_{sat}, $DIC_{pre} - C_{sat}$, where DIC_{pre} is the model concentration of preformed carbon, gives a good approximation of C_{dis}.

Appendix C: Corresponding changes in pCO_2^{atm}

To achieve the equilibrium states of our ensemble ($SE1$–$SE12$), we have been restoring pCO_2^{atm} to 278 µatm (µatm ≈ ppm). This means that the changes in carbon cycling caused by the imposed circulation changes are only seen as changes in ocean carbon storage. In the real world, we would also get an effect on the air-sea equilibirum and on pCO_2^{atm}.

In this section, we translate the observed ΔTC, ΔC_{sat}, ΔC_{soft}, ΔC_{carb}, and ΔC_{res} to the effect on pCO_2^{atm} that would have been seen if it had not been restored. The fact that we are indeed changing the total carbon inventory of the system means that these translations are approximate, since they assume the inventory to be constant. However, the changes in inventory are small compared to the size of the total inventory and therefore these calculations are still reasonably correct.

First, we need to know the Revelle buffer factor, R_C, for the control equilibrium, where R_C is

$$R_C = \frac{\Delta[CO_2]}{[CO_2]} \Big/ \frac{\Delta[DIC]}{[DIC]} \approx \frac{\Delta[CO_2]}{[CO_2]} \Big/ \frac{\Delta[TC]}{[TC_o]} \quad \text{(C1)}$$

where $[CO_2]$ and $[DIC]$ are the concentrations of dissolved CO_2 and DIC in the surface ocean. The difference between the total ocean carbon ($TC_o = M_o(\overline{C_{sat}} + \overline{C_{soft}} + \overline{C_{carb}} + \overline{C_{res}})$) and DIC is very small and is due to the carbon trapped in organic molecules. This difference is small enough to be negligible in these calculations, and henceforth we consider DIC and TC_o to be directly interchangeable in all equations. Note that $\Delta TC = \Delta TC_o$, since the atmospheric contribution to $\Delta TC = 0$.

R_C is calculated by using the carbon system equation solver CO2SYS (Lewis et al., 1998). As input we use the control equilibirum global averages of temperature, salinity and concentrations of A_{pre} and PO_4, which are 3.58 °C, 34.90, 2296 µmol kg^{-1}, 2.15 μmol kg^{-1} respectively. R_C is given as output from CO2SYS. Given the control pCO_2^{atm} of 278 ppm, R_C is 12.4, which we then use as R_C in the rest of our calculations. From the equation solver, we also get the global average ocean concentration of DIC that corresponds to the given conditions. We call this concentration DIC_{ref} and it is 2100 μmol kg^{-1}.

DIC_{ref} is used as input when we next prepare to calculate the alkalinity factor, R_A, of the system. This factor is used to calculate the effect of a change in alkalinity on pCO_2^{atm}. R_A is given by

$$R_A = \frac{\Delta[CO_2]}{[CO_2]} \Big/ \frac{\Delta[A_{pre}]}{[A_{pre}]} \quad \text{(C2)}$$

Again, we use CO2SYS, with the same control state equilibrium parameters as before, but now giving DIC_{ref} instead of pCO_2^{atm}. This time we get a value for pCO_2^{atm} as output. We will denote this output $pCO_{2_{alk}}$. We also let CO2SYS calculate

We can now calculate how a change in TC, in our SE ensemble would affect pCO_2^{atm}, if we were not restoring it:

$$\Delta pCO_2^{atm}\Big|_{TC} = pCO_2^{atm} \cdot -(R_C \frac{\Delta TC}{TC} + R_A \frac{\Delta Alk}{Alk}) \quad \text{(A3)}$$

Here, ΔTC is the change in TC of an ensemble member ($SE1 - SE12$) c.f. the control, as seen in panel a of Figure 2. TC and Alk are total inventories of carbon and alkalinity respectively in the control equilibrium and ΔAlk is the difference in alkalinity inventory between the ensemble member and the control. In this ensemble, ΔAlk is solely due to changes in the biological pump.

The effect a change in the inventory of residual carbon, $M_o \cdot \Delta C_{res}$, would have on pCO_2^{atm}, is calculated in a similar manner as for ΔTC;

$$\Delta pCO_2^{atm}\Big|_{C_{res}} = pCO_2^{atm} \cdot -R_C \frac{M_o \Delta C_{res}}{TC} \quad \text{(A4)}$$

Since the biological pump is not involved in this change, we need not take into account changes related to alkalinity, and therefore that term is removed.

We estimate the effects of changes in the biological pump using equations from Kwon et al. (2011), which they base on the framework described in Ito and Follows (2005). They make simplifications assuming that $[C_{sat}]$ can replace $[DIC]$ in Eq. (A1), and that, to leading order approximation, the sensitivity of pCO_2^{atm} to changes in C_{soft} is independent of the size of the carbon reservoirs in the atmosphere and ocean respectively. These simplifications yield Eqs. (A5) and (A7).

$$\Delta pCO_2^{atm}\Big|_{C_{soft}} = pCO_2^{atm} \cdot \Delta\overline{C_{soft}} \cdot C_{soft_F} \quad \text{(A5)}$$

$$C_{soft_F} = \frac{-R_C}{C_{sat}} + R_{N:C}\frac{R_A}{A_{pre}} \quad \text{(A6)}$$

Equation (A5) gives the change in pCO_2^{atm} that would correspond to an observed ΔC_{soft}. $\Delta\overline{C_{soft}}$ is the change in global average concentration of C_{soft} in the control equilibrium and C_{soft_F} is the scaled buffer factor for C_{soft}, which is based on global average concentrations of C_{sat} and A_{pre} (see Kwon et al. (2011)). The approximation in this case that pCO_2^{atm} is insensitive to the size of the carbon reservoirs in the atmosphere and ocean overestimates the excursion in pCO_2^{atm} due to changes in C_{soft} by about 10–15 %.

For C_{carb}, the corresponding equations are

$$\Delta pCO_2^{atm}\Big|_{C_{carb}} = pCO_2^{atm} \cdot \Delta\overline{C_{carb}} \cdot C_{carb_F} \quad \text{(A7)}$$

$$C_{carb_F} = \frac{-R_C}{C_{sat}} - 2\frac{R_A}{A_{pre}} \quad \text{(A8)}$$

pCO_2^{atm} for a 1 % increase in $\overline{A_{pre}}$. $pCO_{2_{alk}}$ is 278 ppm in the case with all control values and 248 ppm in the case with increased A_{pre}. We take the average of these two calculations, 263 ppm, as $\overline{pCO_{2_{alk}}}$ and $\Delta pCO_{2_{alk}} = 278 - 248 = 30$ ppm. With these values, Eq. (C2) gives $R_A = -11.4$.

We can now calculate how a change in TC, in our SE ensemble would affect pCO_2^{atm}, if we were not restoring it:

$$\Delta pCO_2^{atm}\Big|_{TC} = pCO_2^{atm} \cdot -(R_C \frac{\Delta TC}{DIC} + R_A \frac{\Delta Alk}{Alk}) \quad \text{(C3)}$$

Here, ΔTC is the change in TC of an ensemble member ($SE1$–$SE12$) cf. the control, as seen in panel a of Figure 2. DIC and Alk are total inventories of DIC and alkalinity respectively in the control equilibrium and ΔAlk is the difference in alkalinity inventory between the ensemble member and the control. In this ensemble, ΔAlk is solely due to changes in the biological (soft tissue and carbonate) pump .

The effect a change in the inventory of residual carbon, $M_o \cdot \Delta C_{res}$, would have on pCO_2^{atm}, is calculated in a similar manner as for ΔTC;

$$\Delta pCO_2^{atm}\Big|_{C_{res}} = pCO_2^{atm} \cdot -R_C \frac{M_o \Delta C_{res}}{DIC} \quad \text{(C4)}$$

Since the biological pump is not involved in this change, we need not take into account changes related to alkalinity, and therefore that term is removed.

We estimate the effects of changes in the biological pump using equations from Kwon et al. (2011), which they base on the framework described in Ito and Follows (2005). They make simplifications assuming that $[C_{sat}]$ can replace $[DIC]$ in Eq. (C1), and that, to leading order approximation, the sensitivity of pCO_2^{atm} to changes in C_{soft} is independent of the size of the carbon reservoirs in the atmosphere and ocean respectively. These simplifications yield Eqs. (C5) and (C7).

$$\Delta pCO_2^{atm}\Big|_{C_{soft}} = pCO_2^{atm} \cdot \Delta\overline{C_{soft}} \cdot C_{soft_F} \quad \text{(C5)}$$

$$C_{soft_F} = \frac{-R_C}{C_{sat}} + R_{N:C}\frac{R_A}{A_{pre}} \quad \text{(C6)}$$

Equation (C5) gives the change in pCO_2^{atm} that would correspond to an observed ΔC_{soft}. $\Delta\overline{C_{soft}}$ is the change in global average concentration of C_{soft} in the control equilibrium and C_{soft_F} is the scaled buffer factor for C_{soft}, which is based on global average concentrations of C_{sat} and A_{pre} (see Kwon et al., 2011). The approximation in this case that pCO_2^{atm} is insensitive to the size of the carbon reservoirs in the atmosphere and ocean overestimates the excursion in pCO_2^{atm} due to changes in C_{soft} by about 10–15 %.

For C_{carb}, the corresponding equations are

The only remaining carbon species is C_{sat}. We calculate the effects on pCO_2^{atm} corresponding to our observed ΔC_{sat} directly by solving the carbon system equations using CO2SYS. As input data we use the observed salinity, global average concentration of DIC and surface PO_4 of the control equilibrium, as well as the restored value of pCO_2^{atm} = 278 ppm. We run CO2SYS with the control global average temperature and the SE ensemble member global average temperature. As output, we then get the pCO_2^{atm} at these two temperatures. Thus, we can compute the ΔpCO_2^{atm} we would get as a result of solely changing the temperature and keeping everything else but pCO_2^{atm} constant.

Instead of solving the carbon system equations to get the change in pCO_2^{atm}, Goodwin et al. (2011) suggest using a simplified equation, where the fractional change $\Delta pCO_2^{atm}/pCO_2^{atm}$, is described as proportional to a function of global average ocean temperature;

$$\frac{\Delta pCO_2^{atm}}{pCO_2^{atm}} \sim -\frac{V}{I_B}\frac{\partial C_{sat}}{\partial T}\Delta T_{avg} \quad \text{(A9)}$$

$$I_B = I_A + I_O/R_{global} \quad \text{(A10)}$$

Here, V is the ocean volume (m^3) and $\frac{\partial C_{sat}}{\partial T}$ (mol m^{-3} °C^{-1}) is the change in saturation concentration of DIC per unit change of seawater temperature, in this case global ocean average temperature. I_B is the buffered amount of carbon in the system, or in other words the CO_2 that is "available for redistribution between the atmosphere and ocean" (Goodwin et al., 2007). As described by Eq. (A10), I_B is based on the atmospheric carbon inventory, I_A, and the ocean inventory of DIC, I_O, scaled by the global value for the Revelle buffer factor, which in this case is the same as R_C above.

Author contributions. M. Ödalen, J. Nycander and K. I. C. Oliver designed the model experiments. A. Ridgwell developed the cGENIE model code, and M. Ödalen adapted it for the experimental design. M. Ödalen performed the model simulations and produced the figures. L. Brodeau provided technical expertise for the model setup. M. Ödalen prepared the manuscript with contributions from all co-authors.

Competing interests. No competing interests are present.

Acknowledgements. The simulations were performed on resources provided by the Swedish National Infrastructure for Computing (SNIC) at the National Supercomputer Centre, Linköping University. Kevin Oliver would like to acknowledge the support by UK NERC grant NE/K002546/1 and he is grateful to the International Mereorological Institute for generous support during several visists to Stockholm. This work benefited from helpful discussions with Johan Nilsson.

$$\Delta pCO_2^{atm}\Big|_{C_{carb}} = pCO_2^{atm} \cdot \Delta\overline{C_{carb}} \cdot C_{carb_F} \quad \text{(C7)}$$

$$C_{carb_F} = \frac{-R_C}{\overline{C_{sat}}} - 2\frac{R_A}{\overline{A_{pre}}} \quad \text{(C8)}$$

The only remaining carbon species is C_{sat}. The effect on pCO_2^{atm} corresponding to our observed $\Delta C_{sat,A}$ is estimated using Eq. C3, replacing TC by $\Delta C_{sat,A}$. We calculate the effects on pCO_2^{atm} corresponding to our observed $\Delta C_{sat,T}$ directly by solving the carbon system equations using CO2SYS. As input data we use the observed salinity, global average concentration of DIC and surface PO_4 of the control equilibrium, as well as the restored value of pCO_2^{atm} = 278 ppm. We run CO2SYS with the $PIES278$ global average temperature and the SE ensemble member global average temperature. As output, we then get the pCO_2^{atm} at these two temperatures. Thus, we can compute the ΔpCO_2^{atm} we would get as a result of solely changing the temperature and keeping everything else but pCO_2^{atm} constant.

Instead of solving the carbon system equations to get the change in pCO_2^{atm}, Goodwin et al. (2011) suggest using a simplified equation, where the fractional change $\Delta pCO_2^{atm}/pCO_2^{atm}$, is described as proportional to a function of global average ocean temperature;

$$\frac{\Delta pCO_2^{atm}}{pCO_2^{atm}} \sim -\frac{V}{I_B}\frac{\partial C_{sat}}{\partial T}\Delta T_{avg} \quad \text{(C9)}$$

$$I_B = I_A + I_O/R_{global} \quad \text{(C10)}$$

Here, $\frac{\partial C_{sat}}{\partial T}$ (mol m^{-3} °C^{-1}) is the change in saturation concentration of DIC per unit change of seawater temperature, in this case global ocean average temperature. We calculate this quantity using the temperature restriction on the gas solubility, mentioned in Section B1. V is the ocean volume (m^3) and I_B is the buffered amount of carbon in the system, or in other words the CO_2 that is "available for redistribution between the atmosphere and ocean" (Goodwin et al., 2007). As described by Eq. (C10), I_B is based on the atmospheric carbon inventory, I_A, and the ocean inventory of DIC, I_O, scaled by the global value for the Revelle buffer factor, which in this case is the same as R_C above.

Author contributions. M. Ödalen, J. Nycander and K. I. C. Oliver designed the model experiments. A. Ridgwell developed the cGENIE model code with addition of new tracers. M. Ödalen adapted the code for the experimental design, performed the model simulations and produced the figures. L. Brodeau provided technical expertise for the model setup. M. Ödalen prepared the manuscript with contributions from all co-authors.

Competing interests. No competing interests are present.

Acknowledgements. The simulations were performed on resources provided by the Swedish National Infrastructure for Computing (SNIC) at the National Supercomputer Centre, Linköping University. Malin Ödalen and Jonas Nycander would like to accnowledge the Bolin Centre for Climate Research for financial support. Kevin Oliver would like to acknowledge the support by UK NERC grant NE/K002546/1 and he is grateful to the International Mereorological Institute for generous support during several visists to Stockholm. Andy Ridgwell was supported by EU grant ERC 2013-CoG-617313. This work benefited from helpful discussions with Johan Nilsson.

References

Anderson, L. A. and Sarmiento, J. L.: Redfield ratios of remineralization determined by nutrient data analysis, Global biogeochemical cycles, 8, 65–80, 1994.

Archer, D., Winguth, A., Lea, D., and Mahowald, N.: What caused the glacial/interglacial atmospheric pCO2 cycles?, Reviews of Geophysics, 38, 159–189, 2000a.

Archer, D. E., Eshel, G., Winguth, A., Broecker, W., Pierrehumbert, R., Tobis, M., and Jacob, R.: Atmospheric pCO2 sensitivity to the biological pump in the ocean, Global Biogeochemical Cycles, 14, 1219–1230, 2000b.

Aumont, O., van Hulten, M., Roy-Barman, M., Dutay, J.-C., Ethé, C., and Gehlen, M.: A reactivity continuum of particulate organic matter in a global ocean biogeochemical model, Biogeosciences Discussions, 2016, 1–37, doi:10.5194/bg-2016-374, http://www.biogeosciences-discuss.net/bg-2016-374/, 2016.

Ballarotta, M., Falahat, S., Brodeau, L., and Döös, K.: On the glacial and interglacial thermohaline circulation and the associated transports of heat and freshwater, Ocean Science, 10, 907, 2014.

Bernardello, R., Marinov, I., Palter, J. B., Sarmiento, J. L., Galbraith, E. D., and Slater, R. D.: Response of the ocean natural carbon storage to projected twenty-first-century climate change, Journal of Climate, 27, 2033–2053, 2014.

Broecker, W. S.: "NO", A conservative water-mass tracer, Earth and Planetary Science Letters, 23, 100–107, 1974.

Broecker, W. S.: Glacial to interglacial changes in ocean chemistry, Progress in Oceanography, 11, 151 – 197, doi:http://dx.doi.org/10.1016/0079-6611(82)90007-6, http://www.sciencedirect.com/science/article/pii/0079661182900076, 1982.

Broecker, W. S., Peng, T.-H., Trumbore, S., Bonani, G., and Wolfli, W.: The distribution of radiocarbon in the glacial ocean, Global Biogeochemical Cycles, 4, 103–117, 1990.

Brovkin, V., Ganopolski, A., Archer, D., and Rahmstorf, S.: Lowering of glacial atmospheric CO2 in response to changes in oceanic circulation and marine biogeochemistry, Paleoceanography, 22, 2007.

Cao, L., Eby, M., Ridgwell, A., Caldeira, K., Archer, D., Ishida, A., Joos, F., Matsumoto, K., Mikolajewicz, U., Mouchet, A., et al.: The role of ocean transport in the uptake of anthropogenic CO 2, Biogeosciences, 6, 375–390, 2009.

Comiso, J. C.: Variability and trends of the global sea ice cover, in: Sea ice: an introduction to its physics, chemistry, biology and geology, edited by Thomas, D. N. and Dieckmann, G. S., John Wiley & Sons, 2008.

Edwards, N. R. and Marsh, R.: Uncertainties due to transport-parameter sensitivity in an efficient 3-D ocean-climate model, Climate Dynamics, 24, 415–433, 2005.

Elderfield, H. and Rickaby, R.: Oceanic Cd/P ratio and nutrient utilization in the glacial Southern Ocean, Nature, 405, 305–310, 2000.

Eriksson, E. and Welander, P.: On a Mathematical Model of the Carbon Cycle in Nature, Tellus, 8, 155–175, doi:10.1111/j.2153-3490.1956.tb01207.x, http://dx.doi.org/10.1111/j.2153-3490.1956.tb01207.x, 1956.

Falkowski, P., Scholes, R. J., Boyle, E., Canadell, J., Canfield, D., Elser, J., Gruber, N., Hibbard, K., Högberg, P., Linder, S., Mackenzie, F. T., Moore III, B., Pedersen, T., Rosenthal, Y., Seitzinger, S., Smetacek, V., and Steffen, W.: The Global Carbon Cycle: A Test of Our Knowledge of Earth as a System, Science, 290, 291–296, doi:10.1126/science.290.5490.291, http://science.sciencemag.org/content/290/5490/291, 2000.

Galbraith, E. D. and Martiny, A. C.: A simple nutrient-dependence mechanism for predicting the stoichiometry of marine ecosystems, Proceedings of the National Academy of Sciences, 112, 8199–8204, 2015.

References

Anderson, L. A. and Sarmiento, J. L.: Redfield ratios of remineralization determined by nutrient data analysis, Global biogeochemical cycles, 8, 65–80, 1994.

Archer, D., Winguth, A., Lea, D., and Mahowald, N.: What caused the glacial/interglacial atmospheric pCO_2 cycles?, Reviews of Geophysics, 38, 159–189, 2000a.

Archer, D. E., Eshel, G., Winguth, A., Broecker, W., Pierrehumbert, R., Tobis, M., and Jacob, R.: Atmospheric pCO_2 sensitivity to the biological pump in the ocean, Global Biogeochemical Cycles, 14, 1219–1230, 2000b.

Ballarotta, M., Falahat, S., Brodeau, L., and Döös, K.: On the glacial and interglacial thermohaline circulation and the associated transports of heat and freshwater, Ocean Science, 10, 907–921, 2014.

Bernardello, R., Marinov, I., Palter, J. B., Sarmiento, J. L., Galbraith, E. D., and Slater, R. D.: Response of the ocean natural carbon storage to projected twenty-first-century climate change, Journal of Climate, 27, 2033–2053, 2014.

Broecker, W. S.: Glacial to interglacial changes in ocean chemistry, Progress in Oceanography, 11, 151–197, doi:http://dx.doi.org/10.1016/0079-6611(82)90007-6, http://www.sciencedirect.com/science/article/pii/0079661182900076, 1982.

Broecker, W. S., Peng, T.-H., Trumbore, S., Bonani, G., and Wolfli, W.: The distribution of radiocarbon in the glacial ocean, Global Biogeochemical Cycles, 4, 103–117, 1990.

Brovkin, V., Ganopolski, A., Archer, D., and Rahmstorf, S.: Lowering of glacial atmospheric CO_2 in response to changes in oceanic circulation and marine biogeochemistry, Paleoceanography, 22, PA4202, 2007.

Brovkin, V., Ganopolski, A., Archer, D., and Munhoven, G.: Glacial CO_2 cycle as a succession of key physical and biogeochemical processes, Climate of the Past, 8, 251–264, 2012.

Cao, L., Eby, M., Ridgwell, A., Caldeira, K., Archer, D., Ishida, A., Joos, F., Matsumoto, K., Mikolajewicz, U., Mouchet, A., et al.: The role of ocean transport in the uptake of anthropogenic CO_2, Biogeosciences, 6, 375–390, 2009.

Comiso, J. C.: Variability and trends of the global sea ice cover, in: Sea ice: an introduction to its physics, chemistry, biology and geology, edited by Thomas, D. N. and Dieckmann, G. S., pp. 205–246, John Wiley & Sons, 2008.

DeVries, T. and Primeau, F.: Atmospheric pCO_2 sensitivity to the solubility pump: Role of the low-latitude ocean, Global Biogeochemical Cycles, 23, GB4020, 2009.

Duteil, O., Koeve, W., Oschlies, A., Aumont, O., Bianchi, D., Bopp, L., Galbraith, E., Matear, R., Moore, J., Sarmiento, J., et al.: Preformed and regenerated phosphate in ocean general circulation models: can right total concentrations be wrong?, Biogeosciences (BG), 9, 1797–1807, 2012.

Edwards, N. R. and Marsh, R.: Uncertainties due to transport-parameter sensitivity in an efficient 3-D ocean-climate model, Climate Dynamics, 24, 415–433, 2005.

Eggleston, S. and Galbraith, E. D.: The devil's in the disequilibrium: sensitivity of ocean carbon storage to climate state and iron fertilization in a general circulation model, Biogeosciences Discussions, 2017, 1–29, doi:10.5194/bg-2017-328, https://www.biogeosciences-discuss.net/bg-2017-328/, 2017.

Elderfield, H. and Rickaby, R.: Oceanic Cd/P ratio and nutrient utilization in the glacial Southern Ocean, Nature, 405, 305–310, 2000.

Eriksson, E. and Welander, P.: On a Mathematical Model of the Carbon Cycle in Nature, Tellus, 8, 155–175, doi:10.1111/j.2153-3490.1956.tb01207.x, http://dx.doi.org/10.1111/j.2153-3490.1956.tb01207.x, 1956.

Ganopolski, A., Calov, R., and Claussen, M.: Simulation of the last glacial cycle with a coupled climate ice-sheet model of intermediate complexity, Climate of the Past, 6, 229–244, 2010.

Goodwin, P., Williams, R. G., Follows, M. J., and Dutkiewicz, S.: Ocean-atmosphere partitioning of anthropogenic carbon dioxide on centennial timescales, Global Biogeochemical Cycles, 21, 2007.

Goodwin, P., Follows, M. J., and Williams, R. G.: Analytical relationships between atmospheric carbon dioxide, carbon emissions, and ocean processes, Global Biogeochemical Cycles, 22, 2008.

Goodwin, P., Oliver, K. I. C., and Lenton, T. M.: Observational constraints on the causes of Holocene CO2 change, Global Biogeochemical Cycles, 25, n/a–n/a, doi:10.1029/2010GB003888, http://dx.doi.org/10.1029/2010GB003888, gB3011, 2011.

Hain, M. P., Sigman, D. M., and Haug, G. H.: Carbon dioxide effects of Antarctic stratification, North Atlantic Intermediate Water formation, and subantarctic nutrient drawdown during the last ice age: Diagnosis and synthesis in a geochemical box model, Global Biogeochemical Cycles, 24, 2010.

Headly, M. A. and Severinghaus, J. P.: A method to measure Kr/N2 ratios in air bubbles trapped in ice cores and its application in re-constructing past mean ocean temperature, Journal of Geophysical Research: Atmospheres, 112, n/a–n/a, doi:10.1029/2006JD008317, http://dx.doi.org/10.1029/2006JD008317, d19105, 2007.

Homola, K., Spivack, A. J., D'Hondt, S., Estes, E. R., Insua, T. L., McKinley, C. C., Murray, R. W., Pockalny, R. A., Robinson, R. S., and Sauvage, J.: Preformed Nitrate in the Glacial North Atlantic, AGU Fall Meeting Abstracts, 2015.

IPCC: Contribution of Working Group I to the Fourth Assessment Report of the Intergovernmental Panel on Climate Change, 2007.

Ito, T. and Follows, M. J.: Preformed phosphate, soft tissue pump and atmospheric CO2, Journal of Marine Research, 63, 813–839, 2005.

Keigwin, L. and Schlegel, M.: Ocean ventilation and sedimentation since the glacial maximum at 3 km in the western North Atlantic, Geochemistry, Geophysics, Geosystems, 3, 1–14, 2002.

Kohfeld, K. E. and Ridgwell, A.: Glacial-Interglacial Variability in Atmospheric CO2, in: Surface Ocean-Lower Atmosphere Processes, edited by Le Quéré, C. and S., S. E., pp. 251–286, American Geophysical Union, Washington D.C., 2009.

Köhler, P. and Fischer, H.: Proposing a mechanistic understanding of changes in atmospheric CO 2 during the last 740 000 years, Climate of the Past Discussions, 2, 1–42, 2006.

Kwon, E. Y., Sarmiento, J. L., Toggweiler, J., and DeVries, T.: The control of atmospheric pCO2 by ocean ventilation change: The effect of the oceanic storage of biogenic carbon, Global Biogeochemical Cycles, 25, 2011.

Lauderdale, J. M., Garabato, A. C. N., Oliver, K. I. C., Follows, M. J., and Williams, R. G.: Wind-driven changes in Southern Ocean residual circulation, ocean carbon reservoirs and atmospheric CO2, Climate dynamics, 41, 2145–2164, 2013.

Lewis, E., Wallace, D., and Allison, L. J.: Program developed for CO2 system calculations, ORNL/CDIAC-105, Carbon Dioxide Information Analysis Center, managed by Lockheed Martin Energy Research Corporation for the US Department of Energy Tennessee, 1998.

Locarnini, R. A., Mishonov, A. V., Antonov, J. I., Boyer, T. P., Garcia, H. E., Baranova, O. K., Zweng, M. M., Paver, C. R., Reagan, J. R., Johnson, D. R., Hamilton, M., and Seidov, D.: World Ocean Atlas 2013, Volume 1: Temperature, Tech. Rep. 73, NOAA Atlas NESDIS, 40 pp., 2013.

Löfverström, M., Caballero, R., Nilsson, J., and Kleman, J.: Evolution of the large-scale atmospheric circulation in response to changing ice sheets over the last glacial cycle, Climate of the Past, 10, 1453–1471, 2014.

Lüthi, D. et al.: EPICA Dome C Ice Core 800KYr Carbon Dioxide Data, IGBP PAGES/World Data Center for Paleoclimatology Data Contribution Series, 55, 2008.

Falkowski, P., Scholes, R. J., Boyle, E., Canadell, J., Canfield, D., Elser, J., Gruber, N., Hibbard, K., Högberg, P., Linder, S., Mackenzie, F. T., Moore III, B., Pedersen, T., Rosenthal, Y., Seitzinger, S., Smetacek, V., and Steffen, W.: The Global Carbon Cycle: A Test of Our Knowledge of Earth as a System, Science, 290, 291–296, doi:10.1126/science.290.5490.291, http://science.sciencemag.org/content/290/5490/291, 2000.

Galbraith, E. D. and Martiny, A. C.: A simple nutrient-dependence mechanism for predicting the stoichiometry of marine ecosystems, Proceedings of the National Academy of Sciences, 112, 8199–8204, 2015.

Ganopolski, A., Calov, R., and Claussen, M.: Simulation of the last glacial cycle with a coupled climate ice-sheet model of intermediate complexity, Climate of the Past, 6, 229–244, 2010.

Goodwin, P., Williams, R. G., Follows, M. J., and Dutkiewicz, S.: Ocean-atmosphere partitioning of anthropogenic carbon dioxide on centennial timescales, Global Biogeochemical Cycles, 21, GB1014, 2007.

Goodwin, P., Follows, M. J., and Williams, R. G.: Analytical relationships between atmospheric carbon dioxide, carbon emissions, and ocean processes, Global Biogeochemical Cycles, 22, GB3030, 2008.

Goodwin, P., Oliver, K. I. C., and Lenton, T. M.: Observational constraints on the causes of Holocene CO_2 change, Global Biogeochemical Cycles, 25, GB3011, doi:10.1029/2010GB003888, http://dx.doi.org/10.1029/2010GB003888, gB3011, 2011.

Goodwin, P., Williams, R. G., and Ridgwell, A.: Sensitivity of climate to cumulative carbon emissions due to compensation of ocean heat and carbon uptake, Nature Geoscience, 8, 29–34, 2015.

Goyet, C. and Poisson, A.: New determination of carbonic acid dissociation constants in seawater as a function of temperature and salinity, Deep Sea Research Part A. Oceanographic Research Papers, 36, 1635–1654, 1989.

Hain, M. P., Sigman, D. M., and Haug, G. H.: Carbon dioxide effects of Antarctic stratification, North Atlantic Intermediate Water formation, and subantarctic nutrient drawdown during the last ice age: Diagnosis and synthesis in a geochemical box model, Global Biogeochemical Cycles, 24, 2010.

Headly, M. A. and Severinghaus, J. P.: A method to measure Kr/N2 ratios in air bubbles trapped in ice cores and its application in re-constructing past mean ocean temperature, Journal of Geophysical Research: Atmospheres, 112, D19 105, doi:10.1029/2006JD008317, http://dx.doi.org/10.1029/2006JD008317, d19105, 2007.

Heinze, C., Maier-Reimer, E., and Winn, K.: Glacial pCO_2 reduction by the world ocean: Experiments with the Hamburg carbon cycle model, Paleoceanography, 6, 395–430, 1991.

Homola, K., Spivack, A. J., D'Hondt, S., Estes, E. R., Insua, T. L., McKinley, C. C., Murray, R. W., Pockalny, R. A., Robinson, R. S., and Sauvage, J.: Preformed Nitrate in the Glacial North Atlantic, AGU Fall Meeting Abstracts, 2015.

IPCC: Contribution of Working Group I to the Fourth Assessment Report of the Intergovernmental Panel on Climate Change, 2007.

Ito, T. and Follows, M. J.: Preformed phosphate, soft tissue pump and atmospheric CO_2, Journal of Marine Research, 63, 813–839, 2005.

Ito, T. and Follows, M. J.: Air-sea disequilibrium of carbon dioxide enhances the biological carbon sequestration in the Southern Ocean, Global Biogeochemical Cycles, 27, 1129–1138, 2013.

Ito, T., Follows, M., and Boyle, E.: Is AOU a good measure of respiration in the oceans?, Geophysical research letters, 31, 2004.

Keigwin, L. and Schlegel, M.: Ocean ventilation and sedimentation since the glacial maximum at 3 km in the western North Atlantic, Geochemistry, Geophysics, Geosystems, 3, 1–14, 2002.

Klockmann, M., Mikolajewicz, U., and Marotzke, J.: The effect of greenhouse gas concentrations and ice sheets on the glacial AMOC in a coupled climate model, Climate of the Past, 12, 1829–1846, doi:10.5194/cp-12-1829-2016, https://www.clim-past.net/12/1829/2016/, 2016.

Marinov, I., Follows, M., Gnanadesikan, A., Sarmiento, J. L., and Slater, R. D.: How does ocean biology affect atmospheric pCO2? Theory and models, Journal of Geophysical Research, 113, 2008a.

Marinov, I., Gnanadesikan, A., Sarmiento, J. L., Toggweiler, J. R., Follows, M., and Mignone, B. K.: Impact of oceanic circulation on biological carbon storage in the ocean and atmospheric pCO2, Global Biogeochemical Cycles, 22, 2008b.

Marsh, R., Sobester, A., Hart, E. E., Oliver, K., Edwards, N., and Cox, S.: An optimally tuned ensemble of the" eb_go_gs" configuration of GENIE: parameter sensitivity and bifurcations in the Atlantic overturning circulation, Geoscientific Model Development, 6, 1729–1744, 2013.

Muglia, J. and Schmittner, A.: Glacial Atlantic overturning increased by wind stress in climate models, Geophysical Research Letters, 42, 9862–9868, 2015.

Müller, S. A., Joos, F., Edwards, N. R., and Stocker, T. F.: Water Mass Distribution and Ventilation Time Scales in a Cost-Efficient, Three-Dimensional Ocean Model, Journal of Climate, 19, 5479–5499, doi:10.1175/JCLI3911.1, http://dx.doi.org/10.1175/JCLI3911.1, 2006.

Otto-Bliesner, B. L., Hewitt, C. D., Marchitto, T. M., Brady, E., Abe-Ouchi, A., Crucifix, M., Murakami, S., and Weber, S. L.: Last Glacial Maximum ocean thermohaline circulation: PMIP2 model intercomparisons and data constraints, Geophysical Research Letters, 34, n/a–n/a, doi:10.1029/2007GL029475, http://dx.doi.org/10.1029/2007GL029475, l12706, 2007.

Petit, J.-R., Jouzel, J., Raynaud, D., Barkov, N. I., Barnola, J.-M., Basile, I., Bender, M., Chappellaz, J., Davis, M., Delaygue, G., et al.: Climate and atmospheric history of the past 420,000 years from the Vostok ice core, Antarctica, Nature, 399, 429–436, 1999.

PMIP3: Paleoclimate Modelling Intercomparison Project Phase III , https://pmip3.lsce.ipsl.fr/.

Quere, C. L., Harrison, S. P., Colin Prentice, I., Buitenhuis, E. T., Aumont, O., Bopp, L., Claustre, H., Cotrim Da Cunha, L., Geider, R., Giraud, X., et al.: Ecosystem dynamics based on plankton functional types for global ocean biogeochemistry models, Global Change Biology, 11, 2016–2040, 2005.

Raven, J., Caldeira, K., Elderfield, H., Hoegh-Guldberg, O., Liss, P., Riebesell, U., Shepherd, J., Turley, C., and Watson, A.: Ocean acidification due to increasing atmospheric carbon dioxide, The Royal Society, 2005.

Redfield, A. C.: The influence of organisms on the composition of sea-water, The Sea, 2, 26–77, 1963.

Ridgwell, A., Hargreaves, J. C., Edwards, N. R., Annan, J. D., Lenton, T. M., Marsh, R., Yool, A., and Watson, A.: Marine geochemical data assimilation in an efficient Earth System Model of global biogeochemical cycling, Biogeosciences, 4, 87–104, 2007.

Sarmiento, J. and Toggweiler, J.: A new model for the role of the oceans in determining atmospheric pCO 2, Nature, 308, 621–624, 1984.

Sarmiento, J. L. and Gruber, N.: Ocean biogeochemical dynamics, Princeton University Press, 2006.

Schmittner, A., Green, J. A. M., and Wilmes, S.-B.: Glacial ocean overturning intensified by tidal mixing in a global circulation model, Geophysical Research Letters, 42, 4014–4022, 2015.

Sigman, D. M. and Boyle, E. A.: Glacial/interglacial variations in atmospheric carbon dioxide, Nature, 407, 859–869, 2000.

Sigman, D. M., Hain, M. P., and Haug, G. H.: The polar ocean and glacial cycles in atmospheric CO2 concentration, Nature, 466, 47–55, 2010.

Sikes, E. L., Samson, C. R., Guilderson, T. P., and Howard, W. R.: Old radiocarbon ages in the southwest Pacific Ocean during the last glacial period and deglaciation, Nature, 405, 555–559, 2000.

Sime, L. C., Kohfeld, K. E., Le Quéré, C., Wolff, E. W., de Boer, A. M., Graham, R. M., and Bopp, L.: Southern Hemisphere westerly wind changes during the Last Glacial Maximum: model-data comparison, Quaternary Science Reviews, 64, 104–120, 2013.

Skinner, L., Fallon, S., Waelbroeck, C., Michel, E., and Barker, S.: Ventilation of the deep Southern Ocean and deglacial CO2 rise, Science, 328, 1147–1151, 2010.

Kohfeld, K. E. and Ridgwell, A.: Glacial-Interglacial Variability in Atmospheric CO_2, in: Surface Ocean-Lower Atmosphere Processes, edited by Le Quéré, C. and S., S. E., pp. 251–286, American Geophysical Union, Washington D.C., 2009.

Köhler, P. and Fischer, H.: Proposing a mechanistic understanding of changes in atmospheric CO_2 during the last 740 000 years, Climate of the Past Discussions, 2, 1–42, 2006.

Kwon, E. Y., Sarmiento, J. L., Toggweiler, J., and DeVries, T.: The control of atmospheric pCO_2 by ocean ventilation change: The effect of the oceanic storage of biogenic carbon, Global Biogeochemical Cycles, 25, 2011.

Lauderdale, J. M., Garabato, A. C. N., Oliver, K. I. C., Follows, M. J., and Williams, R. G.: Wind-driven changes in Southern Ocean residual circulation, ocean carbon reservoirs and atmospheric CO_2, Climate dynamics, 41, 2145–2164, 2013.

Lewis, E., Wallace, D., and Allison, L. J.: Program developed for CO_2 system calculations, ORNL/CDIAC-105, Carbon Dioxide Information Analysis Center, managed by Lockheed Martin Energy Research Corporation for the US Department of Energy Tennessee, 1998.

Locarnini, R. A., Mishonov, A. V., Antonov, J. I., Boyer, T. P., Garcia, H. E., Baranova, O. K., Zweng, M. M., Paver, C. R., Reagan, J. R., Johnson, D. R., Hamilton, M., and Seidov, D.: World Ocean Atlas 2013, Volume 1: Temperature, Tech. Rep. 73, NOAA Atlas NESDIS, 40 pp., 2013.

Löfverström, M., Caballero, R., Nilsson, J., and Kleman, J.: Evolution of the large-scale atmospheric circulation in response to changing ice sheets over the last glacial cycle, Climate of the Past, 10, 1453–1471, 2014.

Lüthi, D. et al.: EPICA Dome C Ice Core 800KYr Carbon Dioxide Data, IGBP PAGES/World Data Center for Paleoclimatology Data Contribution Series, 55, 2008.

Marchitto, T. M. and Broecker, W. S.: Deep water mass geometry in the glacial Atlantic Ocean: A review of constraints from the paleonutrient proxy Cd/Ca, Geochemistry, Geophysics, Geosystems, 7, 2006.

Marinov, I., Follows, M., Gnanadesikan, A., Sarmiento, J. L., and Slater, R. D.: How does ocean biology affect atmospheric pCO_2? Theory and models, Journal of Geophysical Research, 113, 2008a.

Marinov, I., Gnanadesikan, A., Sarmiento, J. L., Toggweiler, J. R., Follows, M., and Mignone, B. K.: Impact of oceanic circulation on biological carbon storage in the ocean and atmospheric pCO_2, Global Biogeochemical Cycles, 22, 2008b.

Marsh, R., Sobester, A., Hart, E. E., Oliver, K., Edwards, N., and Cox, S.: An optimally tuned ensemble of the" eb_go_gs" configuration of GENIE: parameter sensitivity and bifurcations in the Atlantic overturning circulation, Geoscientific Model Development, 6, 1729–1744, 2013.

Martin, J. H.: Glacial-interglacial CO_2 change: The iron hypothesis, Paleoceanography, 5, 1–13, 1990.

Marzocchi, A. and Jansen, M. F.: Connecting Antarctic sea ice to deep-ocean circulation in modern and glacial climate simulations, Geophysical Research Letters, 44, 6286–6295, doi:10.1002/2017GL073936, http://dx.doi.org/10.1002/2017GL073936, 2017.

Mehrbach, C., Culberson, C., Hawley, J., and Pytkowicx, R.: Measurement of the apparent dissociation constants of carbonic acid in seawater at atmospheric pressure, Limnology and Oceanography, 18, 897–907, 1973.

Muglia, J. and Schmittner, A.: Glacial Atlantic overturning increased by wind stress in climate models, Geophysical Research Letters, 42, 9862–9868, 2015.

Müller, S. A., Joos, F., Edwards, N. R., and Stocker, T. F.: Water Mass Distribution and Ventilation Time Scales in a Cost-Efficient, Three-Dimensional Ocean Model, Journal of Climate, 19, 5479–5499, doi:10.1175/JCLI3911.1, http://dx.doi.org/10.1175/JCLI3911.1, 2006.

Munhoven, G.: Glacial–interglacial changes of continental weathering: estimates of the related CO_2 and HCO^{3-} flux variations and their uncertainties, Global and Planetary Change, 33, 155–176, 2002.

Skinner, L., McCave, I., Carter, L., Fallon, S., Scrivner, A., and Primeau, F.: Reduced ventilation and enhanced magnitude of the deep Pacific carbon pool during the last glacial period, Earth and Planetary Science Letters, 411, 45–52, 2015.

Takahashi, T., Broecker, W. S., and Langer, S.: Redfield ratio based on chemical data from isopycnal surfaces, Journal of Geophysical Research: Oceans, 90, 6907–6924, 1985.

Toggweiler, J. R., Gnanadesikan, A., Carson, S., Murnane, R., and Sarmiento, J. L.: Representation of the carbon cycle in box models and GCMs: 1. Solubility pump, Global Biogeochemical Cycles, 17, n/a–n/a, doi:10.1029/2001GB001401, http://dx.doi.org/10.1029/2001GB001401, 1026, 2003.

Volk, T. and Hoffert, M. I.: Ocean Carbon Pumps: Analysis of Relative Strengths and Efficiencies in Ocean-Driven Atmospheric CO2 Changes, in: The Carbon Cycle and Atmospheric CO: Natural Variations Archean to Present, edited by Sundquist, E. T. and Broecker, W. S., American Geophysical Union, Washington D.C., 1985.

Wanninkhof, R.: Relationship between gas exchange and wind speed over the ocean, Journal of Geophysical Research, 97, 7373–7382, 1992.

Williams, R. G. and Follows, M. J.: Ocean Dynamics and the Carbon Cycle: Principles and Mechanisms, Cambridge University Press, 2011.

Zeebe, R. E. and Wolf-Gladrow, D. A.: CO2 in seawater: equilibrium, kinetics, isotopes, 65, Gulf Professional Publishing, 2001.

Zhang, X., Lohmann, G., Knorr, G., and Xu, X.: Different ocean states and transient characteristics in Last Glacial Maximum simulations and implications for deglaciation, Climate of the Past, 9, 2319–2333, doi:10.5194/cp-9-2319-2013, http://www.clim-past.net/9/2319/2013/, 2013.

Otto-Bliesner, B. L., Hewitt, C. D., Marchitto, T. M., Brady, E., Abe-Ouchi, A., Crucifix, M., Murakami, S., and Weber, S. L.: Last Glacial Maximum ocean thermohaline circulation: PMIP2 model intercomparisons and data constraints, Geophysical Research Letters, 34, L12706, doi:10.1029/2007GL029475, http://dx.doi.org/10.1029/2007GL029475, l12706, 2007.

Petit, J.-R., Jouzel, J., Raynaud, D., Barkov, N. I., Barnola, J.-M., Basile, I., Bender, M., Chappellaz, J., Davis, M., Delaygue, G., et al.: Climate and atmospheric history of the past 420,000 years from the Vostok ice core, Antarctica, Nature, 399, 429–436, 1999.

PMIP3: Paleoclimate Modelling Intercomparison Project Phase III , https://pmip3.lsce.ipsl.fr/.

Quere, C. L., Harrison, S. P., Colin Prentice, I., Buitenhuis, E. T., Aumont, O., Bopp, L., Claustre, H., Cotrim Da Cunha, L., Geider, R., Giraud, X., et al.: Ecosystem dynamics based on plankton functional types for global ocean biogeochemistry models, Global Change Biology, 11, 2016–2040, 2005.

Raven, J., Caldeira, K., Elderfield, H., Hoegh-Guldberg, O., Liss, P., Riebesell, U., Shepherd, J., Turley, C., and Watson, A.: Ocean acidification due to increasing atmospheric carbon dioxide, The Royal Society, 2005.

Redfield, A. C.: The influence of organisms on the composition of sea-water, The Sea, 2, 26–77, 1963.

Ridgwell, A., Hargreaves, J. C., Edwards, N. R., Annan, J. D., Lenton, T. M., Marsh, R., Yool, A., and Watson, A.: Marine geochemical data assimilation in an efficient Earth System Model of global biogeochemical cycling, Biogeosciences, 4, 87–104, 2007.

Ridgwell, A. J.: Glacial-interglacial perturbations in the global carbon cycle., Ph.D. thesis, University of East Anglia, 2001.

Sarmiento, J. and Toggweiler, J.: A new model for the role of the oceans in determining atmospheric pCO_2, Nature, 308, 621–624, 1984.

Sarmiento, J. L. and Gruber, N.: Ocean biogeochemical dynamics, Princeton University Press, 2006.

Schmittner, A., Green, J. A. M., and Wilmes, S.-B.: Glacial ocean overturning intensified by tidal mixing in a global circulation model, Geophysical Research Letters, 42, 4014–4022, 2015.

Sigman, D. M. and Boyle, E. A.: Glacial/interglacial variations in atmospheric carbon dioxide, Nature, 407, 859–869, 2000.

Sigman, D. M., Hain, M. P., and Haug, G. H.: The polar ocean and glacial cycles in atmospheric CO_2 concentration, Nature, 466, 47–55, 2010.

Sijp, W. P., von der Heydt, A. S., Dijkstra, H. A., Flögel, S., Douglas, P. M., and Bijl, P. K.: The role of ocean gateways on cooling climate on long time scales, Global and Planetary Change, 119, 1–22, doi:https://doi.org/10.1016/j.gloplacha.2014.04.004, 2014.

Sikes, E. L., Samson, C. R., Guilderson, T. P., and Howard, W. R.: Old radiocarbon ages in the southwest Pacific Ocean during the last glacial period and deglaciation, Nature, 405, 555–559, 2000.

Sime, L. C., Kohfeld, K. E., Le Quéré, C., Wolff, E. W., de Boer, A. M., Graham, R. M., and Bopp, L.: Southern Hemisphere westerly wind changes during the Last Glacial Maximum: model-data comparison, Quaternary Science Reviews, 64, 104–120, 2013.

Sime, L. C., Hodgson, D., Bracegirdle, T. J., Allen, C., Perren, B., Roberts, S., and de Boer, A. M.: Sea ice led to poleward-shifted winds at the Last Glacial Maximum: the influence of state dependency on CMIP5 and PMIP3 models, Climate of the Past, 12, 2241–2253, 2016.

Skinner, L., Fallon, S., Waelbroeck, C., Michel, E., and Barker, S.: Ventilation of the deep Southern Ocean and deglacial CO_2 rise, Science, 328, 1147–1151, 2010.

Skinner, L., McCave, I., Carter, L., Fallon, S., Scrivner, A., and Primeau, F.: Reduced ventilation and enhanced magnitude of the deep Pacific carbon pool during the last glacial period, Earth and Planetary Science Letters, 411, 45–52, 2015.

Stocker, T.: Climate change 2013: the physical science basis: Working Group I contribution to the Fifth assessment report of the Intergovernmental Panel on Climate Change, Cambridge University Press, 2014.

Takahashi, T., Broecker, W. S., and Langer, S.: Redfield ratio based on chemical data from isopycnal surfaces, Journal of Geophysical Research: Oceans, 90, 6907–6924, 1985.

Toggweiler, J. R., Gnanadesikan, A., Carson, S., Murnane, R., and Sarmiento, J. L.: Representation of the carbon cycle in box models and GCMs: 1. Solubility pump, Global Biogeochemical Cycles, 17, doi:10.1029/2001GB001401, http://dx.doi.org/10.1029/2001GB001401, 1026, 2003.

Volk, T. and Hoffert, M. I.: Ocean Carbon Pumps: Analysis of Relative Strengths and Efficiencies in Ocean-Driven Atmospheric CO_2 Changes, in: The Carbon Cycle and Atmospheric CO: Natural Variations Archean to Present, edited by Sundquist, E. T. and Broecker, W. S., pp. 99–110, American Geophysical Union, Washington D.C., 1985.

von der Heydt, A. and Dijkstra, H. A.: Effect of ocean gateways on the global ocean circulation in the late Oligocene and early Miocene, Paleoceanography, 21, PA1011, 2006.

Williams, R. G. and Follows, M. J.: Ocean Dynamics and the Carbon Cycle: Principles and Mechanisms, Cambridge University Press, 2011.

Zhang, X., Lohmann, G., Knorr, G., and Xu, X.: Different ocean states and transient characteristics in Last Glacial Maximum simulations and implications for deglaciation, Climate of the Past, 9, 2319–2333, doi:10.5194/cp-9-2319-2013, http://www.clim-past.net/9/2319/2013/, 2013.

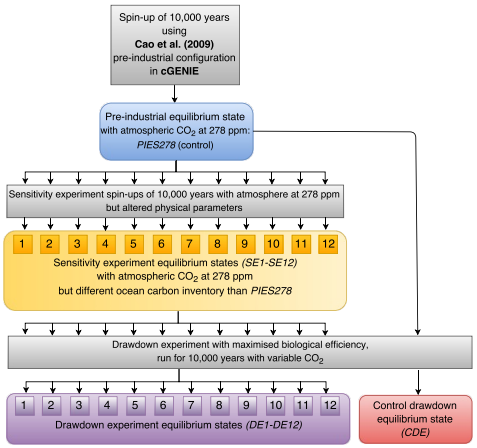

Figure 1. Flow chart showing the experimental setup. Grey boxes are spin-ups and transient stages of simulations (not analysed). Coloured boxes are equilibrium states that are analysed in this study. Throughout the study, the pre-industrial equilibrium state $PIES278$ (light blue box) is used as the control state, with which we compare the sensitivity experiment equilibrium states $SE1 - SE12$ (yellow box). The change in physical characteristics for each SE state compared to the control state $PIES278$ is described in Table 1. The SE:s are then used as a basis for the CO_2 experiments where biological efficiency is maximised. After running the drawdown experiments for 10,000 model years, we achieve a new ensemble of drawdown equilibrium states ($DE1 - DE12$) which are compared to a control drawdown equilibrium state (CDE).

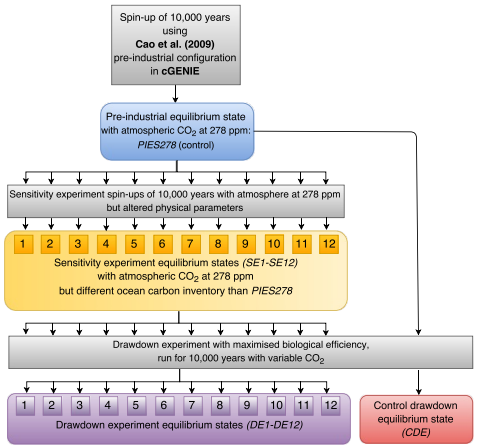

Figure 1. Flow chart showing the experimental setup. Grey boxes are spin-ups and transient stages of simulations (not analysed). Coloured boxes are equilibrium states that are analysed in this study. Throughout the study, the pre-industrial equilibrium state $PIES278$ (light blue box) is used as the control state, with which we compare the sensitivity experiment equilibrium states $SE1–SE12$ (yellow box). The change in physical characteristics for each SE state compared to the control state $PIES278$ is described in Table 1. The SEs are then used as a basis for the CO_2 experiments where biological efficiency is maximised. After running the drawdown experiments for 10,000 model years, we achieve a new ensemble of drawdown equilibrium states ($DE1 - DE12$) which are compared to a control drawdown equilibrium state (CDE).

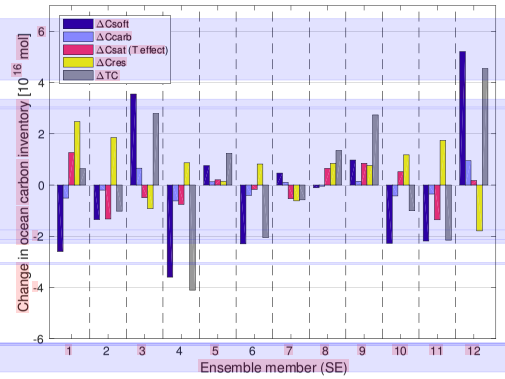

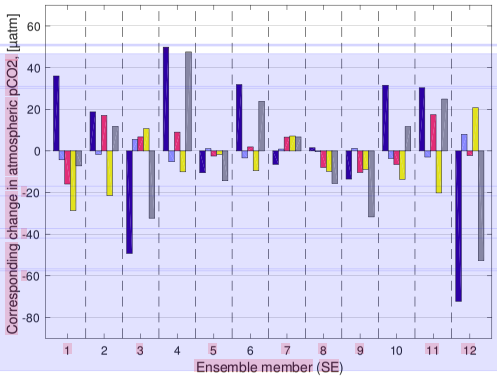

Figure 2. The upper panel shows observed ΔTC (grey bars) for $SE1 - SE12$, as compared to the TC inventory of the control $PIES278$, and the relative contributions by changes in the biological soft tissue (dark blue bars), hard tissue (light purple bars) and solubility (red bars) pumps. The contribution to the change in the solubility pump by changes in preformed alkalinity is so small that it can not be seen in this type of diagram and is therefore excluded. Hence, only the contribution to C_{sat} by the change in temperature is shown. The residual of the theoretical contributions by changes in C_{soft}, C_{carb} and C_{sat} to ΔTC (calculations made using Eqs. (9)–(13)) and the observed model ΔTC is denoted C_{res} (yellow bars). The left hand axis shows magnitude of changes given in 10^{16} mol ($\sim$ 120 Pg C). The lower panel shows pCO_2^{atm} equivalent given in μatm. Hence, this shows how big the difference in pCO_2^{atm} would be between ensemble members if we were not restoring to 278 ppm. Note that a positive (negative) ΔTC indicates a higher (lower) storage of CO_2 in the ocean, which would cause a lower (higher) pCO_2^{atm}.

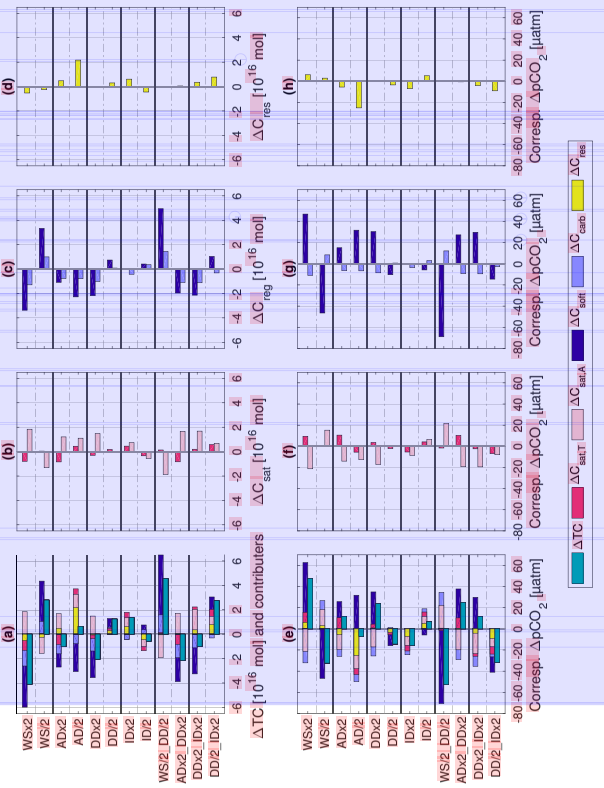

Figure 2. In panel a, green bars show observed ΔTC inventory for $SE1$–$SE12$, as compared to the TC inventory of the control $PIES278$. Other bars show relative contributions to ΔTC inventory by changes in the solubility (due to temperature = red, due to preformed alkalinity = pink, panels a and b), biological soft tissue (dark blue, panels a and c) and hard tissue (light purple, panels a and c) pumps. The residual of the theoretical contributions by changes in C_{soft}, C_{carb} and C_{sat} to ΔTC (calculations made using Eqs. (B2)–(B1)) and the observed model ΔTC is denoted C_{res} (yellow bars). The horizontal axis shows magnitude of changes given in 10^{16} mol ($\sim$ 120 Pg C). The lower panels (e–h) show approximate pCO_2^{atm} equivalent given in μatm. Hence, this shows how big the difference in pCO_2^{atm} would be between ensemble members if we were not restoring to 278 μatm. Note that a positive (negative) ΔTC indicates a higher (lower) storage of CO_2 in the ocean, which would cause a lower (higher) pCO_2^{atm}.

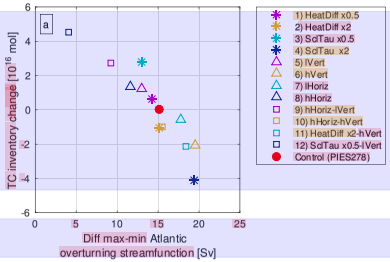

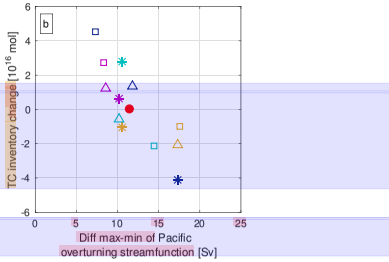

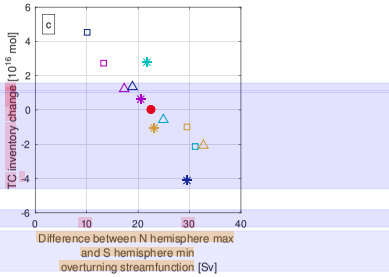

Figure 3. The difference between the maximum and minimum of the zonal average overturning streamfunction, ψ, below 556 m depth, and the change in TC for equilibrium states $SE1$–$SE12$ c.f. the control $PIES278$ (red dot). This is shown for the Atlantic basin, Pacific basin and for a global measure based on hemispheric differences, on the horizontal axis of panels a, b and c respectively.

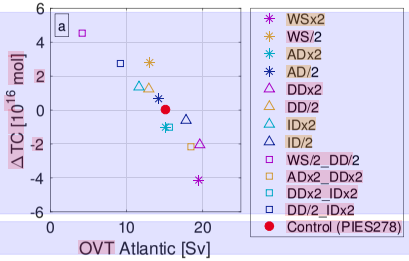

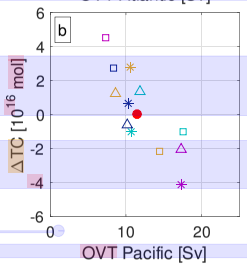

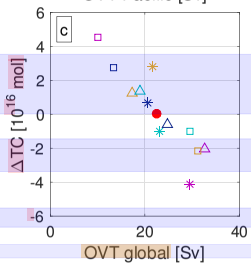

Figure 3. Strength of the overturning circulation in terms of OVT (see Section 3.4), and the change in TC inventory for equilibrium states $SE1$–$SE12$ c.f. the control $PIES278$ (red dot). This is shown for the Atlantic basin, Pacific basin and for the global measure based on hemispheric differences, on the horizontal axis of panels a, b and c respectively.

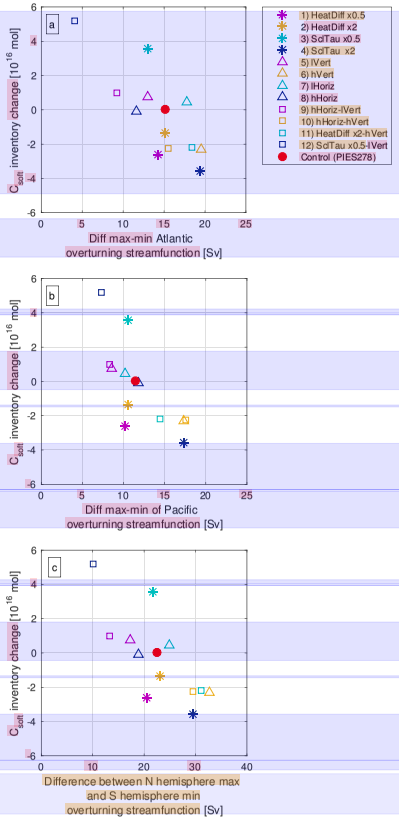

Figure 4. The difference between the maximum and minimum of the zonal average overturning streamfunction, ψ, below 556 m depth, and the change in C_{soft} for equilibrium states $SE1$ – $SE12$ c.f. the control $PIES278$ (red dot). This is shown for the Atlantic basin, Pacific basin and for a global measure based on hemispheric differences, on the horizontal axis of panels a, b and c respectively.

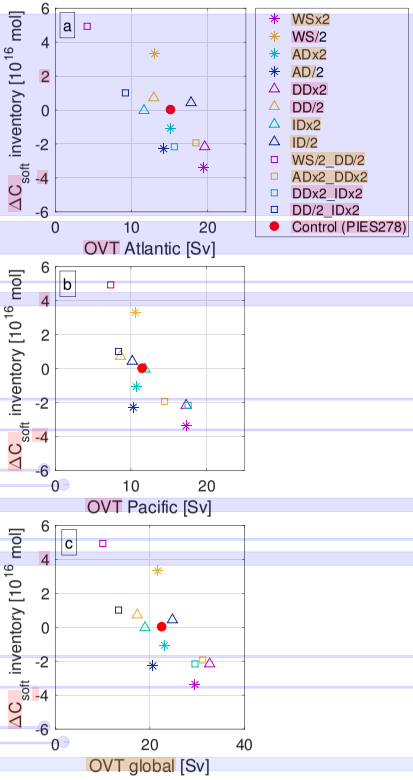

Figure 4. Strength of the overturning circulation in terms of OVT (see Section 3.4), and the change in C_{soft} inventory ($M_o \cdot \Delta C_{soft}$) for equilibrium states $SE1$–$SE12$ c.f. the control $PIES278$ (red dot). This is shown for the Atlantic basin, Pacific basin and for the global measure based on hemispheric differences, on the horizontal axis of panels a, b and c respectively.

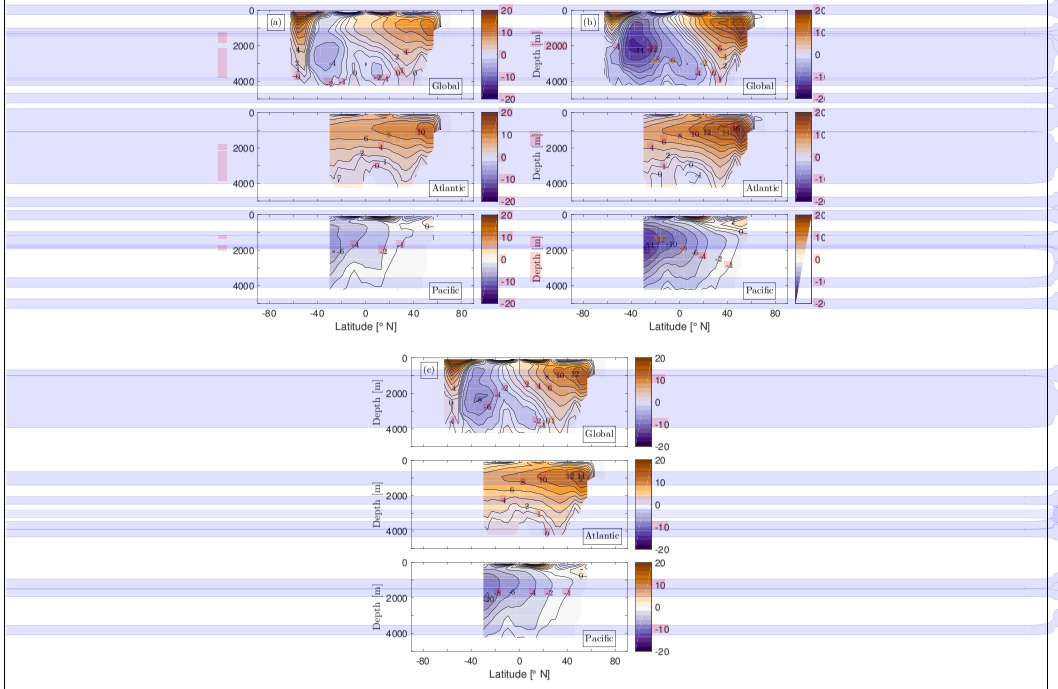

Figure 5. Zonal average overturning streamfunction (ψ) in Sverdrup Sv for a) $SE5$, with low vertical diffusivity, b) $SE6$, with high vertical diffusivity and c) the control $PIES278$. The upper panel shows the global ψ, the middle panel shows only the Atlantic sector and the lower panel shows only the Pacific sector. The southernmost limit for the Atlantic and Pacific sectors is -30° N.

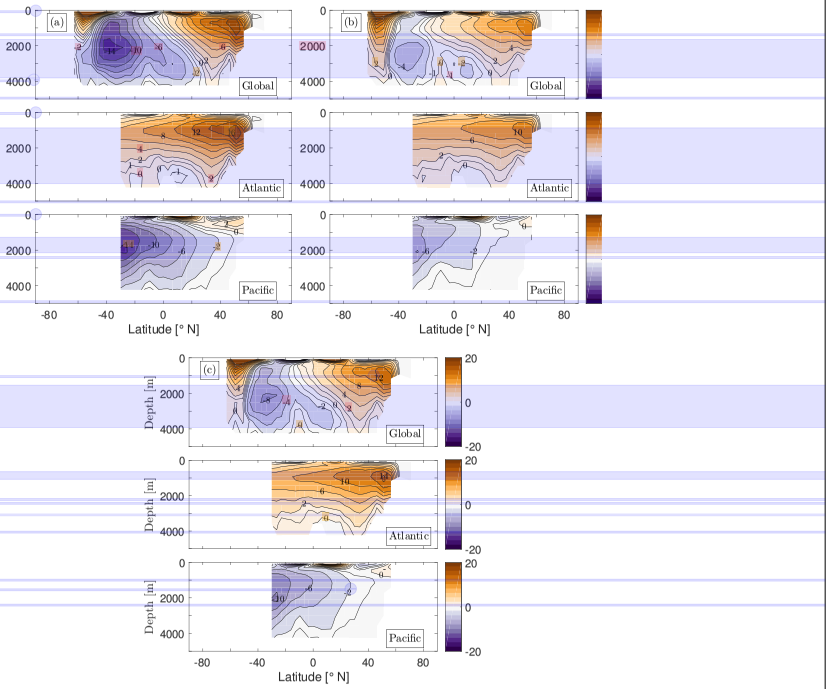

Figure 5. Zonal average overturning streamfunction (ψ) in Sverdrup Sv for a) $DDx2$, with high diapycnal diffusivity, b) $DD/2$, with low diapycnal diffusivity, and c) the control $PIES278$. The upper panel in each subfigure shows the global ψ, the middle panel shows only the Atlantic sector ,and the lower panel shows only the Pacific sector. The southernmost limit for the Atlantic and Pacific sectors is -30° N.

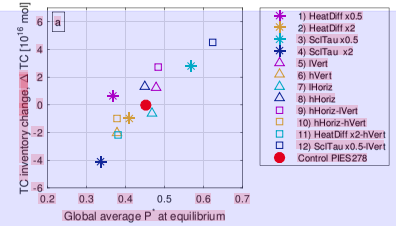

Figure 6. Panels showing (whole) global ocean $\overline{P^*}$ for the different ensemble members $SE1 - SE12$ plotted versus a) ΔTC (10^{16} mol), b) the inventory change of C_{soft}, hence $M_o \cdot \Delta C_{soft}$, and c) the CO_2 drawdown potential (ppm) of each ensemble member, which is the lowering of pCO_2^{atm} achieved by maximising biological efficiency (making $\overline{P^*}$ get equal to 1), see Eq. (3). Ensemble member characteristics are described in Table 1.

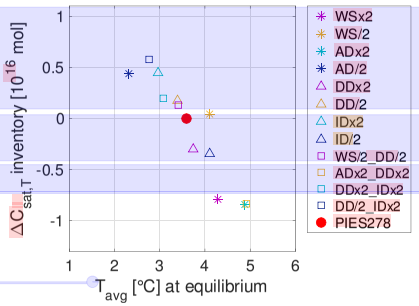

Figure 6. Global ocean average temperature (T_{avg}) and the changes in TC that are due to solubility changing with temperature ($\Delta C_{sat,T}$) for the ensemble members $SE1$–$SE12$ compared to the control simulation $PIES278$ (red dot).

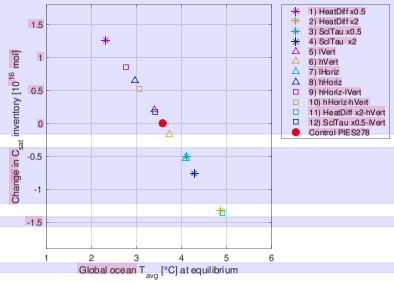

Figure 7. Global ocean average temperature (T_{avg}) and the changes in C_{sat} for the ensemble members $SE1-SE12$ compared to the control simulation $PIES278$ (red dot).

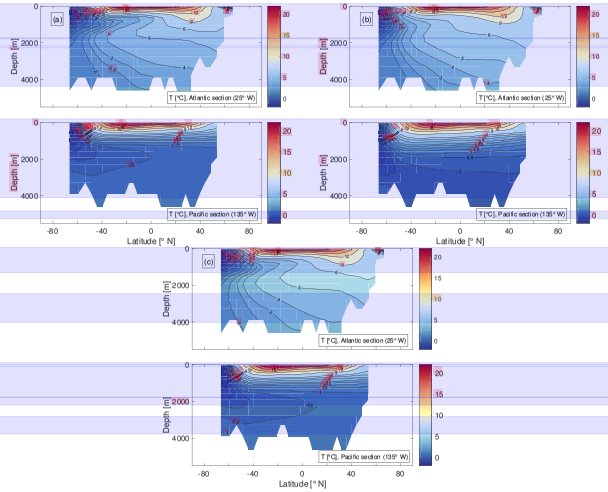

Figure 8. Sections of temperature (°C) for a) $SE5$, with low vertical diffusivity, b) $SE6$, with high vertical diffusivity and c) the control $PIES278$. The upper panel of each subfigure shows a section through the Atlantic, at 25° W and the lower panel shows a section through the Pacific, at 135° W. Both sections also cover latitudes that are in the Southern Ocean (south of -30° N).

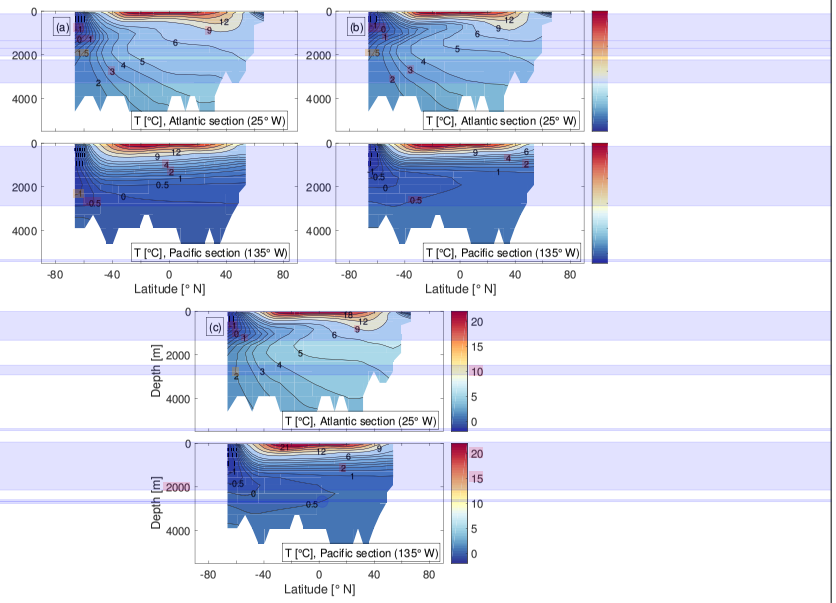

Figure 7. Sections of temperature (°C) for a) $DDx2$, with high diapycnal diffusivity, b) $DD/2$, with low diapycnal diffusivity, and c) the control $PIES278$. The upper panel of each subfigure shows a section through the Atlantic, at 25° W and the lower panel shows a section through the Pacific, at 135° W. Both sections also cover latitudes that are in the Southern Ocean (south of -30° N).

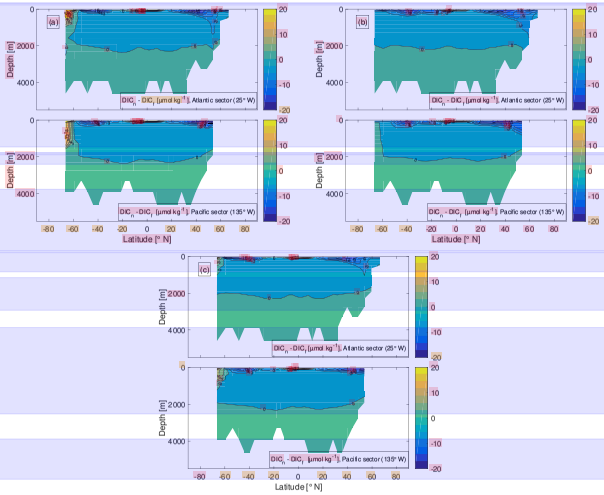

Figure 9. Example sections of the DIC concentration difference $DIC_n - DIC_f$, where DIC_n is the concentration in model simulations with normal gas exchange for CO_2 and DIC_f is the concentration in model simulations with artificially fast gas exchange for CO_2. The panels show $DIC_n - DIC_f$ for a) $SE1$, with halved atmospheric heat diffusivity, b) $SE4$, with doubled wind stress and c) the control equilibirum $PIES278$. The upper panel of each subfigure shows a section through the Atlantic, at 25° W and the lower panel shows a section through the Pacific, at 135° W. Both sections also cover latitudes that are in the Southern Ocean (south of -30° N).

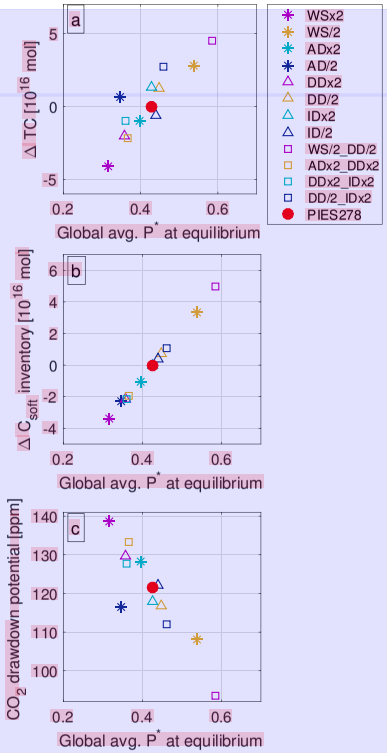

Figure 8. Panels showing (whole) global ocean $\overline{P^*}$ for the different ensemble members $SE1$–$SE12$ plotted versus a) change in total carbon inventory (ΔTC, 10^{16} mol), b) the inventory change of C_{soft}, hence $M_o \cdot \Delta C_{soft}$ (10^{16} mol), and c) the CO_2 drawdown potential (ppm) of each ensemble member, which is the lowering of pCO_2^{atm} achieved by maximising biological efficiency (making $\overline{P^*}$ get equal to 1), see Eq. (1). Ensemble member characteristics are described in Table 1.

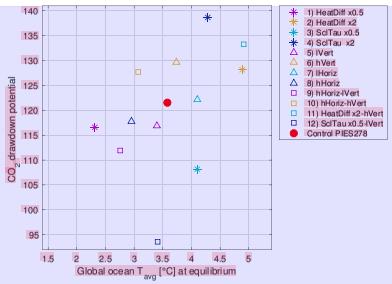

Figure 10. Global ocean average temperature (T_{avg}, °C) in relation to drawdown potential for CO_2 (DP, ppm) for all ensemble members $SE1 - SE12$ and the control $PIES278$ (red dot).

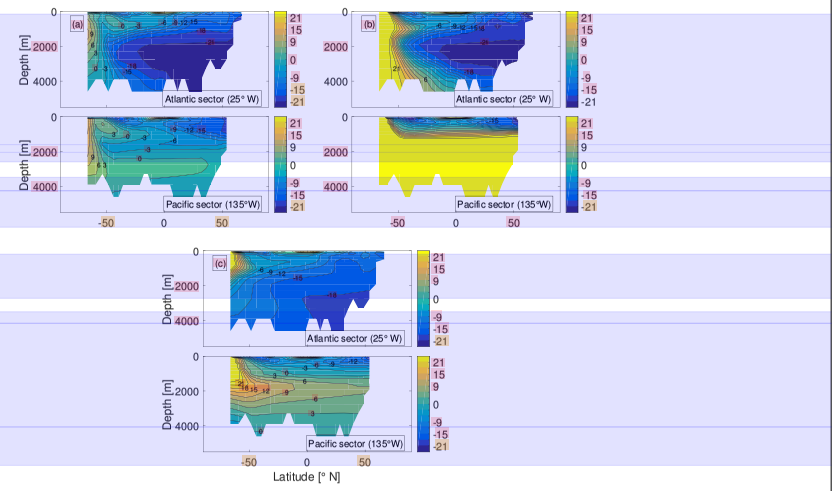

Figure 9. Example sections of $C_{dis} = DIC_{pre} - C_{sat}$ (Appendix B3). The panels show C_{dis} ($\mu molkg^{-1}$) for a) $WSx2$, with doubled wind stress, b) $AD/2$, with halved atmospheric heat diffusivity and c) the control equilibirum $PIES278$. The upper panel of each subfigure shows a section through the Atlantic, at 25° W and the lower panel shows a section through the Pacific, at 135° W. Both sections also cover latitudes that are in the Southern Ocean (south of -30° N).

Table 1. List of sensitivity experiment equilibrium states $SE1-SE12$, abbreviated ensemble member description, and specification of which one or two physical characteristics have been altered compared to the control $PIES278$. The nature of the change is specified within parenthesis.

Ensemble member	Abbreviated description	Adjusted parameter (adjustment)
SE1	'HeatDiff x0.5'	Atmospheric heat diffusivity (halved)
SE2	'HeatDiff x2'	Atmospheric heat diffusivity (doubled)
SE3	'SclTau x0.5'	Wind stress intensity (halved)
SE4	'SclTau x2'	Wind stress intensity (doubled)
SE5	'lVert'	Ocean vertical diffusivity (halved)
SE6	'hVert'	Ocean vertical diffusivity (doubled)
SE7	'lHoriz'	Ocean horizontal diffusivity (halved)
SE8	'hHoriz'	Ocean horizontal diffusivity (doubled)
SE9	'hHoriz-lVert'	Ocean horizontal, and vertical diffusivity (doubled, halved)
SE10	'hHoriz-hVert'	Ocean horizontal, and vertical diffusivity (doubled, doubled)
SE11	'HeatDiff x2 hVert'	Atmospheric heat diffusivity (doubled) and ocean vertical diffusivity (doubled)
SE12	'SclTau x0.5 lVert'	Wind stress intensity (halved) and ocean vertical diffusivity (halved)

Table 1. List of sensitivity experiment equilibrium states $SE1-SE12$, abbreviated ensemble member description, and specification of which one or two physical characteristics have been altered compared to the control $PIES278$. The nature of the change is specified within parenthesis.

Ensemble member	Abbreviated description	Adjusted parameter (adjustment)
SE1	'WSx2'	Wind stress intensity (doubled)
SE2	'WS/2'	Wind stress intensity (halved)
SE3	'ADx2'	Atmospheric heat diffusivity (halved)
SE4	'AD/2'	Atmospheric heat diffusivity (doubled)
SE5	'DDx2'	Ocean diapycnal diffusivity (doubled)
SE6	'DD/2'	Ocean diapycnal diffusivity (halved)
SE7	'IDx2'	Ocean isopycnal diffusivity (halved)
SE8	'ID/2'	Ocean isopycnal diffusivity (doubled)
SE9	'WS/2_DD/2'	Wind stress intensity (halved) and ocean diapycnal diffusivity (halved)
SE10	'ADx2_DDx2'	Atmospheric heat diffusivity (doubled) and ocean diapycnal diffusivity (doubled)
SE11	'DDx2_IDx2'	Ocean diapycnal, and isopycnal diffusivity (doubled, doubled)
SE12	'DDx2_ID/2'	Ocean diapycnal, and isopycnal diffusivity (doubled, halved)

Table 2. Diagnostic variables for observations (Obs.), the control $PIES278$ (Ctrl.) and the ensemble members $SE1 - SE12$. The variables are global ocean averages of temperature (T_{avg}, °C) and pH (pH_{avg}), surface ocean average pH, the sea ice cover (%), the global average of the nutrient utilisation efficiency (expressed in terms of $\overline{P^*}$) and a measure of the strength of the global ocean overturning circulation, ψ, which is the difference between the Northern hemisphere maximum and the Southern hemisphere minimum ($1\ \text{Sv} = 1 \cdot 10^6\ \text{m}^3\ \text{s}^{-1}$) below 556 m. Observational estimate for T_{avg} has been calculated using World Ocean Atlas 2013, Locarnini et al. (2013)) and the pre-industrial estimate for pH is given by Raven et al. (2005). Modern day sea ice cover is given as an interval due to seasonal variability Comiso (2008). The observational estimate for $\overline{P^*}$ is given by Ito and Follows (2005)

Ens. mem.	T_{avg} (°C)	pH_{avg} (SWS)	pH_{surf} (SWS)	Sea ice cover (%)	Global $\overline{P^*}$	Global $\psi_{max} - \psi_{min}$ (Sv)
Obs.	3.49	-	∼8.2	3 to 6	0.36	–
Ctrl.	3.58	7.90	8.16	5.4	0.45	22.5
SE1	2.31	7.89	8.15	10.6	0.37	20.6
SE2	4.88	7.91	8.17	0.7	0.41	23.2
SE3	4.10	7.84	8.16	6.7	0.57	21.6
SE4	4.28	7.97	8.16	2.7	0.34	29.4
SE5	3.39	7.87	8.15	6.1	0.48	17.4
SE6	3.73	7.94	8.16	4.1	0.38	32.6
SE7	4.10	7.90	8.16	5.3	0.47	24.8
SE8	2.96	7.88	8.16	5.4	0.45	19.0
SE9	2.76	7.85	8.15	6.0	0.48	13.4
SE10	3.07	7.93	8.16	3.7	0.38	30.0
SE11	4.91	7.93	8.17	0.0	0.38	31.1
SE12	3.41	7.80	8.15	7.4	0.62	10.1

Table 2. Diagnostic variables of the pre-industrial control states ($PICs$) of PMIP2 and CMIP5/PMIP3 (temperature and salinity as read from Fig. 9.18. of WG1 in IPCC AR5 and AMOC as given in Table 1 in Muglia and Schmittner (2015)) compared to similar diagnostics for our ensemble $SE1$–$SE12$ and control state $PIES278$.

Variables	$PICs$ of PMIP2 and CMIP5/PMIP3	Ödalen et al. cGENIE $SE1$–$SE12$ and $PIES278$
Potential temperature (°C), N. Atlantic	2.9 – 6.4[1]	4.6 – 8.0[2]
Potential temperature (°C), S. Atlantic	-1.6 – 2.0[3]	-0.3 – 3.7[4]
Salinity, N. Atlantic	34.8 – 35.5[1]	35.3 – 35.6[2]
Salinity, S. Atlantic	34.6 – 35.0[3]	34.9 – 35.1[4]
AMOC ($1Sv = 10^6 m^3 s^{-1}$)	12.64 – 23.02[5]	2.0 – 18.0[6]

[1] North Atlantic PMIP grid point: 55.5°N, 14.5°W, 2,184 m depth
[2] North Atlantic cGENIE closest corresponding grid cell: 51-56°N, 10-20°W, 1,738-2,100 m depth
[3] South Atlantic PMIP grid point: 50°S, 5°E, 3,636 m depth
[4] South Atlantic cGENIE closest corresponding grid cell: 46-51°S, 0-10°E, 3,008-3,576 m depth
[5] Muglia and Schmittner (2015), PMIP3 pre-industrial control ensemble AMOC at 25°N, average with interval of one standard deviation [6] cGENIE maximum Atlantic overturning. Ensemble member $WS/2\_DD/2$ (see Table 1) has a collapsed AMOC circulation (2.0 Sv). The average of this variable for all other SEs is 13.8 Sv (range 8.3 – 18.0 Sv).

Table 3. Correlation coefficients of the changes in strength of the zonal average overturning streamfunction ($\psi_{max} - \psi_{min}$) below 556 m depth in different geographical regions and the changes in carbon species. Global means the difference between the Northern Hemisphere maximum and the Southern Hemisphere minimum overturning.

($\psi_{max} - \psi_{min}$) in region	ΔTC	ΔC_{sat} (T effect)	ΔC_{soft}	ΔC_{res}	$\Delta C_{soft} + \Delta C_{res}$
Atlantic	-0.924	-0.485	-0.793	0.476	-0.871
Pacific	-0.810	-0.256	-0.733	0.402	-0.832
Global	-0.893	-0.488	-0.756	0.445	-0.836

Table 3. Diagnostic variables for observations (Obs.), the control $PIES278$ (Ctrl.) and the ensemble members $SE1$–$SE12$. The variables are global ocean averages of temperature (T_{avg}, °C) and pH (pH_{avg}), surface ocean average pH, the sea ice cover (%), the global average of the nutrient utilisation efficiency (expressed in terms of $\overline{P^*}$) and a measure of the strength of the global ocean overturning circulation, OVT (see Section 3.4). Observational estimate for T_{avg} has been calculated using World Ocean Atlas 2013, Locarnini et al. (2013)) and the pre-industrial estimate for pH is given by Raven et al. (2005). Modern day sea ice cover is given as an interval due to seasonal variability Comiso (2008). The observational estimate for $\overline{P^*}$ is given by Ito and Follows (2005)

Ens. mem.	Experiment name	T_{avg} (°C)	pH_{avg} (SWS)	pH_{surf} (SWS)	Sea ice cover (%)	Global $\overline{P^*}$	Global OVT (Sv)
Obs.	-	3.49	-	∼8.2	3 to 6	0.36	–
Ctrl.	PIES278	3.58	7.90	8.16	5.4	0.43	22.5
SE1	WSx2	4.28	7.97	8.16	2.7	0.32	29.4
SE2	WS/2	4.10	7.84	8.16	6.7	0.54	21.6
SE3	ADx2	4.88	7.91	8.17	0.7	0.40	23.2
SE4	AD/2	2.31	7.89	8.15	10.6	0.35	20.6
SE5	DDx2	3.73	7.94	8.16	4.1	0.36	32.6
SE6	DD/2	3.39	7.87	8.15	6.1	0.45	17.4
SE7	IDx2	2.96	7.88	8.16	5.4	0.43	19.0
SE8	ID/2	4.10	7.90	8.16	5.3	0.44	24.8
SE9	WS/2_DD/2	3.41	7.80	8.15	7.4	0.59	10.1
SE10	ADx2_DDx2	4.91	7.93	8.17	0.0	0.37	31.1
SE11	DDx2_IDx2	3.07	7.93	8.16	3.7	0.36	30.0
SE12	DD/2_IDx2	2.76	7.85	8.15	6.0	0.46	13.4

Table 4. Correlation coefficients of the changes in OVT (see Section 3.4), sorted by geographical regions, and the anomaly in each carbon species for the SE-ensemble (relative to $PIES278$).

OVT in region	ΔTC	$\Delta C_{sat,T}$	$\Delta C_{sat,A}$	ΔC_{soft}	ΔC_{carb}	ΔC_{res}	$\Delta C_{soft} + \Delta C_{res}$
Atlantic	-0.92	-0.64	0.65	-0.80	-0.69	-0.25	-0.89
Pacific	-0.81	-0.43	0.72	-0.75	-0.74	-0.27	-0.84
Global	-0.89	-0.63	0.67	-0.77	-0.70	-0.30	-0.87